University of Reading

Using SO_2, Thermal and SAR Time-Series Data to Investigate Cyclicity at Bagana Volcano, Papua New Guinea

MPhil

Department of Meteorology

Rebecca Faye Couchman-Crook

July 2020

Word Count: 17,568

Abstract

Bagana is a young (300-400 years) polygenetic andesitic volcano situated on Bougainville Island, Papua New Guinea, that lends itself to satellite remote sensing due to its largely inaccessible location. Bagana is unusual in the amount of SO_2 it outputs, and its high rate of lava extrusion. Previous work noted with lava mass fluxes from Interferometric Synthetic Aperture Radar (InSAR) data that there is cyclicity of a few months over a 14 month period, and others examined trends in the SO_2 degassing against thermal data, suggesting there were two eruption behaviours demonstrated.[1,2] Using a unique combination of data sources, this study has found evidence of cyclicity in SO_2, thermal infra-red and InSAR data, where the significant cycles identified are at 16 days (SO_2) and 133 days (thermal). Additionally, this study showed there are three observed eruption styles at Bagana. There is evidence to indicate that SO_2 peaks are related to elevated thermal signals on a 4-5 month cycle. These peaks coincide with lava flows imaged by Sentinel-2 that provide some verification for the conclusions drawn. This may provide insight as to Bagana's cycles compared with other volcanoes in similar arc settings, with the most comparable processes seen at Soufrière Hills Volcano, with its 8-14 day cycle in SO_2, and Popocatépetl with its 1.7-7 month dome-building cycle.

Declaration of Original Authorship

Declaration: I confirm that this is my own work and the use of all material from other sources has been properly and fully acknowledged.

REBECCA FAYE COUCHMAN-CROOK

Contents

Chapter One – Introduction

1.1 Introduction to Bagana

Bagana volcano, on the island of Bougainville in Papua New Guinea (Fig. 1.1), presents a rare opportunity to examine a very young (likely 300-400 years old), polygenetic, andesitic volcano.[3] It reaches 1850 m above sea level (a.s.l.) (Fig.1.2), and has a summit crater 200 m across, with a low dome up to 40 m above the crater rim.[3]

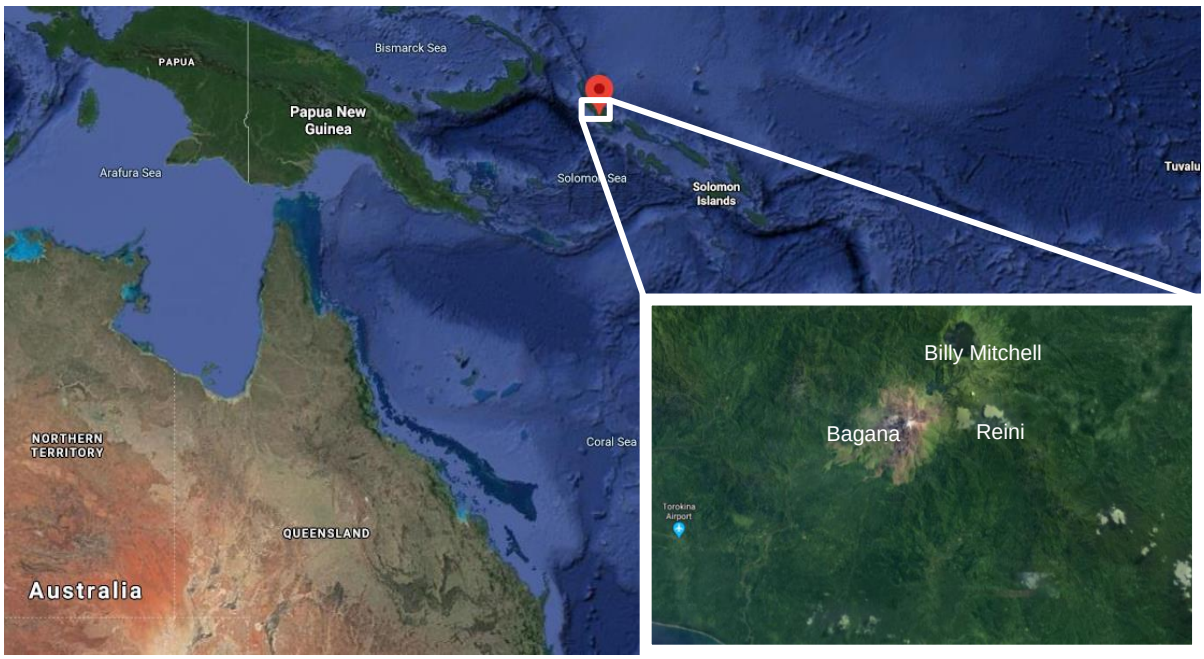

Figure 1.1 A location map of Bagana, part of Papua New Guinea, and adjacent to the Solomon Islands. The red marker shows Bougainville Island.[4]

Bagana has a high emission rate of gas in passive mode, with a persistent SO_2 plume. Bagana has the third-highest SO_2 mass flux of persistently active volcanoes worldwide, at 1204 x 10^6 kg/y at the start of this study (2017).[5] The plume is water-vapour and SO_2-rich, sometimes containing ash that reaches heights ranging from low-level ash venting to a more vigorous plume of 3-4 km above sea level.[3,5]

There is also a high rate of lava extrusion (~1 m^3/s) measured over decades at Bagana.[3] The lava flows on Bagana reach maximum lengths of approximately 4 km on the southern flank, with channels that broaden downslope to be 100-300 m wide with branching flows 60-150 m wide and high levees.[1,6,7] Lava flows comprise crystal-rich andesite, and appear to be delivered in distinct batches.[8]

Figure 1.2 A view of Bagana, Bougainville Island seen from south-west coast.[9]

Typical behaviour are pulses of activity lasting many months, with slow-moving channelised lava accompanied by minor ash and high levels of SO_2 emission.[1] Bagana has modest Vulcanian eruptions every few weeks to months, with larger explosive events every few years. Most of these are smaller than 4 on the Volcanic Explosivity Index (VEI); however, there is field evidence of larger eruptions that produced sustained ash columns and pyroclastic density currents.[1,6,10]

1.2 Geological Setting of Bagana

1.2.1 Bagana's Tectonic Setting

Primarily, the convergence of the Pacific plate and the Australian plate are responsible for volcanoes in the area of Papua New Guinea (Fig. 1.3). South-west of Bougainville Island, the Solomon Sea plate is subducting at a 75° angle to the north-east at the New Britain Trench at a rate of about 100 mm/yr.[11,12]

The depth to the subducting plate is 150 km below Bagana.[12] North-east of Bougainville Island, the Ontong Java Plateau is subducting much more slowly to the south-west along

the North Solomon Trench. There are areas of faulting throughout Bougainville, and these may provide conduits for magma transport.[13]

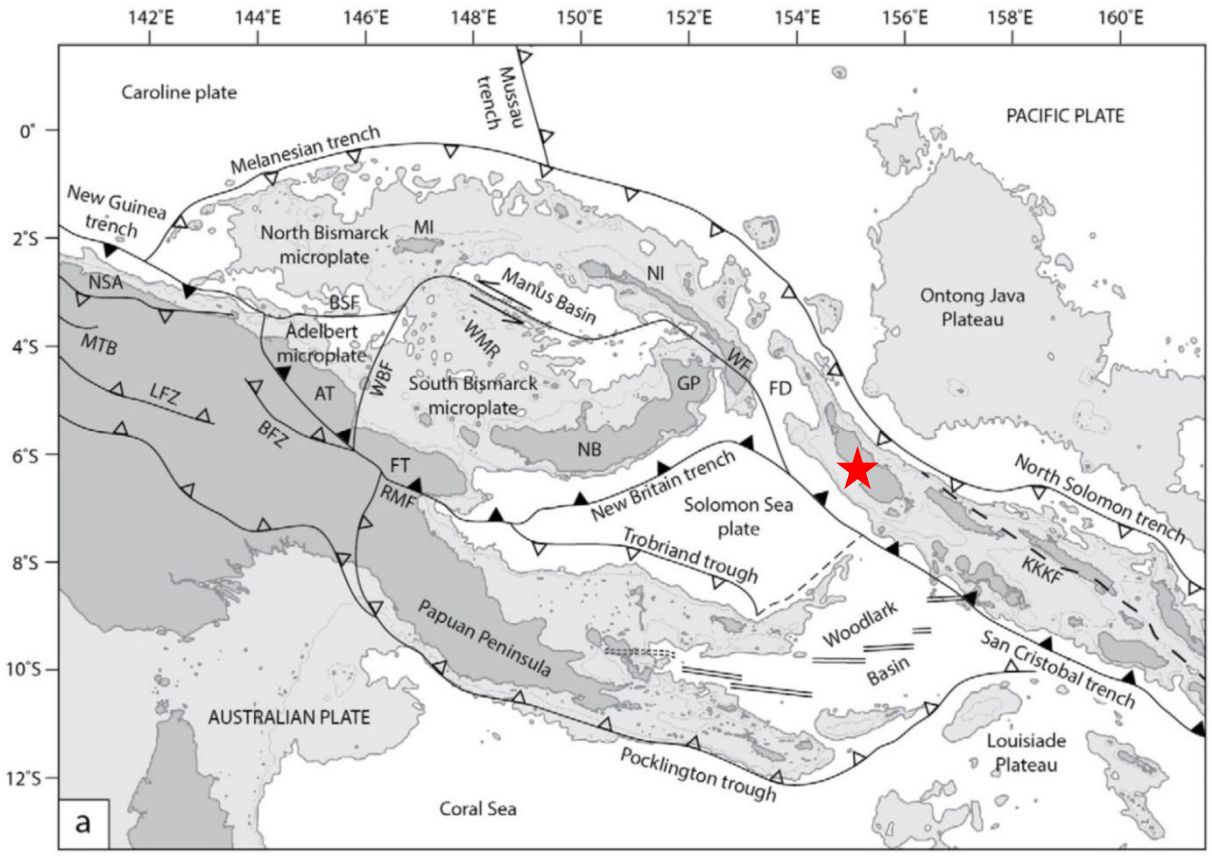

Figure 1.3 A map of the tectonic plates surrounding Bougainville Island, Papua New Guinea. The red star indicates the location of Bagana.[14]

Seismicity is a prominent feature of the geology in the area. With the Solomon Sea plate and Ontong Java Plateau surrounding Bougainville Island on the North Bismarck plate (Fig. 1.3), there are stresses built up on all sides from subducting plates, causing frequent events in the Benioff zone beneath Bagana. Particularly strong events are not uncommon, with notable recent examples occurring on 17th December 2016 and January 22nd 2017, both at a magnitude of 7.9.[15]

1.2.2 Historical Volcanoes Neighbouring Bagana

Billy Mitchell is a volcano 6 km north-northeast of Bagana (Figs. 1.1 and 1.4), which last erupted 370 ± 19 years before the present.[16] The eruption was a Plinian event, dacitic in composition, with a total erupted volume of 13.5 km^3.[3,16] A Plinian eruption prior to this occurred 937±19 years before the present, with an estimated volume of 7 km^3.[3]

Inclusions of dacite are found in Bagana lavas, which may provide a link to the Billy Mitchell magma source.[3]

To the east of Bagana is Reini, an eroded lava cone (see Figs. 1.1 and 1.4). It has a whole rock geochemistry similar to Bagana.[13,16] Reini's oldest activity predates the Billy Mitchell 1 and 2 eruptions, and there is also field evidence that it was active between the two Plinian events.[3,16]

1.2.3 Eruptive History of Bagana

The eruptive history of Bagana is documented since the early 1800s.[17] A large explosive event in 1884 resulted in a number of fatalities, and the volcano was reported as having been in eruption for 15-20 years.[18] A systematic aerial photograph record of the volcano was begun in 1943, continuing through the 1960s, and field observations continued throughout this period. The first mapping of lava flows was made in 1967 by Blake and Miezitis (1968), and has since been revised multiple times.[3,13] Fig. 1.4 shows the latest version of this (modified from Wadge et al. (2018)).[3]

Recent work by Wadge et al. (2018) revealed lava flows have been active 73% of the time between 1943 and 2017.[3] They mapped lava flows and identified areas of changed topography using Shuttle Radar Topography Mission data (SRTM) and InSAR. The slow and sustained emplacement of lava allowed the estimation of flux. Wadge et al. (2018) calculated an average rate of lava extrusion for the period 1945-2014 of 1.0±0.5 m^3/s, and determined that the summit has risen 150 m in 70 years, with an increase in volume of 2.2 ±0.9 km^3.[3] This growth rate suggests an age of a round 300 years for Bagana.[1,3]

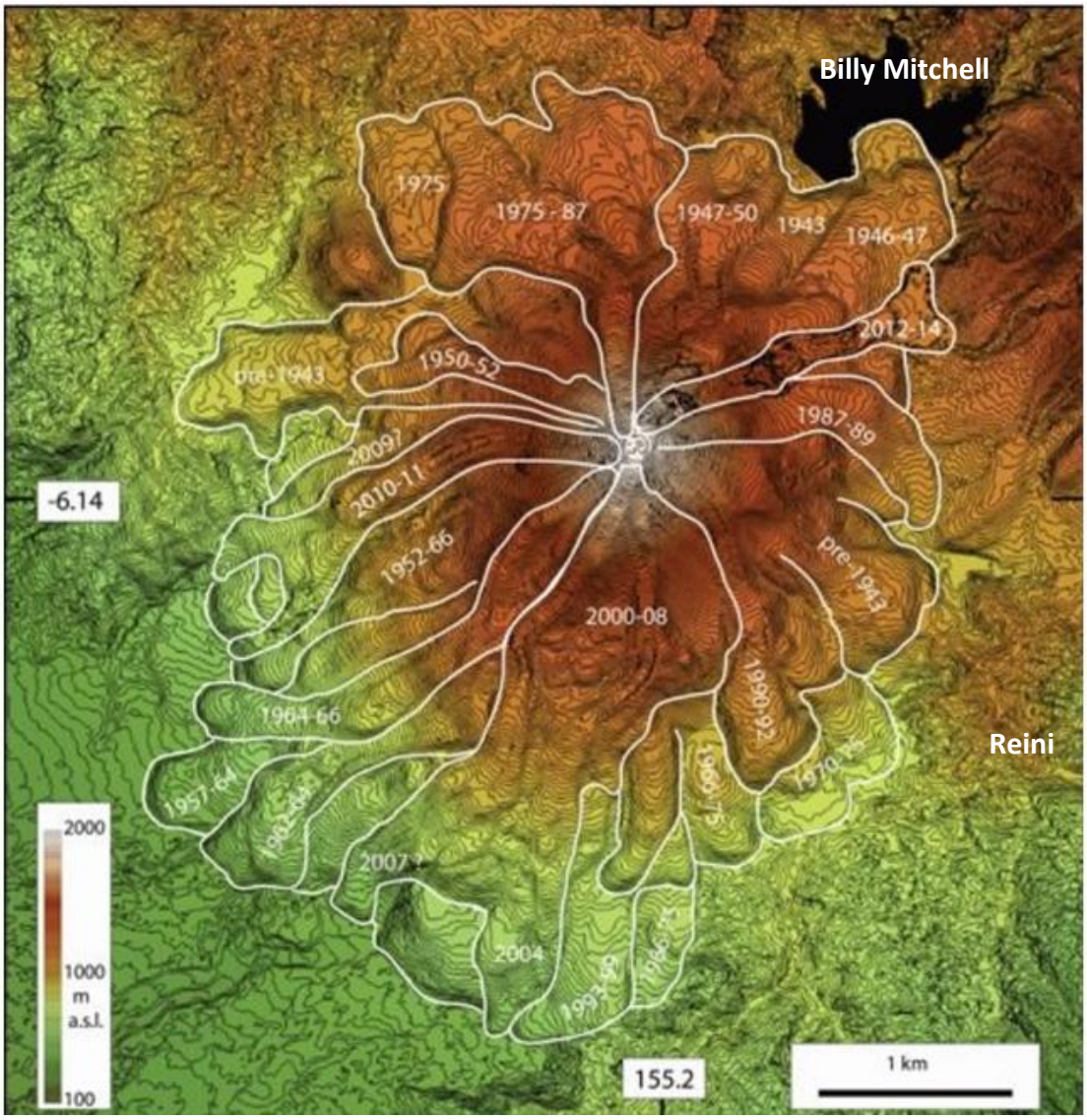

Figure 1.4 Map of the outlines of lava flows at Bagana volcano from 1943-2017. The topography is derived from TanDEM-X global data with 10 m contour intervals (modified from Fig. 4. from Wadge et al., 2018).[3]

1.3 Motivation for the Study

Recent work on Bagana has revealed that on a decadal timescale, the magma flux at the surface is fairly constant.[3] However, pulsatory behaviour is evident during the emplacement of lavas over periods of a few months shown by TerraSAR-X amplitude change detection images.[1] Similarly, there is evidence that the volatile flux is pulsatory at scales of months, with studies focussing on the high SO_2 content of the permanent plume

at its summit.[2] Detailed investigations at Bagana are needed to better understand eruption cycles and related pulsatory behaviour, and to enhance understanding of the processes governing Bagana's behaviour.

The use of remotely sensed data for the purpose of investigating at Bagana is vital, as there are no regular series of ground instrumental observations due to its remote location, with much of the lower slopes covered in thick vegetation, and little funding to maintain monitoring systems. Furthermore, remote sensing is suitable for the study of Bagana, as its slow-moving silicic flows can be understood by less-frequent observations than if they were basaltic, faster-moving ones.[1] Additionally, there are people living in the potential path of pyroclastic density currents and lava flows, which are rare but significant hazards associated with this volcano.

Relatively little work has been done on Bagana, compared to other andesitic arc stratovolcanoes, such as Volcán de Colima in Mexico, and Soufrière Hills Volcano, Montserrat. In addition, Bagana is comparatively young compared to its contemporaries, so there is much to be gained from exploring new datasets to better understand the development of young andesitic volcanoes in an arc setting.

1.4 Aims of the Research

The focus of this study is to investigate the pulsatory nature of Bagana volcano through the identification and interpretation of cyclic behaviour using satellite remote sensing data, namely SO_2, InSAR, radar amplitude and thermal data. This combination of data sources is unusual in the study of Bagana, and across volcanic cyclicity studies in general, which do not typically incorporate the combination of these datasets.

This work aims to improve understanding of the physical processes that govern the behaviour of Bagana, particularly the pulsation of magma and SO_2 flux through the volcano from SO_2 (Chapter 2) and thermal (Chapter 3) data analysis. A comparison of these two datasets and the cycles identified is provided (Chapter 4). A better characterisation of the behaviour will be gained through a new time-series database, covering a previously un-studied time interval from 2016-2019, with new sources of data (InSAR and Amplitude) utilised to enhance the validity of interpretations (Chapter 5).

This will provide unique insights to understand eruption processes governing Bagana's cyclic behaviour which may be applied to other andesitic lava dome forming volcanoes in similar settings across the globe, in an original way not common in volcanic cyclicity studies.

Chapter Two – SO_2 Cyclicity at Bagana - Is Cyclicity Seen in the Output of SO_2 at Bagana? And How Does This Compare to Other SO_2 Cycles at Other Similar Volcanoes?

2.1 Introduction

The aims of these research questions are to identify any weekly to yearly cyclicity present in the SO_2 data from Bagana, building on the work of Wadge et al. (2012).[1] How unusual this cyclicity is in relation to other similar andesitic volcanoes will also be established, in terms of length of cycle, volume and flux of SO_2. Bagana has a continuous plume of SO_2 at its summit, which may provide a valuable insight into the processes governing the behaviour of Bagana volcano.[2]

The method for this section is based on the work of McCormick Kilbride et al. (2019), because it provides a comparative study to this, utilising SO_2 data from the Ozone Monitoring Instrument (OMI).[2] McCormick Kilbride et al. (2019) analyse the SO_2 over a 17 year period, which provides an historical record with which to compare results from this study.[2] There is also a year's overlap in the data which allows direct comparison of values obtained from each study to evaluate the repeatability of the methods from each. This study seeks to provide a repeatable methodology based on less subjective cloud cover analysis, relying on inbuilt classifiers in the SO_2 data, instead of visual classification.

Furthermore, cyclicity was not the focus of McCormick Kilbride et al. (2019), and so through the use of Fast Fourier Transform analysis, the work from this study adds a new dimension to other SO_2 studies of Bagana, which dealt with linear time-series data.[2]

2.2 Objectives

The objectives to achieve these aims are:

- To acquire the SO_2 data from OMI necessary to undertake the analysis over the 2016-2019 period;

- To develop a method for analysing the OMI data and working out totals based on McCormick Kilbride et al. (2019) and seeking to improve the repeatability of this;

- To conduct a time-series analysis on the SO_2 data, using the coding language R, and Fast Fourier Transform, to identify cycles;

- To conduct a literature review examining equivalent cycles at other andesitic volcanoes in similar settings.

2.3 A Review of SO_2 Cyclicity at Andesitic Volcanoes

Cyclic behaviour of andesitic lava dome forming volcanoes has been studied at individual examples (e.g. Popocatépetl, Soufriere Hills Volcano) but not often have comparative studies on them specifically been made to the degree in this study. This section provides a literature review of potentially analogous andesitic arc volcanoes which show cyclicity of SO_2 emissions. These will be used to draw comparisons with the data and the cyclicity observed at Bagana Volcano, to try to better understand Bagana's behaviour. An equivalent study based on thermal radiation is discussed in Chapter 3.

2.3.1 Popocatépetl

Popocatépetl is situated on the Trans-Mexican Volcanic Belt, with its crater morphology created by a series of pre-1994 eruptions.[19,20] From 1994, after initial clearing of the vent with ash-rich eruptions, a cycle of lava dome building began and Popocatépetl is now one of the top five SO_2 volcanic emitters globally.[21]

Passive degassing is gas released from a volcano at all times, regardless of whether an eruption is occurring. The passive degassing seen at Popocatépetl manifests as "puffing", which is thought to be caused by fractures in the lava dome narrowing due to gravity under a waning gas supply, and then expansion after pressure build-up, resulting in an oscillation in the degassing behaviour.[21] Application of a Fourier Transform to the time-series of SO_2 flux data shows a peak in the SO_2 flux at 200-400 s, corresponding to the "puffing".[21] This behaviour is different to that seen at volcanoes such as Santiaguito and Soufrière Hills.[21]

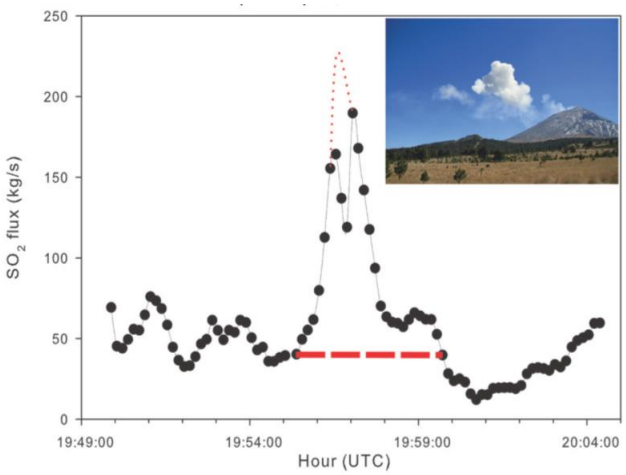

Figure. 2.1 Explosion Type 1 – SO_2 peak, with an explosion and return to normal levels (Campion et al., 2018).[21]

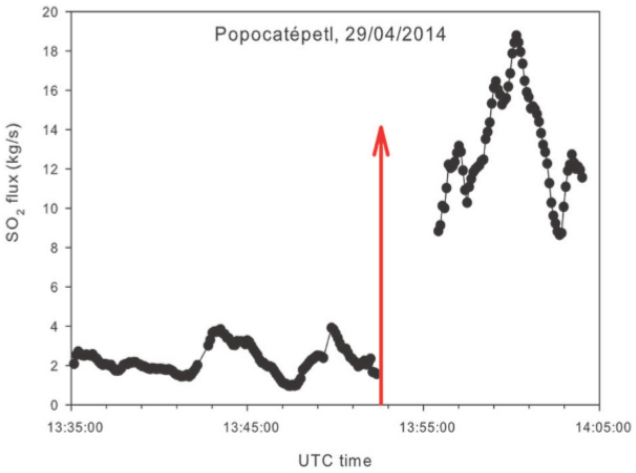

Figure 2.2 Explosion Type 2 – low passive degassing, with an explosion and large amounts of ash, levels of SO_2 return to normal (Campion et al., 2018).[21]

There are two types of explosive activity resulting in ash emissions at Popocatépetl. Firstly, where there is a peak in the SO_2 emissions, followed by a small explosion with ash reaching a few km a.s.l. and SO_2 levels returning to normal (Fig. 2.1).[21,22] The second type has a low SO_2 passive degassing level, followed by an explosion, producing large amounts of ejecta and ash >10 km a.s.l., after which the SO_2 level returns to a normal passive degassing level (Fig. 2.2).[21,22]

2.3.2 Santiaguito

The 1902 Plinian eruption of Santa Maria volcano, Guatemala, produced a crater that, since 1922, has been the site of ongoing eruptive activity at the Santiaguito lava dome complex. Santiaguito comprises four overlapping domes, contributing to a total dome size of 1.1 km^3.[23] The currently active vent at Santiaguito is El Caliente, which is an open cone with a crater 200 m in diameter.[23,24,25,26]

Using tiltmeters placed around the El Caliente vent, as well as seismic and infrasound measurements, Johnson et al. (2014) showed that the lava in the vent undergoes inflation and deflation associated with degassing and explosions.[24] Their data shows that the vent either rapidly inflates resulting in an explosion, or it quietly deflates.[24] There is thought to be a fairly steady gas supply, with elevated degassing every 26-30 minutes.[24] Gas accumulation is thought to cause the tilting as the degassing lags the inflation, with the peak gas flux occurring during the deflation.[24] In addition, due to the absence of seismicity during inflation, and no lava when it deflates, the cycles are thought to be

driven by gas with the edifice becoming temporarily impermeable.[24] Similar cycles have been observed at other volcanoes, such as Stromboli [27] and Semeru [28], however these were solely explosive and non-periodic; therefore not as useful a comparison as Soufrière Hills, which has a similar sinusoidal shape to its tilt, but does have accompanying seismic swarms during inflation, which Santiaguito lacks.[24]

2.3.3 Soufrière Hills Volcano

The Soufrière Hills Volcano (SHV) on Montserrat, in the Lesser Antilles island arc, is a Pelean lava dome complex, which most recently erupted from 1995-2010.[29] SHV has been widely studied for the cyclicity present in its seismicity, ground deformation, SO_2 and lava extrusion.[29,30,31,32] Cyclicity has been noted at four different time scales, multi-hour, multi-day, multi-year and multi-decadal.[29,33,34,35]

The multi-week cycle is approximately 50 days, with several studies showing a range of 35-49 days.[33,34,36] The shorter cycles (multi-hour and multi-day) are overprinted by a gradual deflation, present in the tilt and seismic data from 1997.[34] They are characterised by a quick onset of tilt and seismicity, with a dome collapse or Vulcanian explosion within a few days of a new cycle.[34,37] The shorter cycles have initially high extrusion rates, and additionally often a change in direction of the lava flow.[34,35] Multi-week cycles have also been observed in SO_2 data, where Nicholson et al. (2013) used Fourier Transforms on UV-DOAS SO_2 data to identify a ~50 day cycle, and a 10-14 day cycle.[30] This work was supported by the findings of Flower and Carn (2015) who used OMI SO_2 data and found a ~54 day cycle, as well as two shorter cycles of 8 and 12 days.[32]

The multi-year cycle is between 1.5 and 3 years, identified in two different data streams.[29,30] This behaviour represents phases of more extrusive behaviour interspersed with pauses.[29] The average length of an extrusive phase was 1.7 years and the average repose length was 1.4 years.[29] This behaviour is controlled by deeper processes in the magma chamber, as opposed to the shallower controls on the shorter cycles.[29,37] Nicholson et al. (2013) identified a 2-3 year cycle in SO_2 data, but this cycle may be independent of the extrusive phases as the two data streams do not correlate.[30,31]

Table 2.1 Volcano SO_2 cycles

Volcano	Cycle Length	Method and Characteristics	Source
Popocatépetl	"Puffing" ~3-7 minutes	UV cameras used to measure the SO_2 flux; Fourier Transform analysis to results, identified a peak at 200-400 s, corresponding to an oscillating behaviour in the degassing	Campion et al. (2018)
Santiaguito	26 min	SO_2 UV imagers in 2008-9 used to observe gas fluctuations, explosions and non-explosive elevated degassing. Divergent movement on the rim of crater.	Johnson et al. (2014)
Soufrière Hills Volcano, SHV	8 hour cycle – vent clearing 8-14 day cycle 30-50 day – dyke clearing	SO_2, tilt and seismicity data identify a cycle length of 30-50 days. Characterised by a sudden onset of tilt and seismicity and high extrusion rates, followed by a dome collapse or Vulcanian explosion within a few days.	Sparks and Young, (2002); Nicholson et al. (2013); Flower and Carn (2015); Costa et al. (2013).
Soufrière Hills Volcano, SHV	1.4-3 years	UV-DOAS SO_2 shows 2-3 year cycle that is likely independent from the 1.4/1.7 year cycle shown in extrusive phases, linked to a deep magma source.	Nicholson et al. (2013); Wadge et al. (2014)

2.4 Data Acquisition

The OMI instrument was launched on 15th July 2004 on board the Aura satellite.[38] OMI has a spatial resolution at nadir of 13 x 24 km in the UV (ultraviolet) band used for SO_2 retrievals, increasing to 28 x 160 km at the far swath edge. It orbits 14-15 times per day, with two passes over Bagana. However, only the day-time pass is used for SO_2 retrievals because the sensor relies on UV radiation to detect SO_2. The sensor and algorithm employed by OMI can detect SO_2 two orders of magnitude smaller than its forerunner,

the Total Ozone Mapping Spectrometer (TOMS), making it a better choice for detecting volcanic plumes and passive degassing.[38] The morning pass (ascending node) of OMI has been used for each 24 hour period, this occurs at around 14:00 local time (03:00 UTC).

Two files for each scene are needed, both are in the HDF-EOS5 format, and can be downloaded from the Goddard Earth Sciences Data and Information Services Center.[39] One file contains the SO_2 value for each pixel and has orbit metadata, such as the solar zenith angle and the radiative cloud fraction. This file is known as OMSO2, and is processed using a Principal Component Analysis (PCA) algorithm (or an extension of) which decreases the noise present on SO_2 retrievals.[40] They are taken in global mode in UV on the sunlit part of the orbit, and comprise 1600 lines of 60 pixels each, with each first pixel belonging to a column, which is called a row.[38]

The thickness of SO_2 is provided in Dobson Units (DU, 0.01 mm at standard temperature and pressure) for four different heights in the atmosphere, each with a Centre of Mass Altitude (CMA).[38] For the Planetary Boundary Layer (PBL), the CMA is 0.9 km, which is the layer used in this study. Ordinarily volcanic degassing SO_2 retrievals are recommended from the Lower Tropospheric Layer (TRL), and this has a CMA of 2.5 km.[38] However, this is higher than the summit of Bagana, which stands at ~1900 m (above sea level). Therefore, the PBL was considered to be a better fit, using a local Air Mass Factor (AMF) correction and assuming the height of the plumes to be around 1.5 km, as this is the nearest height to the summit available and corresponds with the reported plume heights.[2]

The accompanying file for each scene contains the areas for each pixel, which vary from ~300 km^2 at nadir, to more than ten times this at the edge of the swath.[41] The files are called OMPIXCOR, and are generated alongside each orbit file, so they are specific to each orbit. They contain area values for two different tiling methods; 'FoV75', which corresponds to overlapping pixel areas, and Tiled, which are neatly stacked pixels mainly used for plotting results.[41] For this method, the 'FoV75' areas were used as recommended in the OMPIXCOR guidelines.[41] This results in an overestimation of the total mass loading, due to overlapping areas above and below each pixel being counted twice.

On some days (about once per month) there is no file for the area of interest. This is due to the "zoom-in" mode of OMI; thus no total can be retrieved for this day. On other days

(about twice per month) the edge of the swath cuts the area of interest into two. For these days, the two files are downloaded and then the totals are added together. Though, when the edges of the two swaths are removed for improved data quality, the resulting value is often zero kt.

2.5 Sources of Uncertainty

The quality of data retrievals for OMI is reduced by a number of external and internal factors that produce noise in the data. Some of these can be corrected for, but some of them are endemic in the data.

2.5.1 Cloud Cover

Sources of noise for SO_2 retrievals include extensive cloud cover and other aerosols altering retrievals. The time of the overpass of OMI over Bagana is at ~14:00 local time. The sea surrounding Bagana is in the southwest Pacific "warm pool" with some of the highest sea surface temperatures on Earth.[42] This produces very high levels of convective cloud. A value of <0.3 for Radiative Cloud Fraction (RCF) within the OMI data files is used as a measure of whether a pixel is cloud-free, with smaller values being favourable for SO_2 retrievals.

OMI calculates the RCF by multiplying the effective cloud fraction and the assumed cloud radiance, divided by the measured radiance.[43] The cloud data for Level 2 products is facilitated by the OMCLDO2 algorithm and product, which uses the O_2-O_2 absorption band around 477 nm and a Differential Optical Absorption Spectroscopy (DOAS) type fit.[44] The result is that a thin cloud that might cover all of a pixel will have a low effective cloud fraction, so care should be taken when drawing comparisons between an effective or geometric cloud fraction.[44] The value can only be a rounded decimal of 0.1, 0.2 and so on, up to 1.0.

Cloud fraction and visible band images from MODIS-Aqua for January 2016 were examined to determine if cloud might be obscuring signals on some days. The Cloud Fraction here is the ratio of the number of cloudy pixels to the total number of pixels in a given area, and is an instantaneous value.[45] One would expect that cloud would be

present mostly during the afternoon, given the region that Bagana is in, and this can be confirmed by the MODIS-Aqua observations to be most often the case.

To confirm that the RCF totals recorded by OMI were valid, some scenes were compared with visual MODIS-Aqua images of the area at the same time, and Cloud Fraction Aqua-MODIS images. This provides an independent measure of cloud cover in the sky above Bagana. It could be seen that the RCF measurements do well to single out the pixels that are best to use for an SO_2 measurement, based on where there is agreement with other sources of cloud cover. Therefore they can be used as a non-subjective solution to removing spurious data from the files when calculating the mass loading totals.

2.5.2 Solar Zenith Angle

Solar Zenith Angle (SZA) is a factor that normally needs to be taken into account when calculating SO_2 mass loading totals, with less than 70° SZA providing the best quality data. However, as Bagana is situated very close to the equator, this is not an issue.

2.5.3 OMI Row Anomaly and Fill Values

Since 25th June 2007, the OMI Row Anomaly has affected Level 1B radiance data, resulting in unusable data for those affected rows.[38] Any anomalous or missing values that are given "fill values" for a pixel must also be disregarded when performing calculations or they will greatly skew the results. The OMI Row Anomaly (ORA) is handled by highlighting affected rows and putting large negative fill values, which can then be used to omit them. The OMI handbook does state that data from all rows can be used when studying volcanic OMI data, omitting those affected by the row anomaly, but additionally omitting the swath edges results in better data quality, as the areas of these pixels are very large.[38]

2.5.4 Processing Noise

The algorithm used on the data, when it is processed to a Level 2 product, is a revised version of the PCA algorithm from Li et al. (2013), called OMSO2VOLCANO.[40,46] This processing leads to a noise on retrievals of around 0.5 DU, and so this can be set as a threshold on retrievals so that only values for SO_2 above 0.5 DU are used.

2.5.5 Air Mass Factor and Centre of Mass Altitude

Having a suitable Centre of Mass Altitude (CMA) will affect retrievals. Using the Lower Troposphere (TRL) data, which is recommended as the default for degassing volcanoes, would result in a decrease of 65% in the mass loading figure, creating an underestimate if used for Bagana.[2,38] Thus, the Planetary Boundary Layer (PBL) data is used, which has a CMA of 0.9 km. The PBL could lead to an overestimation due to the height discrepancy between the assumed altitude and the actual altitude of the plume. Additionally, there is a higher risk of local contamination of pixels due to other SO_2 sources such as pollution, compared to the TRL data.

To convert corrected slant columns to SO_2 vertical columns densities, an Air Mass Factor (AMF) is applied, which was used in the original Band Residual Difference (BRD) algorithm.[47] However, with the improved PCA algorithm, SO_2 Jacobians are instead used to allow for comparison of both the BRD and PCA algorithms. The SO_2 Jacobians are representing the sensitivity of radiances to the SO_2 column, used like a weighting factor they are a look-up table covering different measurement conditions. These can be thought of as having a constant effective AMF of 0.36.[47] This is assuming a cloud and aerosol-free sky, slant column ozone of 1000 DU, 5% surface albedo and 1 DU of SO_2. The AMF is also dependent on variables such as viewing geometry.[48] Additionally, retrievals can be improved by applying a local AMF value, stored in a look-up table (0.547 for Bagana).[2,47] Putting this value into Equation 2.1 below gives SO_2 values corrected for the viewing geometry and atmospheric ozone.[48]

$$SO_2(corrected) = \frac{0.36}{AMF} SO_2(operational)$$

Equation 2.1

By applying this to the PBL layer, the local AMF brings the altitude of the plume to above 1 km.[2,38] This is suitable at Bagana, as often the plume does not reach much above the summit, at 1900 m a.s.l., unlike the TRL layer data.

2.5.6 Region of Interest Coordinates

The use of one set of region-of-interest coordinates most likely will have little impact on the retrieval totals, as they include most instances of SO_2. However, for those scenes

where there is an obvious plume outside the coordinates of the box as seen on OMI files of the entire area, the area of study is extended to encompass the wider plume. In total, 30 out of 1090 instances in the entire time-series (2016-2019) needed the area of interest extended.

2.6 Method

The technique for retrieving SO_2 mass loadings is modified from methods used in McCormick Kilbride et al. (2019).[2] The McCormick Kilbride et al. (2019) method involves qualitative steps to deduce cloud cover, which posed issues for reproducibility in this study.[2] Thus RCF was used to screen out invalid pixels in this study's method to reduce subjectivity in cloud classification (see section 2.5.1). To allow comparisons with the conclusions of Bagana's activity between this study and McCormick Kilbride et al. (2019), the two sets of SO_2 results are contrasted against one another in Section 2.6.3.[2]

The Ozone Mapping and Profiler Suite (OMPS) was not considered as an alternative source of SO_2 data for this study, due to the poorer resolution offered compared to OMI. It would not have been easy to draw comparisons between the OMPS totals and the OMI totals, due to the different pixel sizes and viewing geometry and timing. Further still, this would have posed issues comparing with the McCormick Kilbride et al. (2019) study.[2]

2.6.1 Method Outline

The method of retrieval takes into account all SO_2 mass loading values retrieved from available OMI files, regardless of the cloud cover on the day, and relies on the inbuilt cloud cover (RCF) filtering of pixels to get rid of anomalous values, implemented via a commented Python script (Appendix A).

For days which have values of 0.00 kt as their calculated total, the cloud cover for each of those days has been classified into four categories (Minimal cloud, Partial Cloud, Mostly Cloud, Total Cloud) manually (see Appendix B). If it is "minimal" (0-15% cover) then the scene is deemed to be a "true" 0.00 kt value, representing a day of no gas plume activity. If the cloud cover percentage is higher (i.e. categories of Partial Cloud, Mostly Cloud, Total Cloud), then the "null" values are deemed to be a result of the cloud cover, and are filled

by an average of the two previous and two subsequent values retrieved akin to McCormick Kilbride et al. (2019).[2] This is an improvement on the method from McCormick Kilbride et al. (2019), as they treat all null values as false and fill the nulls with an average.[2] The times when they have many consecutive null values (a series of ten values, which happens ten times in their dataset) they treat them as true null values to minimise error. This approach led to a 56% increase in mass loading totals reported.

The different parameters used to calculate mass loading totals for this study are:

- Masked edges: Rows 0:3, Rows 54:59
- OMI Row Anomalies blocked: Rows 27:45, Rows 53:54
- Radiative cloud fraction of <0.3
- Local AMF correction of 0.547 using Equation 2.1
- Noise threshold of 0.5 DU
- Solar Zenith angle <70°
- Ascending node data (day-time)
- Longitude: 153.8 to 156.3, Latitude: -7.4 to -4.7, extended when larger plumes occur.

2.6.2 Uncertainties

The method introduces the potential for over- and under-estimation of the monthly mass loading. Uncertainties occur when cloud cover is thick over an entire month, as was the case for June 2016, where cloud cover was either Mostly or Total cloud, resulting in no values. Therefore, the data before July 2016 has been disregarded.

Each value for a scene is assumed to be a minimum value as, given the time of acquisition being mid-afternoon and peak time for cloud and rain formation, the SO_2 present has probably undergone deposition of mass, and so the actual mass could have been higher.

The typical lifetime of the plume, given the region, is about 22.5 hours.[2] The scenes are also a “snapshot” so the plume may be, theoretically, up to 24 hours old when detected. This could therefore result in an underestimation of the amount released.

Overestimation could occur when values are substituted on days where there is no data available and an average has been used to fill the gap. If the average is higher than the true figure, then more SO_2 will have been recorded for the day than is accurate.

2.6.3 Comparison of OMI SO_2 data with McCormick Kilbride et al. (2019)

The SO_2 mass loading totals for Bagana for the time period 1st July 2016 - 30th September 2017 obtained in this study are compared with those from McCormick Kilbride et al. (2019).[2] This is to check the reproducibility of the data, as both methods require qualitative steps; namely, assessing cloud cover, and extending the bounding box for results when larger plumes are present. The two time-series alongside each other allows for us to see the longer-term behaviour of Bagana. The data for the comparison were gained via email correspondence from B. McCormick Kilbride.[49]

2.6.3.1 Daily

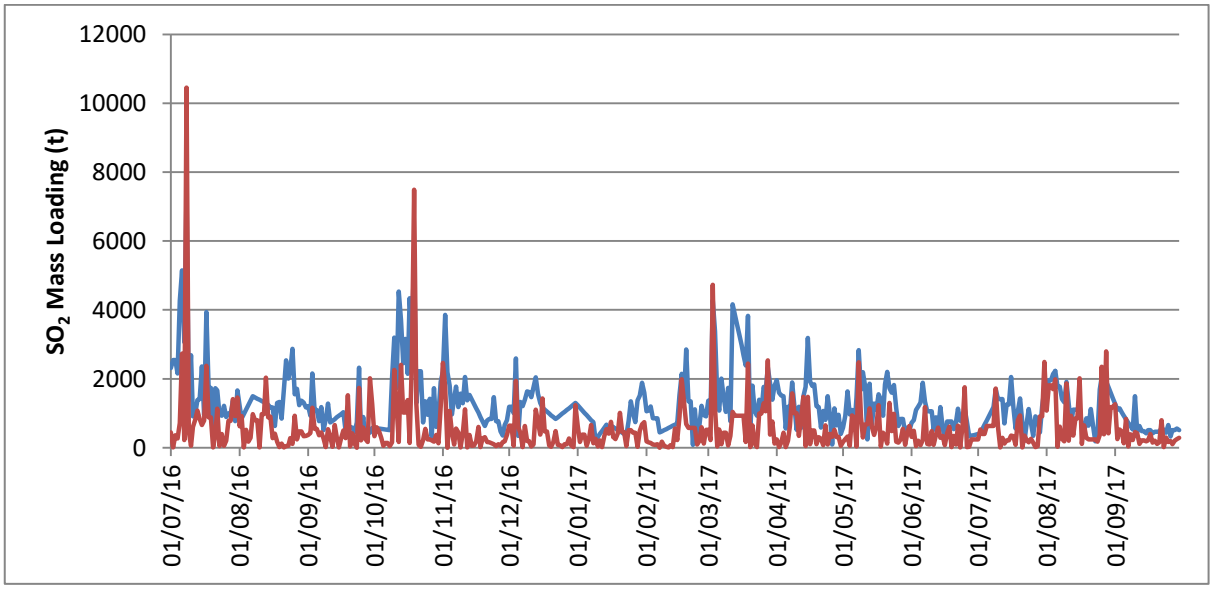

Figure 2.3 The daily OMI SO_2 mass loadings comparing McCormick Kilbride et al. (2019) in blue with this study (Couchman-Crook, 2020) in red.[2,49]

A comparison of the daily totals (Fig. 2.3), reveals that many of the daily peaks (e.g. early July 2016, mid-October 2016) are higher in the values from this study (red line) than McCormick Kilbride et al. (2019).[2,49] However, in general, the overall baseline level of SO_2 recorded at Bagana is lower in this study than McCormick Kilbride et al. (2019).[2,49]

2.6.3.2 Monthly

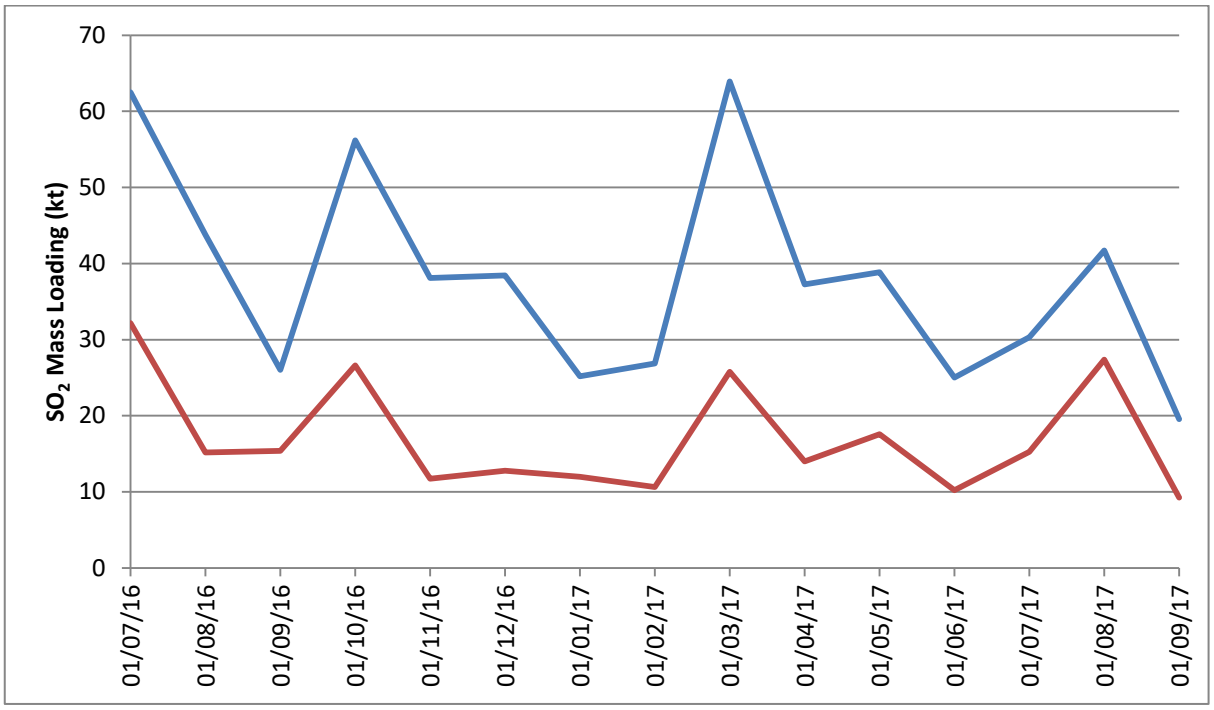

Figure 2.4 The monthly OMI SO_2 mass loadings comparing McCormick Kilbride et al. (2019) in blue with this study (Couchman-Crook, 2020) in red. [2,49]

A comparison of the monthly SO_2 totals (Fig. 2.4) shows that the monthly totals recorded by this study (in red) are lower than those of McCormick Kilbride et al. (2019).[2,49] The peaks and troughs of the monthly totals, however, match very well across the two datasets, showing that the trends are likely to be true, although, the magnitude of those peaks and troughs is under question. This study provides a more conservative estimate of the monthly totals at Bagana than McCormick Kilbride et al. (2019), by a factor of two.[2,49]

2.6.3.3 Discussion

McCormick Kilbride et al. (2019) present a method that has been replicated by this study, with true peaks and trough trends shown in the data.[2,49] However, the magnitude of the peaks differs by a factor of two between the values in McCormick Kilbride et al. (2019) and this study, which has lower totals.[2,49] This shows that this study has more conservative estimates, which might draw into question the assumption that Bagana has the third-highest SO_2 degassing total globally. Notably, in McCormick Kilbride et al. (2019), the comparison of their annual totals with those of Carn et al. (2017), found that Carn et al. (2017) SO_2 mass loading totals were 40-100% higher.[2,50] They did notice that

there were “relatively similar trends”, though arguably there is a much stronger matching of trends between McCormick Kilbride et al. (2019) and this study.[2]

The difference in values from this study may come from the size of the bounding box used over Bagana, over which the mass loading total was calculated. In cases of larger plumes in both studies the bounding box was expanded. The choice of the bounding box and where the plume ends is subjective in both methods, therefore there will be variation in results.

The code used to extract the totals was also different. The one for this study was written in Python, but many studies, McCormick Kilbride et al. (2019) included, use a programme written in the programming language IDL to extract the values.[2,51]

In the description of cloud cover, there was also subjectivity in the selection of cloud-free scenes. The McCormick Kilbride et al. (2019) method used cloud-free scenes assessed subjectively for calculating SO_2 totals with minimum error, and then filled all null values with averages from these values.[2] There was no nuance to denote cloud-free days that had true values of no SO_2 released at the time of that acquisition. The method used in this study is more reliant on the RCF value featured in the data files taking out affected pixels. The subjectivity in this study comes on days where there is a null value for the SO_2 mass loading, and establishing the cloud cover on that day, and therefore the implications for calculating a total or leaving a value of 0.0 kt (see Section 2.6.1). However, this would only seek to give a greater truth to the values seen, rather than a blanket approach for all null values used in McCormick Kilbride et al. (2019), which led to an increase of 56% in reported totals.[2]

In conclusion, caution should be taken with trying to draw direct comparisons between absolute values obtained from each study, and with combining them to extend the data series. However, the observed trends in SO_2 emission through time are comparable between studies, and therefore can be used to investigate cyclicity at Bagana.

2.7 Fast Fourier Transform of SO_2 Time-Series

In order to identify the cycles present in the time-series data, a data analysis needs to be carried out. There are many methods that can be utilised to do this, but by far the most widely used across disciplines and best understood is the Fourier Transform.

2.7.1 Introduction

A Fourier Transform provides a way to move representation of data from the time domain into the frequency domain (for a detailed summary, see R. Crockett (2019)).[52] The general properties of the Fourier Transform (FT) related to time-series analysis are symmetry and linearity.

The Fast Fourier Transform (FFT) function within the statistical programme R uses a non-normalised Discrete Fourier Transform (DFT), which takes the main features of symmetry and linearity from the Fourier Series and Transform. However, the major difference is the sampling interval, which will have a limiting effect on the resolution achievable by a DFT. The maximum resolvable frequency is lower for odd datasets than even, and this is the Nyquist frequency, equal to half the sampling frequency. Other constraints on an FFT include: the lowest non-zero frequency resolvable is 1/T; data-padding/truncating is sometimes required to move the data so that an intermediate frequency becomes a harmonic of the converted time-series; issues with missing data within a time-series, which should be omitted by cutting short the time-series, or filled with a replacement value or estimate.

2.7.2 Applying the FFT to the SO_2 Time-Series

The programming language of choice was R, as it is most suited to statistical computing, and there was more guidance available related to geoscience time-series analysis, than in other comparable languages, such as Matlab and Python.

The method to apply the FFT in R was adapted from examples in the book “A Primer on Fourier Analysis for the Geosciences” by R. Crockett (2019).[52] This uses the inbuilt function of *‘fft()’* in R, to apply a non-normalised DFT to the dataset. From this, power spectrums and spectrograms can be produced to analyse cycles in the data.

An FFT was used to look for cycles in the daily SO_2 data, using OMI data from 1st July 2016 – 25th June 2019. There is a multi-week gap in the data from June 2016 as a result of issues with the instrument; therefore, the data timeline starts from July 2016, despite being collected since January 2016. Additionally, in June 2019, an overprinting of any SO_2 signature from Bagana was caused by a large nearby volcanic eruption that dominated signals for several days, therefore the time-series has been stopped prior to this. Unfortunately this reduces the timescale over which one can detect longer cycles, as the dataset covers just three years.

An anomalously large peak mass loading (from Bagana) on 29th March 2018 caused an overshadowing of more delicate cycles present in the data. The decision was made to remove this to allow easier interpretation of the remaining frequencies identified when carrying out the FFT analysis, it has been left in for the other analyses in this study.

2.8 Results

The full time-series (Fig. 2.5) 1st July 2016 - 25th June 2019, shows the daily mass loading totals of SO_2 from Bagana, spanning three years. Clear peaks can be seen at intervals throughout the time-series (e.g. ~10 days), with some waxing-waning visible around some peaks (e.g. ~80-130 days). Also notable is the lower baseline of SO_2 from ~910-1090 days, where there is an absence of peaks.

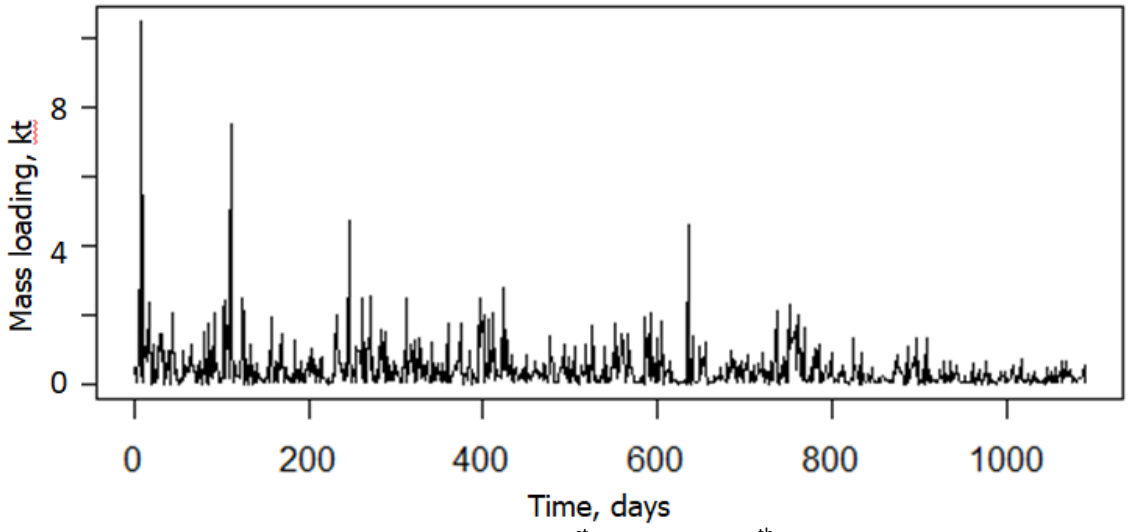

Figure 2.5 The SO_2 mass loading time-series from 1st July 2016 - 25th June 2019, shown on a daily timescale.

Fig. 2.6 shows an FFT spectrogram with output results from 1st July 2016 - 25th June 2019. High-amplitude bars (darkest grey) near to frequency 0.01, and at frequency ~0.065 reveal cycles every approximately 100 and 15-16 days, respectively (shown in more detail in Fig. 2.7). Less prominent dark grey bars are observed at frequency 0.44 and 0.08 which continue for a greater extent, and correspond to a cyclicity of every 2-3 and 12-13 days, respectively.

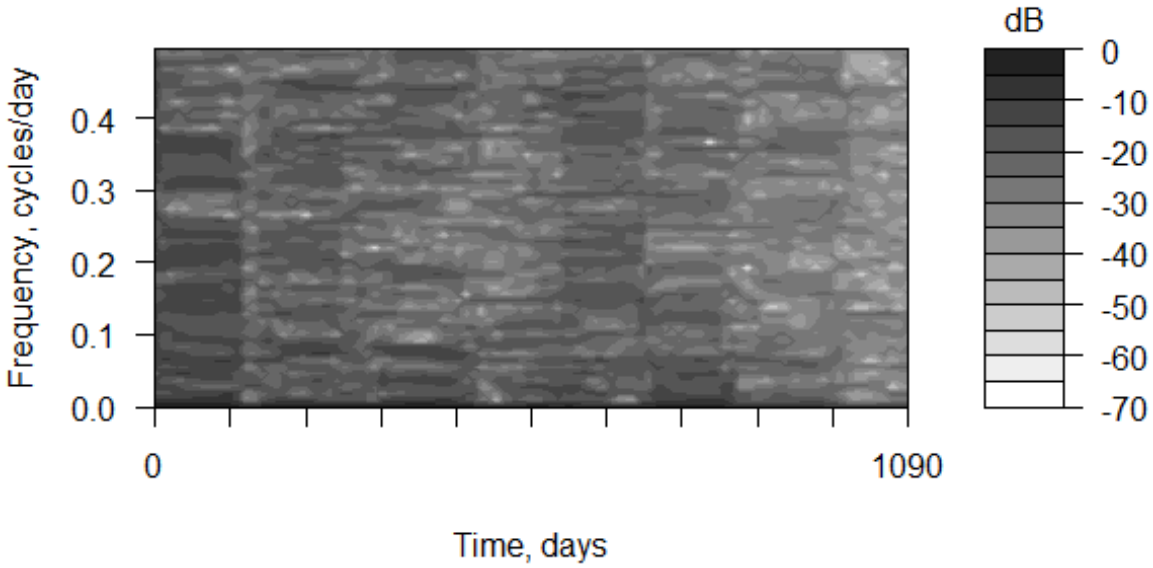

Figure. 2.6 Spectrogram of SO_2 mass loadings from 1st July 2016 - 25th June 2019, focussing on the 0.0 to 0.5 frequency range. The graphic was produced with the 'Simplespectro' programme in R (Crockett, 2019).[52] Each window is 109 days on the time axis, and the default step length 10.9 days.

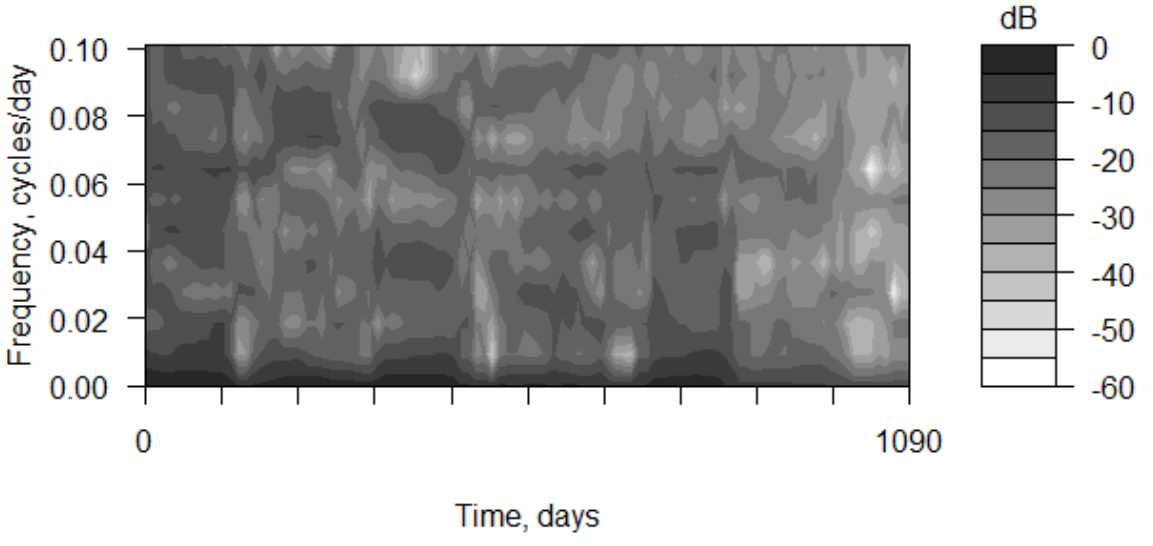

Figure. 2.7 Spectrogram of SO_2 mass loadings from 1st July 2016 - 25th June 2019, focussing on the 0.0 to 0.1 frequency range. Each window is 109 days on the time axis, and the default step length 10.9 days.

By increasing the window of the FFT to 400 days, an increase resolution in the frequency domain is gained by sacrificing resolution in the time domain. This results in the spectrogram in Fig. 2.8. This shows the extended dark grey bar across the first part spectrogram centred on the frequency of 0.08 (12.5 days), showing this cycle dies out with time. Also, the large dark grey signal at the bottom is separated out, to show a dark grey signal centred around 0.01 (100 days). The signal for ~0.065 (~15-16 days) is prominent further along in the time-series. All these cycles fade at the end of the time-series, agreeing with a reduction of activity in general from the OMI SO_2 mass loadings in Fig. 2.5.

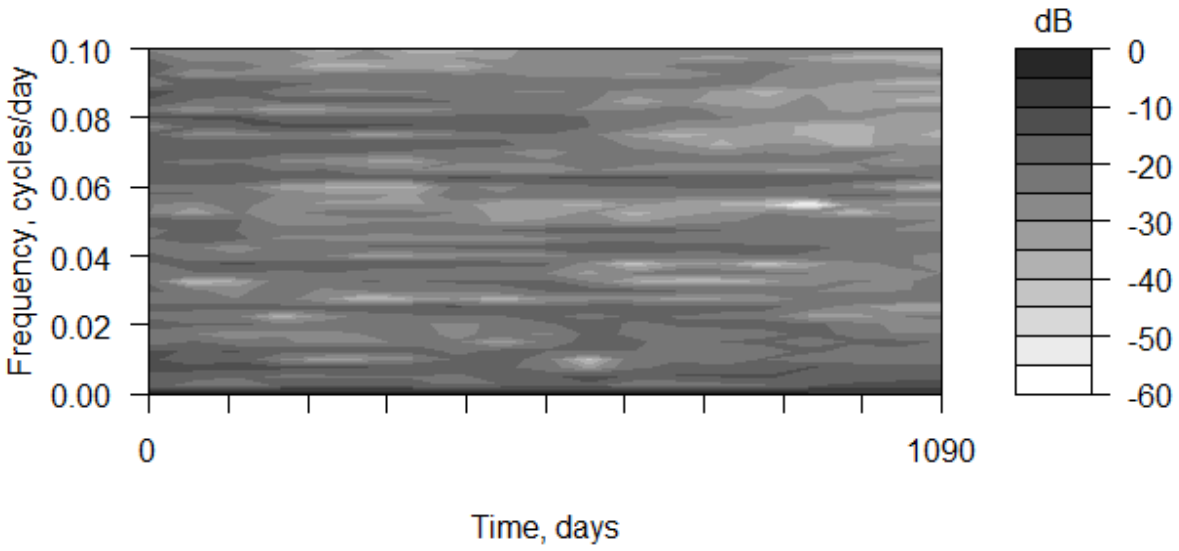

Figure. 2.8 A spectrogram of SO_2 mass loadings from 1st July 2016 - 25th June 2019, focussing on the 0 to 0.1 cycles per day range, with an FFT window of 400 days. Showing darkest grey signals centred on 0.08 (12 days) and 0.01 (100 days) at the earlier part of the time-series. Further along in time there is a dark grey bar at ~0.065 (15-16 days).

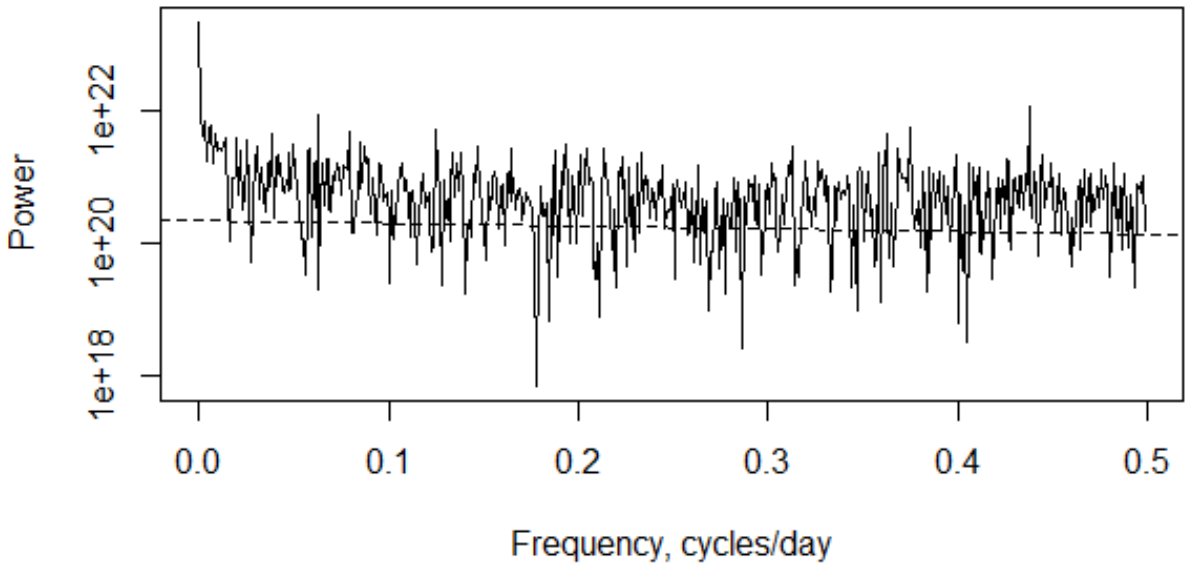

Figure. 2.9 The Power Spectrum of the SO_2 Mass Loadings time-series. The power law is given with a dashed line.

The power spectrum (Fig. 2.9) of the SO_2 data is characteristic of a noisy time-series, with the frequency peaks of interest hidden with surrounding “noise”.

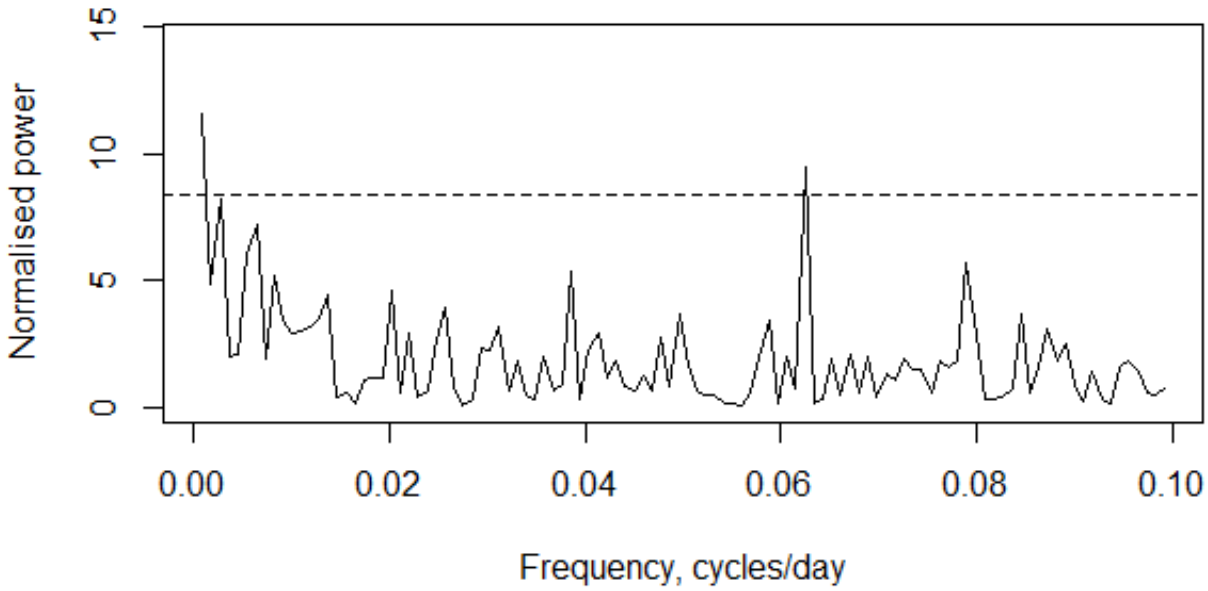

Figure 2.10 A Lomb periodogram of the SO_2 time-series, with 95% confidence interval (CI). The peaks that cross the CI are at ~0.003 (333 days) and ~0.062 (16 days).

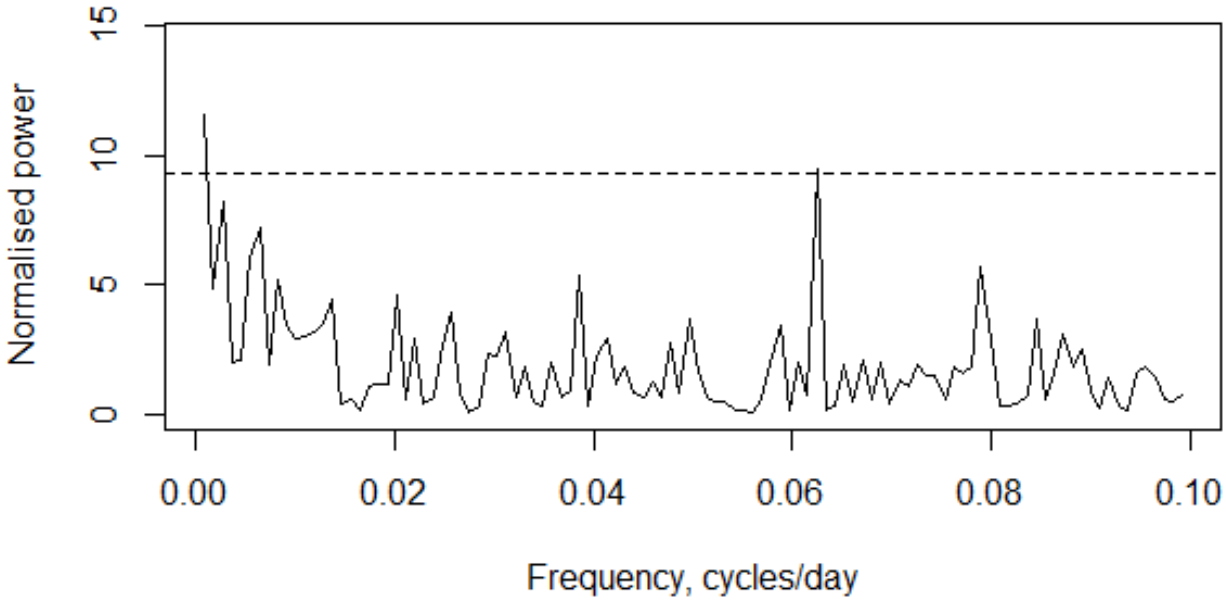

Figure 2.11 The Lomb periodogram, showing the 98% confidence interval (CI) for the frequency range of 0 to 0.1. The significant peak is at ~0.062 cycles per day (~16 days).

The Lomb periodogram looks to assess the confidence in frequencies in the dataset. Focussing on the longer frequency cycles (0.0-0.1), the peaks that cross the 95% confidence interval line (apart from that at 0) are peaks at 0.003 (333 days) and 0.062 (~16 days) (Fig. 2.10). The 333-day cycle is drawn into question due to the length of the time-series as a whole being just 3 years, in these conditions, the Lomb periodogram tends to exaggerate the power of the extremes of the data. The most significant peak in the dataset looks to be at 0.062, which crosses the 98% confidence interval dashed line (Fig. 2.11).

In summary, the cycles shown by the spectrograms and Lomb periodogram suggest 2-3 days, 12-13 days, 15-16 days, 100 days and 333 days as potential cycles of interest at Bagana.

2.9 Discussion

2.9.1 SO_2 Evidence for Cyclicity at Bagana from 2016-2019

2.9.1.1 Linear Time-Series Features

The daily mass loading totals of SO_2 from Bagana for the full time-series reveals that there are a larger number of peaks with higher magnitude in the first part of the time-series than the end (Fig. 2.5), showing the overall SO_2 signal decreases through time. There are families of peaks (e.g. ~100-250 days) present in the data, which show periods of heightened degassing activity. There is also a low baseline signal from 910-1090 days, which indicates a time of quiescence in the degassing. There may be evidence of waning signals (e.g. ~80-130 days), which show a steady decrease in activity, after an initial peak.

2.9.1.2 Spectrogram Features

Spectrograms are interpreted by the colour-bar showing the relative strength of different frequencies through time in the given dataset. Darker grey colours (values 0 to -10 dB) denote more significant cycles than light –grey or white colours (-50 to -60 dB).

The colour-scale of the spectrogram (Fig. 2.6) suggests that cycles at lower frequencies are more prominent, given the dark grey focussed at the base of the spectrogram. This would fit with suggested analogues for natural geophysical time-series of this nature being like a red-noise model. White noise has a power spectrum profile that consists of evenly spread dips and troughs throughout all frequencies. Red noise has a power spectrum profile where the peaks are weighted towards the lower frequencies. This means longer period cycles are more prominent and significant in the time-series. This is demonstrated on Fig. 2.9, as the dashed line of the power law trends downwards at higher frequencies.

Through time it is also apparent that all the observed frequency cycles with strong power drop off, as shown by the light grey/white colouring on the right-hand side of the spectrogram (Figs. 2.6, 2.7 and 2.8), consistent with the linear time-series data (Fig. 2.5).

The key cycles indicated by the spectrogram are at ~0.44 (2-3 days), ~0.08 (12 days), ~0.062 (16 days), and ~0.01 cycles per day (100 days) as these last for an extended period across the spectrogram, but do reduce in time.

2.9.1.3 Lomb Periodogram Features

The Lomb periodogram confirms the ~0.062 (~16 days) and the ~0.003 (333 days) cycles per day as the most significant, with the certainty being higher for ~0.062 (98%). The 333 day cycle has a few opportunities to present in the dataset, making it harder to ascertain this cycle's significance. The 16-day cycle has the potential to be a systematic one, due to the revisit time of the same ground-track of the satellite being 16 days. However, due to the certainty being higher for the 16-day cycle, it is likely to be non-systematic.

2.9.2 Bagana in the Context of SO_2 Cycles of Other Andesitic Volcanoes

The shorter cyclicity seen at other analogous volcanoes (Table 2.1), namely the 26 minute cycle at Santiaguito and 3-7 minute "puffing" at Popocatépetl, are not comparable with the cycles identified in this study. This is not to say they are not present at Bagana, but with a sampling interval of 1 day, it is unlikely that they would be picked up at that sampling resolution due to the Nyquist frequency (half the sampling rate).

Similarly, the 1.4-3 year cycle observed at SHV is on a scale too long for the 3 year dataset that is presented in this study to be comparable (Table 2.1). Therefore, longer period cycles such at this, if they were present at Bagana, would need a dataset spanning decades.

The 8-14 day cycle from SHV is the most similar to the most significant cycle identified at Bagana (16 days). This shorter cycle at SHV is governed by shallow processes within the conduit and shallower magma storage, compared to the longer cycles governed by deeper processes. Therefore, the 16 day cycle at Bagana may indicate that the source of the cyclicity comes from a process within a shallow storage system (e.g. a dyke).

The 30-50 day cycle identified at SHV may be analogous to the 100 day cycle identified at Bagana, though it was a less significant one than the 16 day cycle. This 100 day cycle could indicate a longer-period cyclicity caused by a deeper process governing the degassing, such as deeper magma storage variations. This supports discussion in Wadge et al. (2012), in which is explored how the multi-week cycle seen at SHV would translate to a dyke storage mechanism at Bagana, in relation to pulsatory lava flow behaviour observed on an average cycle of 105 days (4 pulses over 14 months).[1]

The quiescence observed between 910-1090 days could indicate that there is a "choking" in the SO_2 flow restricting the amount of gas being released, which may be related to the formation of a new dome within the last year of the dataset. However, it may instead be the case that the process producing the large amounts of SO_2 previously, such as magma upwelling into a shallow storage system, has waned, resulting in less degassing overall.

2.10 Conclusion

From the data analysis conducted on the SO_2 data, cyclicity can be observed at a periodicity of ~2-3 days, ~12-13 days, ~16 days, ~100 days and ~333 days. The most significant cycle with 98% confidence is a 16 day cycle. A clear reduction in SO_2 activity is also notable at the end of time-series, thought to show a period of quiescence at Bagana and a potential choking of the conduit, or a waning of magma supply.

When compared to the gas-based cycles at the other volcanoes in similar settings, the significant 16 day cycle fills an intermediate time-period, perhaps most similar to SHV's 8-14 day cycle, governed by shallow processes. Additionally, the less-significant 100 day cycle could be similar in process to the 30-50 day cycle observed at SHV, with support from the 105 day lava flow cycle identified in Wadge et al. (2012).[1]

Chapter Three – Thermal Cyclicity at Bagana - Is Cyclicity Seen in the Thermal Data at Bagana?

3.1 Introduction

The aims of this question are to identify any cycles found in the thermal data and suggest mechanisms for them. To this end, MIROVA thermal data (Middle Infra-Red Observation of Volcanic Activity) has been acquired for Bagana to coincide with the dataset acquired for SO_2 emissions. This chapter presents the results of a time-series analysis on the thermal data, using R and Fast Fourier Transform (FFT) methods to identify any cycles, as observed in the SO_2 data. Equivalent cycles at other andesitic volcanoes in similar settings will be examined in order to better understand in the interpretation of the thermal data for Bagana Volcano.

3.2 Objectives

The aims will be achieved through the following objectives:

- To gather the thermal data from Middle Infra-Red Observation of Volcanic Activity (MIROVA) for the time period July 2016 - June 2019.

- To conduct a literature review examining equivalent cycles at other andesitic volcanoes in similar settings.

- To conduct a time-series analysis on the thermal data, using R and Fast Fourier Transform (FFT) methods, and present the results and interpretation of any cycles identified.

3.3 A Review of Thermal Event Cyclicity Shown by the Presence of Dome Growth and Lava Flows at Andesitic Volcanoes

This section provides a literature review of potentially analogous andesitic arc volcanoes which show thermal cyclicity through lava extrusions and dome growth activity. As thermal signatures are taken for proxies of these events at Bagana, this literature review

uses both to identify thermal cycles at the analogous andesitic volcanoes. These cycles will be used to draw comparisons with this study's observed cyclicity at Bagana.

3.3.1 Popocatépetl

From 1994, a cycle of lava dome building began, and between 1996 and 2015, at least 37 lava domes have been successively built and then destroyed by explosive activity.[19,20,21] Three types of activity have been noted at Popocatépetl: passive degassing, explosions, and ash emissions with lava domes.[21]

The lava domes at Popocatépetl typically grow over a few days to weeks and the cyclicity specifically has been the focus of studies by Mendoza-Rosas et al. (2017) and Gómez-Vazquez et al. (2016).[19,20,21] The domes are destroyed, often fully, by single or multiple Vulcanian explosions in the crater, with one ash cloud reaching 13 km a.s.l. in 1997, and another reaching 13.5 km a.s.l. with accompanying pyroclastic density currents in 2001.[20] Extrusion rates for domes peaked in December 2000, reaching 28.5 m^3/s, and a total dome volume of 6.9 $x10^6$ m^3.[20] A new dome can begin to form within a few days after the previous dome is destroyed, or it can take several weeks.[19,20] Gómez-Vazquez et al. (2016) reported a clustering of high and low rate emplacement of domes at Popocatépetl, giving two regimes.[20] Smaller domes were emplaced during both regimes, but larger ones occur only during the high regimes.[20] Alongside this, Mendoza-Rosas et al. (2017) noted that the dimensions of the emplaced domes are governed by the magma volatile content, and the capacity of the dome to release the volatiles.[19] The highest SO_2 is associated with dome growth, but the emitted gas is not proportional to the amount of lava extruded.[21] The current rate of lava production is less than other dome-building volcano eruptions, such as Merapi (2006, 3.3-3.6 m^3/s) and Mt. St. Helens (1980).[20,21,53]

3.3.2 Volcán de Colima

Volcán de Colima is situated 5.5 km south of the larger, extinct Nevado de Colima, and Volcán Cántaro, together comprising the 12 km wide Colima Volcanic Complex.[54] This sits within the Trans Mexican Volcanic Belt that also includes Popocatépetl.[54] It is a basaltic-andesitic stratovolcano and is Mexico's most active andesitic volcano.[55]

Based on historical records of activity (~440 years) Luhr and Carmichael (1980) suggested an approximately 100 year cycle of activity culminating in a major explosive eruption,

completely destroying the lava dome.[54] Luhr (2002) suggested Colima is in a third eruption cycle.[56] In 2015, Volcán de Colima experienced an intense phase of activity resulting in partial dome collapse and the production of pyroclastic density currents.[57] This was the most intense phase of explosive activity experienced by the volcano since the 1913 sub-Plinian/Plinian eruption that represented the end of the second cycle. Reyes-Dávila et al. (2016) examined the 2015 activity as a potential end to the third phase of activity, as they noticed an increase in juvenile scoria in the pyroclastic density currents, similar to the 1913 eruption.[57,58] However, based on geochemical analysis, they concluded that the change in behaviour was not the same, and therefore did not constitute the end of the ~100 year cycle.[58]

3.3.3 Santiaguito

Santiaguito comprises four overlapping domes, with the currently active vent being El Caliente, which is an open cone with a crater 200 m in diameter.[23,24,25,26]

El Caliente has near-continuous dacitic-andesitic lava flows, accompanied by ash explosions approximately every half hour.[23,24] These lava flows reach lengths of up to 3.9 km.[59] The extrusion rate has values of between 0.1-0.7 m^3/s, and 0.5 m^3/s.[24,59] Harris et al. (2003) noted that the lava extrusion occurs in 3-11 year cycles of higher rates, followed by lower rates of extrusion.[26]

Thermal anomalies are present at the current vent and two on the flanks of Santiaguito. The thermal anomaly present at the vent has a ring pattern, established by observing the El Caliente vent with thermal cameras.[59] Using visible imagery, it can be seen that the outer ring has smaller vents which release fine material. There is a blocky ring within this, and then a central hot region which is smooth, and may represent the most recent lava.[59] Work by Holland et al. (2011) shows this to be a permeable, fractured surface, allowing continuous degassing, with pathways being forced open when the pressure built reaches a certain point, and then the pathways collapse and are “healed” until the pressure builds again.[24,60]

3.3.4 Merapi

Located in central Java, Merapi is one of the most active volcanoes in Indonesia.[53] Merapi is persistently degassing, with 6500 tonnes of gases per day emitted, 200 tonnes of that being SO_2.[61]

Merapi exhibits a long-period cyclicity that can be seen when analysing the extruded lavas; it has 200 years of lower VEI eruptive activity with intermediate composition lavas, and then 300-600 years of high eruptive activity with more mafic magma and increasingly more evolved magma mixed with the mafic magma.[62] For the past ~200 years activity has been characterised by slow extrusion rates and lava domes.[53] Merapi has a background extrusion rate of 0.03 m^3/s, but every ~7 years (on average) it rises to 1-4 m^3/s in eruptions lasting a few weeks.[53,63] This is supported by findings of Voight et al. (2000) which suggest that during the twentieth century there was an eruption every 4-6 years of VEI 1-3, with some larger historical eruptions of VEI 4.[61] The cycles of this more violent explosive behaviour have a recurrence of 25-54 years, and generate pyroclastic density currents, tephra falls and pose threats afterwards in the form of lahars.[64]

Table 3.1 Volcano thermal and dome growth cycles

Volcano	Cycle Length	Method and Characteristics	Source
Popocatépetl	1.7/7 months	New domes identified by a change in texture or colour from previous dome, by using aerial photography. The ratio of the Cumulative Volume and the Cumulative Number of Domes emplaced gives the average volume of the domes emplaced. 38 domes from 1996-2015 give a ~6 monthly cycle. Using a cumulative graph (Mendoza-Rosas et al., 2017, Fig. 1.) from 1996-2003, 27 domes were emplaced, giving a 1.7 month cycle. The overall average of 6 months is more representative of the recent behaviour in the phase since 2012.	Gómez-Vazquez et al. (2016); Mendoza-Rosas et al. (2017)
Colima	100 years	Dome growth, Vulcanian explosions and partial dome collapse culminating in a Plinian/sub-Plinian eruption every ~100 years for the past few centuries, resulting in complete dome collapse and partial removal of the edifice.	Luhr and Carmichael (1980); Luhr (2002); Reyes-Davila et al. (2016)
Santiaguito	3-11 years	Using Landsat data to extract lava extrusion rates gives 3-6 year phases of high lava extrusion, and then a 3-11 year cycle of lower extrusion rate. Lower extrusion phases seem to be lasting longer more recently, and the peak and difference between the two phases is getting less.	Harris et al. (2003)
Merapi*	4-6 years	Raised lava extrusion rates for a few weeks. Supported by records of historical eruptions for past 200 years.	Voight et al. (2000); Ratdomopurbo et al. (2013)

** Merapi also exhibits 500-800 year cycles, but these are much longer than the timescales in this study, so are noted here but not considered in this comparison table.*

3.4 Data Acquisition

The MIROVA system is a hotspot detection algorithm that works in near-real time. It utilises data from the Moderate Resolution Imaging Spectroradiometer (MODIS) aboard the Terra and Aqua satellites. MIROVA provides radiative power information within 1-4 hours of the satellite overpass, focussing on the Middle Infrared (MIR) at 3.4 and 4 μm, which has the lowest attenuation from the atmosphere.[65] This allows for the detection, location and measurement of heat radiating from volcanic activity. MIROVA calculates the radiative power from the linear relationship between the radiative power and the radiance detected in the MIR region, multiplied over the number of pixels, with a best-fit regression coefficient of 18.9.[65,66]

MODIS is hosted by two platforms: Terra and Aqua, launched by NASA in 1999 and 2002, respectively. They are in a Sun-synchronous orbit at 705 km, providing global coverage every 1-2 days and a resolution of 1 km^2 at nadir. The data is available from February 2000 to the present.[67]

The data are obtained by email from Prof. Diego Coppola at the University of Turin. The data can be delivered in a Microsoft Excel spreadsheet for the time period specified by the user, featuring a column with the timestamp and another with the radiative power totals. These can then be manipulated into other forms, and notably for this work, the data were converted into a comma separated values (.csv) file to allow for manipulation within the 'RStudio' programme.

The data are also available via a webpage, where the user can specify the volcano of interest from the automated catalogue of collections.[68] The most recent data acquired over the volcano are available as images, as well as the last month or year of data in a graph. On each volcano's webpage there are images of the radiative source which are automatically collected with the (presumed) volcanic source at their centre.

Data were acquired for this study from 1st July 2016 - 25th June 2019, to coincide with the data time-series length of the SO_2 data acquired and analysed in Chapter 2 to allow comparisons to be drawn between the two datasets (see Chapter 4).

3.5 Sources of Uncertainty

MIROVA is only able to detect hotspots where radiation exceeds a threshold, and therefore it can only be used as a proxy for the presence of lava, either as a dome or flows. For visual confirmation of lava flows, data must be sourced elsewhere to verify the MIROVA data (see Chapter 5).

To manipulate the time-series with an FFT algorithm (see Section 2.7), missing values must be filled with zeros. These values are “missing” as they represent the days when there was no heat recorded, therefore zeros should be a true reflection of conditions.

However, the thermal infrared channels used to detect the hotpots can struggle to “see” through thick cloud. This is common at Bagana, especially in the afternoons, due to the strong tropical convection that often forms clouds.

Scenes from the day-time can introduce noise in the form of reflected sunlight, so where possible night-time scenes were used.[2]

3.6 Method

3.6.1 Method Outline

The data are collected up to twice daily, with the highest value recorded in that 24 hour period taken as the value for the entire day. Missing values have been filled with zeros to allow for FFT to be undertaken on the time-series. The time-series has not been padded, and no additional processing steps are required.

3.6.2 Uncertainties

The filling of missing values with zeros to allow a time-series FFT analysis to be undertaken will skew the amount of days recorded with a zero value, so may skew cycles identified at a frequency of zero.

The removal of the lowest reading from any day with two recorded passes means any variation in the proxy lava output is reduced, and may give a false impression of a high reading for the whole of the 24 hours.

3.7 Applying the Fast Fourier Transform to the Thermal Time-Series

The Fast Fourier Transform (FFT) was applied to carry out a time-series analysis of the thermal data using the programming language, R, following Crockett (2019) (see Section 2.7 & 2.8).[52]

An FFT was used to look for cycles in the daily thermal data from 1st July 2016 - 25th June 2019. This time period was used to match the OMI SO_2 data and enable comparisons to be drawn. Issues with the OMI SO_2 data meant that the thermal data time-series was cut short. The 1090-day length of the data set has approximate limitations of a few days at the higher frequency end and ~1000-days at the low frequency end.

3.8 Results

The full time-series shows the radiative power daily totals from Bagana (Fig. 3.1). Peaks in the thermal data can be clearly seen throughout the time-series, and the magnitude of these does not drop off through time. Three patterns can be observed: families of peaks (e.g. at ~50 days, ~100 days, ~250 days), low baseline signals (e.g. at 130-210 days, 920-1090 days), and finally potential waning signals with initially high peaks and then a tail as activity drops off (e.g. at ~50-130 days, ~240-300 days, ~530-580 days).

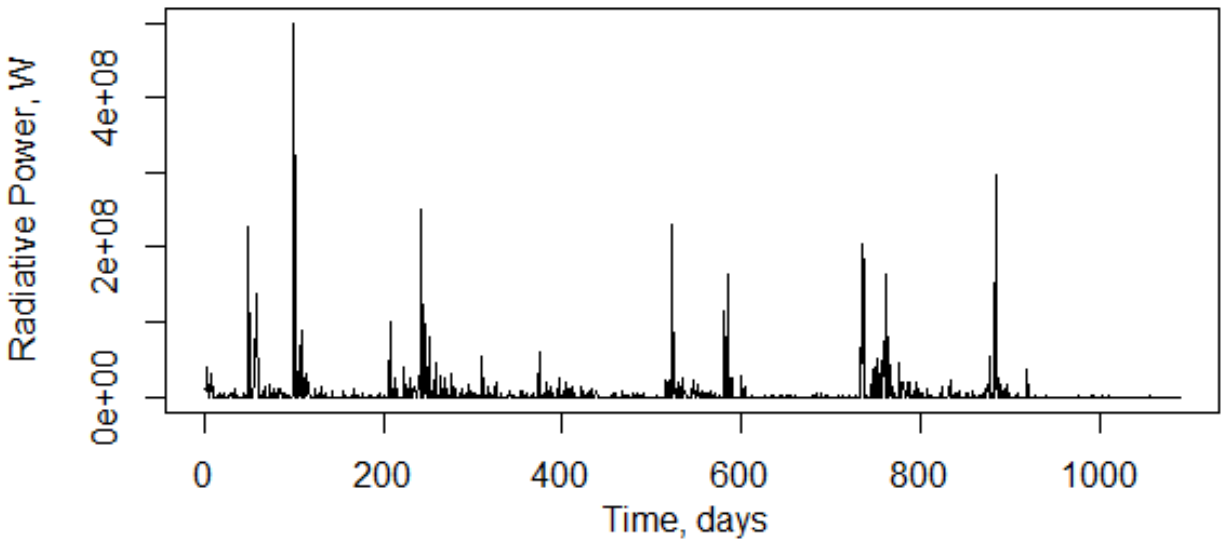

Figure. 3.1 The radiative power daily time-series recorded by MIROVA, from 1st July 2016 - 25th June 2019.

Figures 3.2 and 3.3 both show output results from 1st July 2016 - 25th June 2019, with high-amplitude bars at frequency zero, which, due to the filling of missing values as discussed, is expected from an FFT. In Fig. 3.3 the highest frequency is 0.1 cycles, to show the detail of the longer cycles present in Fig. 3.2. On Fig. 3.3 there are also a number of prominent dark grey bars (fading to mid-grey) between 0 and 0.1 (0.01, 0.04, and 0.08), which continue across the spectrogram, compared to other cycles which show a darkest grey bar for just one time window. This can also be seen at 0.42-0.44 (2-3 days) on Fig. 3.2, though this is thought to relate to noise in the dataset. All the cycles seem to die out in the last time window of the spectrograms (Figs. 3.2 and 3.3), which correlates with a quiet period visible without any peaks, at the end of the time-series in Fig. 3.1. The regularly spaced darkest grey bars at the centre of the spectrogram could be an artefact from sampling.

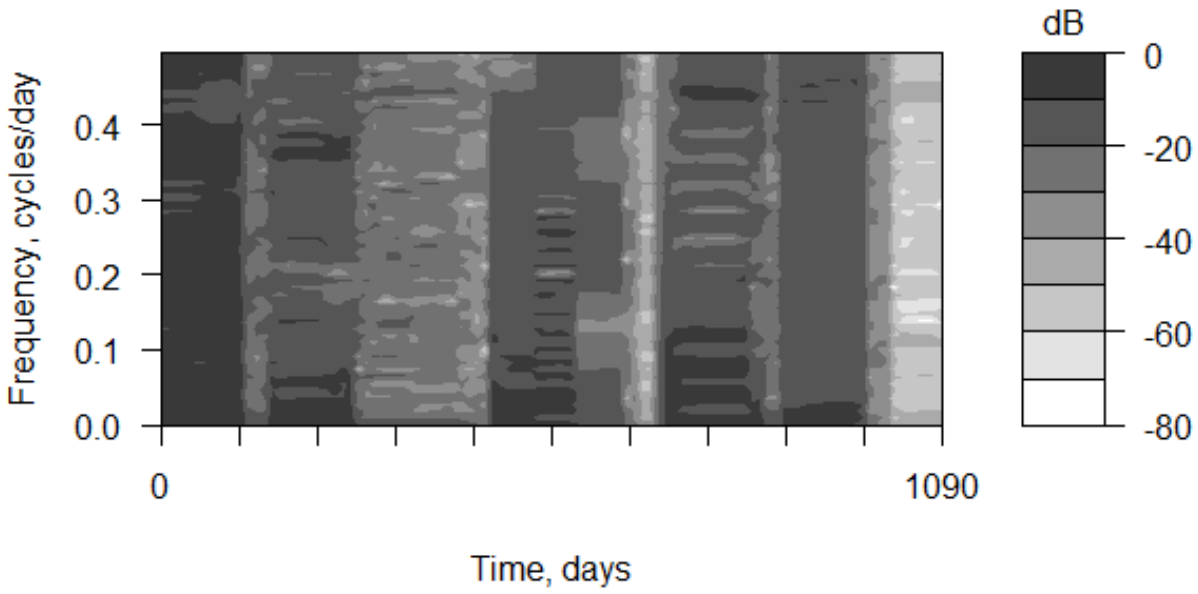

Figure 3.2 Spectrogram of daily thermal radiative power at Bagana, from 1st July 2016 - 25th June 2019. The graphic was produced with the 'Simplespectro' programme in R (Crockett, 2019).[52] Each window is 109 days on the time axis, and the default step length 10.9 days.

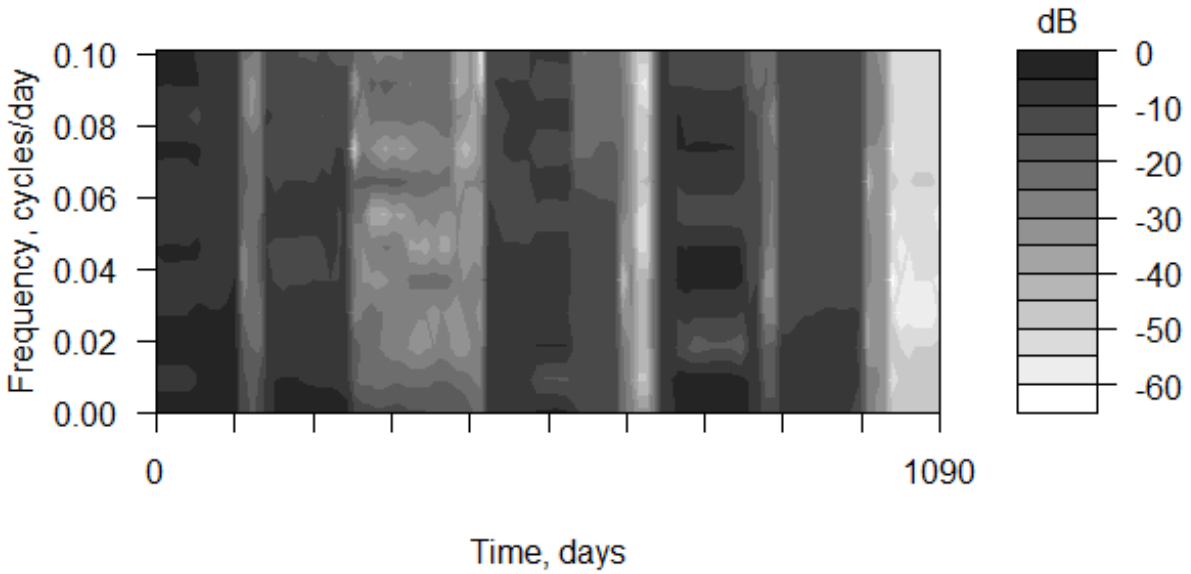

Figure. 3.3 A section of the spectrogram of daily thermal radiative power at Bagana, from 1st July 2016 - 25th June 2019, with a 10.9 day time-step and each window is 109 days on the time axis. The graphic was produced with the "Simplespectro" programme in R (Crockett, 2019).[52]

By increasing the window of the FFT to 400 days, the resolution in the frequency domain is increased by sacrificing resolution in the time domain. This results in the spectrogram in Fig. 3.4, showing a clearer, more-continuous darkest grey line for ~0.0075 cycles per day (133 days) as the most prominent feature. Using this window size, a continuous darkest grey line across the spectrogram is visible centring on ~0.44 (2-3 days), with other dark grey lines featured towards the end of the time-series centred around 0.45 (Fig. 3.5). This shows that there is likely to be strong cyclicity around these frequencies.

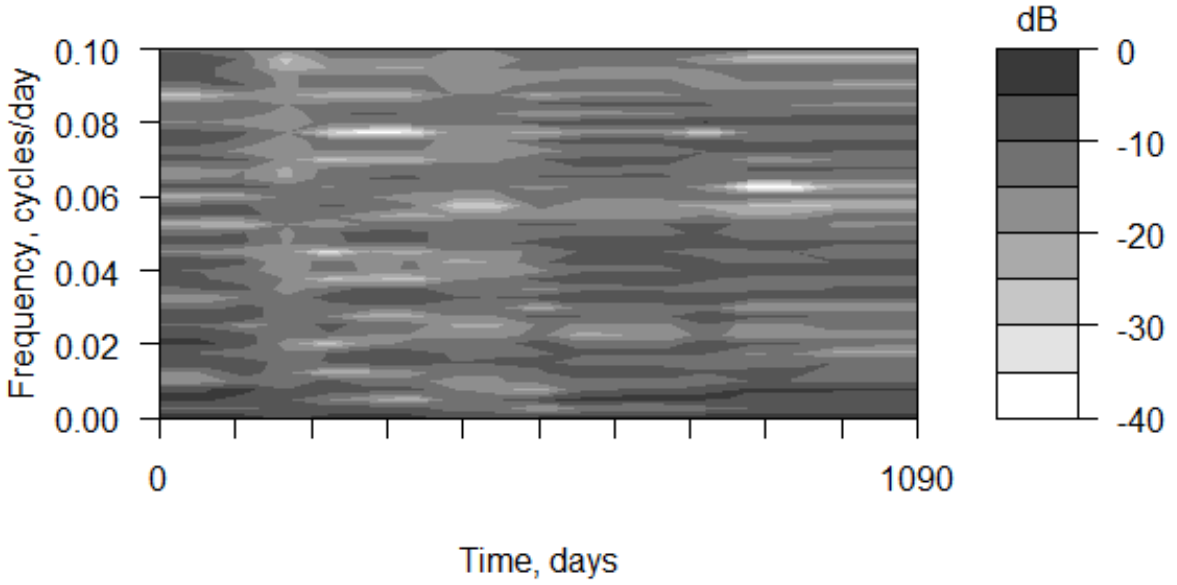

Figure. 3.4 A spectrogram focussing on the 0 to 0.1 cycles per day range, with an FFT window of 400 days. There is a prominent, near-continuous line at ~0.0075, and lesser cycles at 0.035 to 0.05, and clustered around 0.08.

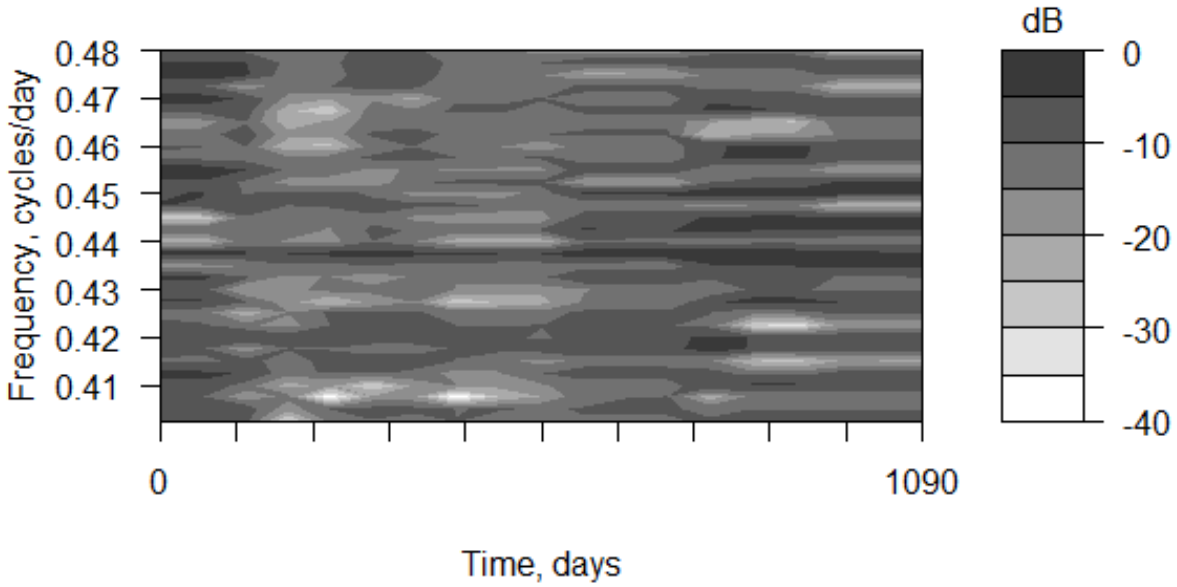

Figure. 3.5 A spectrogram focussing on the 0.4 to 0.48 cycles per day range, with an FFT window of 400 days. There is a continuous line centred ~0.44, with others around this value.

The power spectrum (Fig. 3.6) of the results is characteristic of a 'noisy' time-series. This means it shows multiple tiny fluctuations in-between the more prominent peaks.

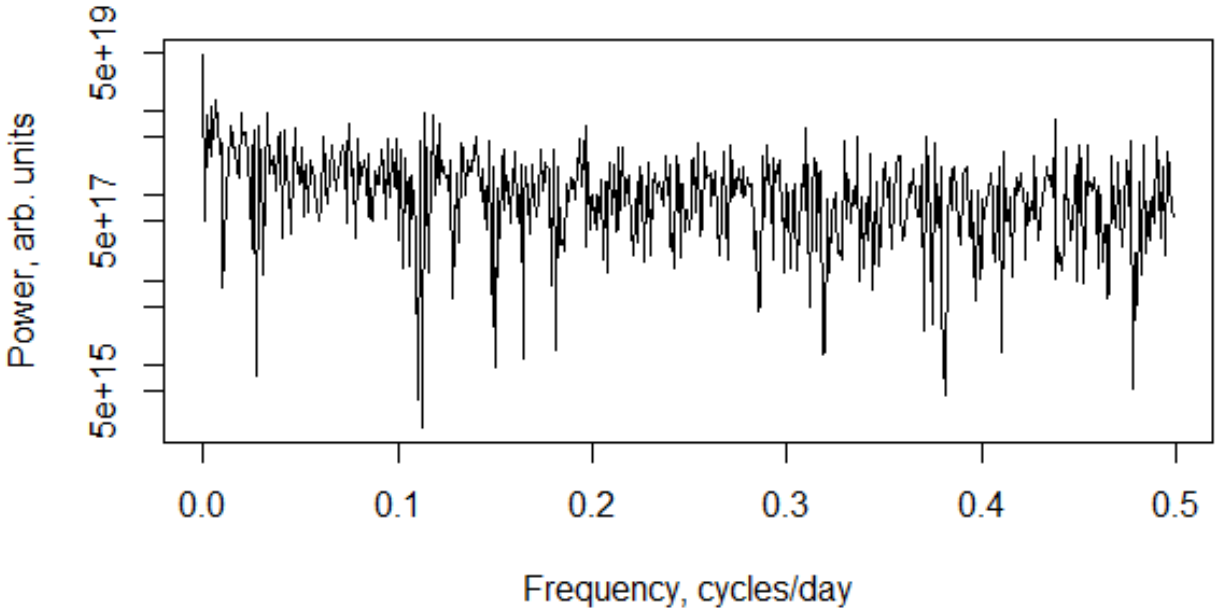

Figure. 3.6 The power spectrum of the thermal radiative power time-series from MIROVA, for the time period 1st July 2016 - 25th June 2019.

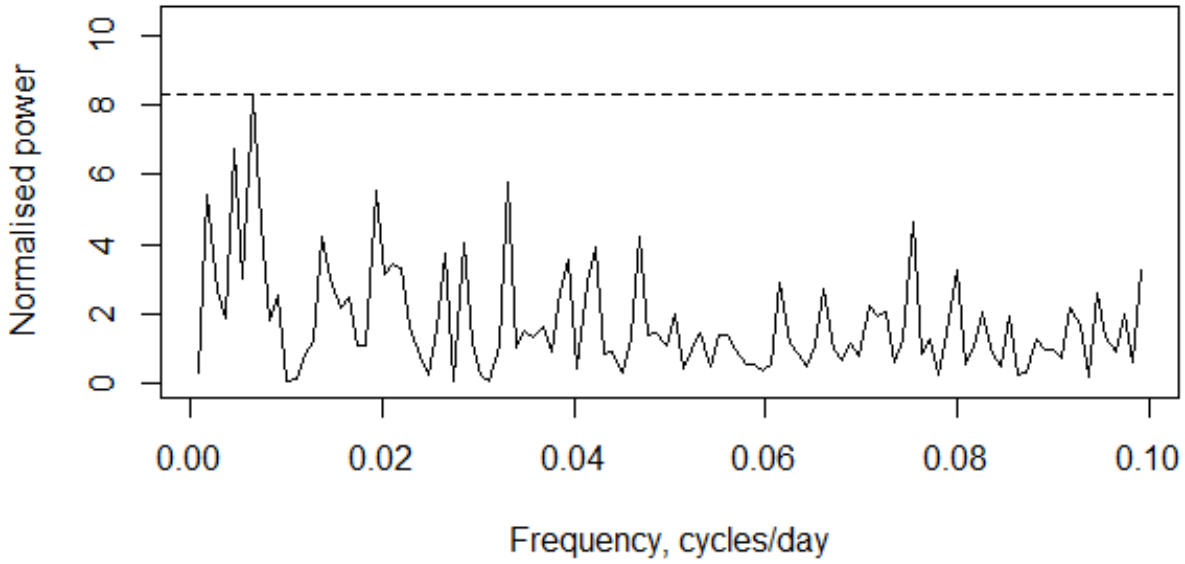

Figure. 3.7 The Lomb periodogram of the thermal radiative power time-series, with 95% confidence interval (CI) for the frequency range of 0 to 0.1.

The Lomb periodogram (Fig. 3.7) with a 95% confidence interval (dashed line), reveals a significant peak at ~0.0075 cycles per day (133 days), when focussing on the longer frequency cycles.

In summary, cycles identified by the FFT spectrograms and the periodogram show cycles of interest may be 2-3 days and 133 days.

3.9 Discussion

3.9.1 Thermal Evidence for Cyclicity at Bagana from 2016-2019

3.9.1.1 Linear Time-Series Features

There is a noticeable quiet period for the final 200 days of the thermal time-series at Bagana (Fig. 3.1). This indicates a reduction in thermal activity, perhaps associated with no active lava flows or lava dome growth. There is also evidence of waning behaviour, with peaks followed by further peaks at increasingly diminutive levels (e.g. 240-300 days).

3.9.1.2 Spectrogram Features

The spectrogram (Fig. 3.2) shows a wide distribution of dark grey colours (values 0 to -10 dB), suggesting strong cycles throughout the dataset; however, many of those highlighted at the first time-step of the spectrogram do not continue throughout the time period. This indicates that the cycles are not present later in the dataset. The key spectrogram cycles identified were at ~0.44 (2-3 days) and ~0.0075 (~133 days).

3.9.1.3 Power Spectrum and Lomb Periodogram Features

This distribution of strong cycles throughout the frequency range suggests that a white noise model would suit this data distribution better than a typical red noise model commonly used for geophysical data modelling, supported by the flat shape of the power spectrum (see Fig. 3.6). A white noise model has equal frequency peaks either side of zero, giving its power spectrum profile a characteristically flat shape.

The Lomb periodogram (Fig. 3.7) confirms at a 95% CI that the ~133 day cycle is the most significant in the thermal time-series data. The 2-3 day cycle is likely some form of noise

or sampling artefact, as the sampling interval for the data is 1 day. Any shorter periods of a few days are likely to be highly uncertain.

3.9.2 Bagana in the Context of Thermal Cycles of Other Andesitic Volcanoes

When compared to the thermal and lava dome growth cycles at the other volcanoes in similar settings (Table 3.1), it is most close in length to the cycles seen at Popocatépetl. The cycles observed at other analogous volcanoes are longer than the dataset obtained for Bagana (3 years). More data would need to be collected to observe longer period cycles at Bagana.

The behaviour exhibited at Popocatépetl, of passive degassing, explosions, and ash emissions with lava domes, are reflective of reported behaviour at Bagana. This shows it may be a good analogue for Bagana to enhance interpretation of behaviour, however the SO_2 cycles present there were much shorter than any found by this study at Bagana. This may suggest that a time-series needs to be created with a finer resolution to see if these shorter (<1 day) cycles are present.

3.10 Conclusion

From the FFT analysis conducted on the thermal data, cyclicity can be observed at a periodicity of ~2-3 days and ~133 days.

There is evidence to support cyclic behaviour at Bagana over the 2016-2019 period: (i) a direct search in the time-series from the MIROVA dataset that reveals a breadth of active features over time intervals from 50 to about 150 days; (ii) FFT derived spectrograms show features with a period of ~ 50 days; and (iii) power spectrums and a Lomb periodogram show strong evidence for a 133 day cycle being the most statistically significant cycle.

Chapter Four – SO_2 and Thermal Cyclicity Comparison - Do the SO_2 and Thermal Time-Series Both Show the Same Trends and Cyclicity at Bagana?

4.1 Introduction

The aim of this chapter is to examine the trends and cycles found in both the SO_2 and MIROVA thermal data from Bagana, building on the data analysis in Chapters two and three. A variety of timescales will be utilised to assess any offsets in the data, and reveal insights to the processes governing the behaviour of the cycles and trends, and whether the cycles of the two datasets are linked.

As a point of reference for this study, McCormick Kilbride et al. (2019) used thermal MODVOLC data to analyse the trends alongside the SO_2 time-series.[2] However, this study uses thermal data from a different source (MIROVA), but it is helped by the information and conclusions in McCormick Kilbride et al. (2019) to put into context this study's results in regard to the longer term trends of Bagana.[2] It is also worth noting that that MIROVA and MODVOLC are both derived from the data from MODIS, so comparisons are justified.

4.2 Objectives

The objectives to achieve these aims are:

- Compare the thermal data with the SO_2 data, by plotting the linear datasets alongside one another at a variety of timescales.

- Plot the thermal data against the corresponding SO_2 values to get the R^2-value of the correlation.

- Compare the temporal lengths of cycles found in the thermal and the SO_2 data from the FFT analysis performed (see Section 2.8 and Section 3.8).

4.3 Comparison of SO_2 and Thermal Remote Sensing Datasets

4.3.1 SO_2 and Thermal Data Plotted Against Time

4.3.1.1 Daily

Plotting the thermal (in red) and SO_2 (in blue) datasets on the same time axis (1st July 2016 - 25th June 2019) reveals some similarities, and other notable differences.

When plotted on a daily timescale (Fig. 4.1), the time-series shows infrequent correlation. There is a matching of elevated activity in both time-series in October 2016, March 2017 and July 2018. However, there is no matching of peaks at July 2016, September 2016, December 2017, February 2018, April 2018 and December 2018.

Notably, the SO_2 time-series shows quiescence from October 2018 onwards. There is one prominent peak in the corresponding MIROVA thermal data during this time, and then a subsequent fall off in any recorded hotspot values. This indicates a reduction in activity at Bagana, reflected in both time-series that could indicate cycles of heightened activity followed by periods of quiescence, longer than can be identified by the three-year time-series in this study. This is supported by findings in McCormick Kilbride et al. (2019; Section 4.2.1, Fig. 6 and Section 4.2.2), where pauses in activity are noted.[2]

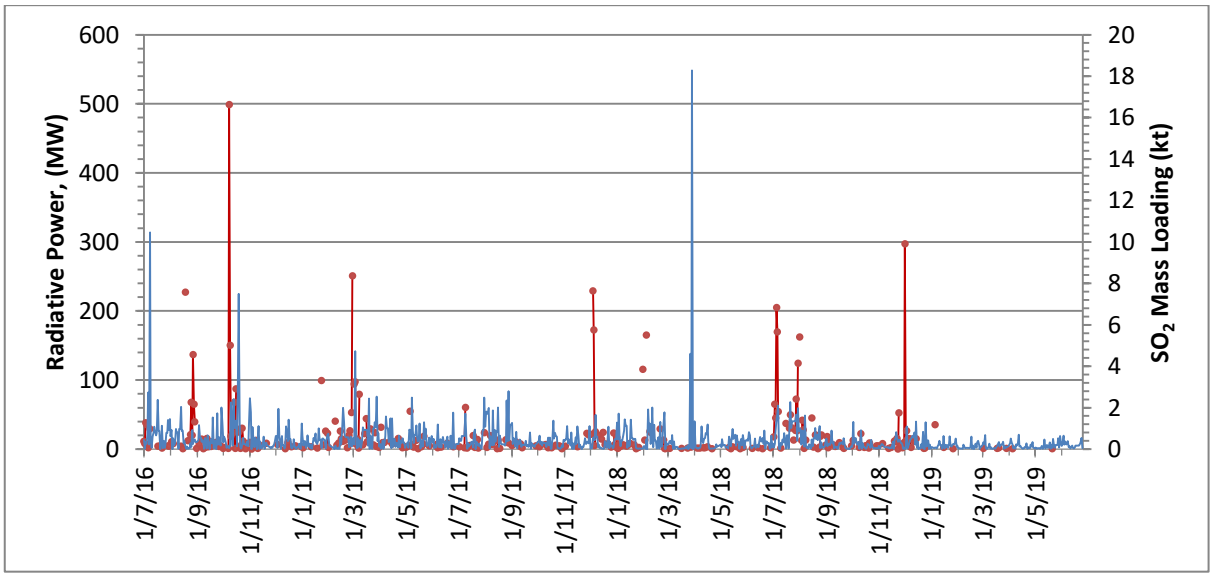

Figure 4.1 The SO_2 and MIROVA thermal data plotted on a daily timescale, with MIROVA values in red and SO_2 values in blue.

4.3.1.2 Weekly

On a weekly timescale (Fig. 4.2), the same peaks and troughs as observed in the daily time-series data are evident, with similar matching and mismatching as before.

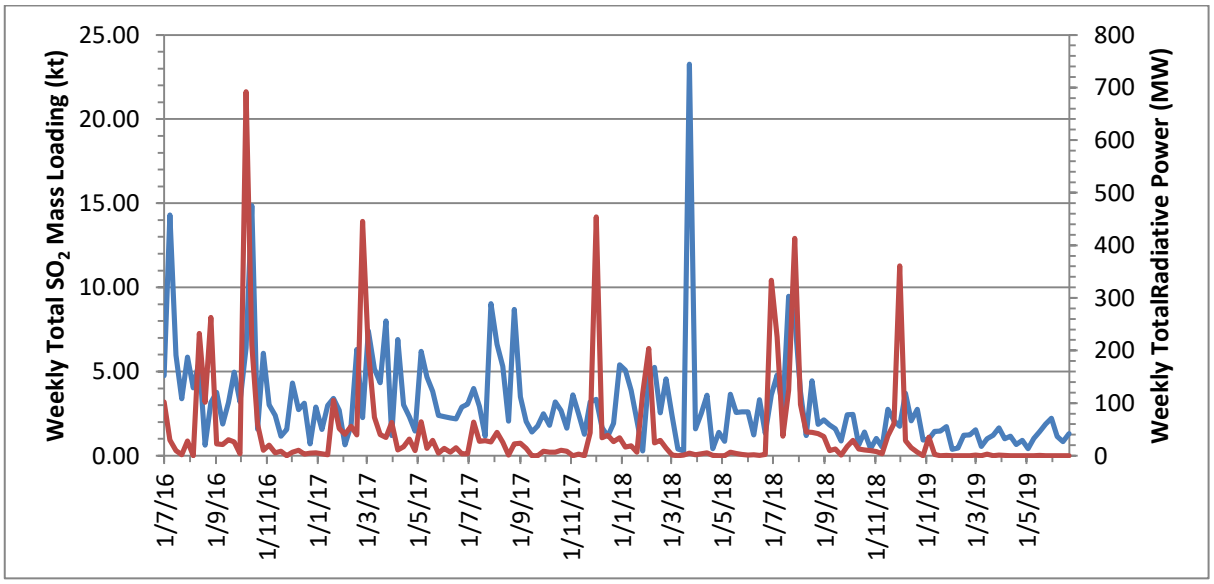

Figure 4.2 The SO_2 and MIROVA thermal data plotted on a weekly timescale, with MIROVA values in red and SO_2 values in blue.

4.3.1.3 Monthly

On a monthly time scale, it appears that months high in SO_2 are preceded by a month high in thermal radiative power on two occasions. There are also more occasions of the matching of the peaks in the two data sets (October 2016, July 2018 and December 2018). This may indicate that there is a more generic link between the two data streams, but on a smaller sampling level the relationship is harder to see.

It is also worth noting that both datasets have a reduction in activity to a much lower baseline activity rate from February 2019. This is evident (Fig. 4.3) in the linear gradient of baseline values from July 2016 - February 2019. This supports two hypotheses. Firstly, that the overall activity at Bagana wanes at the end of the time-series, supported by the spectrograms in Section 2.8 and 3.8. Secondly, that the processes linking the two time-series are also linked, as they decline together.

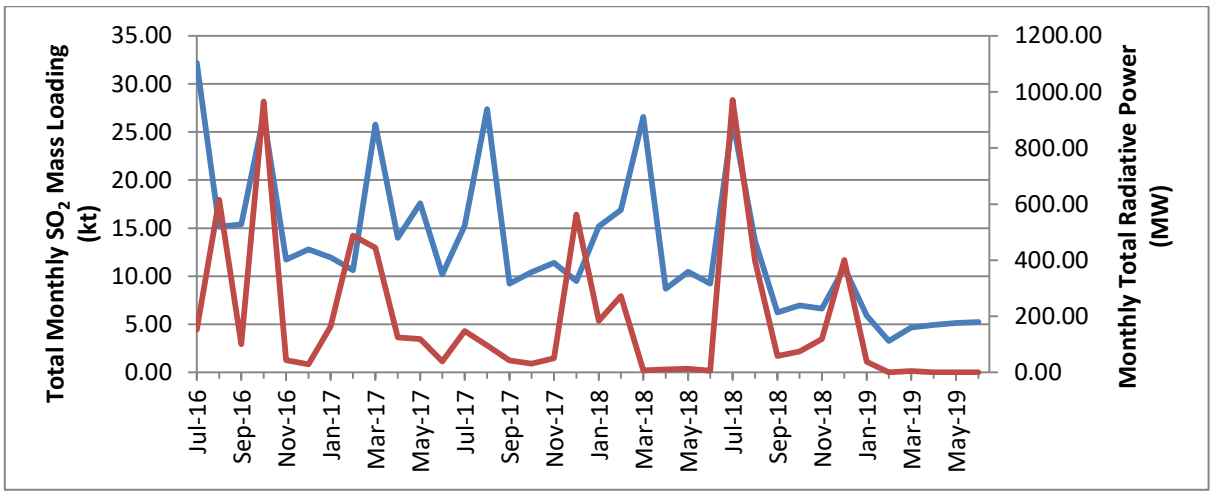

Figure 4.3 The SO_2 and MIROVA thermal data plotted on a monthly timescale, with MIROVA values in red and SO_2 values in blue.

4.3.2 SO_2 Monthly Totals Plotted Against Thermal Monthly Totals

Plotted on a monthly timescale against one another (Fig. 4.4), the SO_2 and thermal data show a slight positive correlation. This was undertaken to see if a relationship existed that on a given day, a high SO_2 value would coincide with a high thermal radiative power value, to show the degree of any dependence of one on the other.

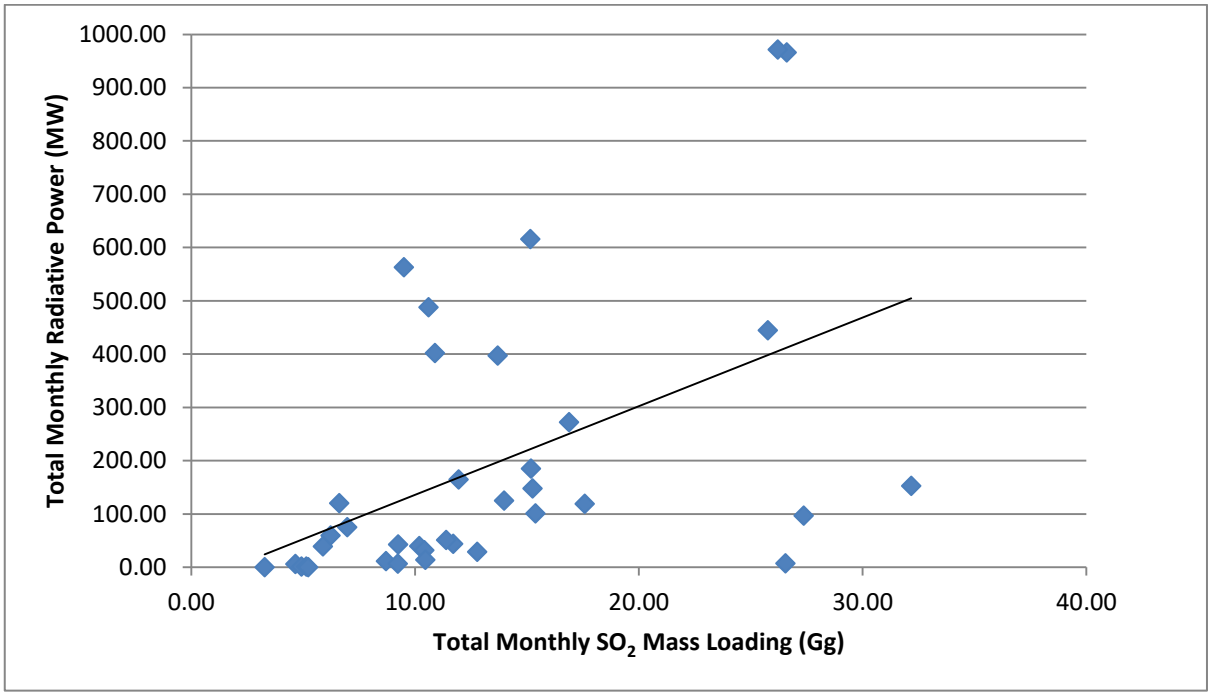

Figure 4.4 The monthly mass loading totals for SO_2 and radiative power totals for thermal data plotted against one another. The regression line shows a weakly positive relation.

Using the inbuilt Microsoft Excel function of *RSQ*, an R^2 value was calculated for the monthly totals. This had a result of 0.23 (unitless). This would indicate a weak correlation. The totals are not meaningfully correlated, as this is supported by worse R^2 values for the weekly and daily timescales.

4.3.3 SO_2 and Thermal Cycle Comparisons

The cycles identified using FFT analysis for the SO_2 and thermal data (Chapters 2 and 3, respectively) are shown in Table 4.1. The SO_2 data show more short-term cycles, with the most significant being a cycle of 16 days. The thermal time-series has a longer significant cycle of 133 days, which does not match with longer cycles seen in the SO_2 data, but is close to the 100 day cycle seen. However, 133 days is roughly 4.5-5 months, and notably in Fig. 4.3, this periodicity in peaks can be seen in the SO_2 data on a monthly basis, suggesting perhaps there is a more general relationship between the two time-series. This also further supports finding of the pulsatory behaviour of flows on a 105 day cycle found in Wadge et al. (2012).[1] The joint cycle of 2-3 days is close to the sampling interval of the data (1 day), and close to the Nyquist frequency (half the sampling rate – the maximum frequency beyond which aliasing occurs). It is also not a significant cycle for each data set; therefore it is likely to be due to the background noise in the data rather than a true cycle. This is further supported by Flower et al. (2016), which found that there is an inherent 3.2 day cyclicity present in OMI data, from the ORA.[69]

Table. 4.1 The FFT cycles of both the SO_2 and thermal data from Chapters 2 and 3 for Bagana. Those cycles in bold are statistically significant according to the Lomb periodogram. The 105 day cycle from Wadge et al. (2012) is included.[1]

SO_2 (days)	**Thermal (days)**
2-3	2-3
12-13	
16	
100	
	(105 Wadge et al. (2012))
	133
333	

4.4 Discussion

A benefit of using these two sources of data (OMI and MIROVA) is that obtaining the data required and processing it is relatively quick, and both are provided open source. This allows for replication of the science measurements in this study.

Both datasets, in particular the SO_2 time-series, are noisy. On a daily timescale, general increases in activity can be lost against the background day-to-day fluctuations. On a monthly timescale, the general trend of increase or decrease in activity is more obvious, and the correlation in the datasets is more evident. In general, it is shown that thermal peaks in activity precede or match with SO_2 peaks. This supports the findings of McCormick Kilbride et al. (2019; Section 4.2.1, Fig. 8), where the peaks in thermal activity were interpreted as lava extrusion, and the accompanying SO_2 peaks as degassing of these flows, and that there was a first-order relationship between them.[2]

The plotting of the data on a monthly timescale has allowed for comparisons to also be drawn against the FFT findings for significant cycles in both datasets. The thermal FFT results indicate a significant cycle of 133 days, which roughly equates to 4.5-5 months. This periodicity is also seen in the peaks of SO_2 in the monthly plotted totals (Fig. 4.3), indicating that the governing processes may be linked may be linked. Care needs to be taken, however, as the level of certainty is somewhat reduced due to the differing sampling rates, with thermal being daily, and the SO_2 monthly in this case. This is supported by evidence from Wadge et al. (2012) of a lava flow periodicity of 105 days.[1]

Using the SO_2 and thermal data streams together helps to build a more complete picture of the processes that might be causing the behaviour at Bagana, and can provided more evidence to support interpretations. McCormick Kilbride et al. (2019; Section 4.2.1), failed to draw a definitive conclusion of the relationship between the SO_2 and thermal trends for the time period 2000-2017, using Terra-SAR-X data, OMI SO_2 data and MODVOLC hotspot numbers.[2] This was due in part to the different and longer sampling times. The MIROVA algorithm used in this study is more sensitive than the MODVOLC hotspot algorithm. The Sentinel-1 and Sentinel-2 SAR data included in Chapter 5 are on a more frequent revisit time (12 days) than the Terra-SAR-X data, allowing for more certainty in the cause and effect of the trends seen.

The increase in thermal activity in months prior to and at the same time as the SO_2, may suggest that lava flows or dome collapse are allowing more degassing to take place. This would be analogous to behaviour and results observed at Popocatépetl (see Section 3.3.1). Higher levels in SO_2 were associated with periods of dome growth.

The peak in March 2018 (of ~18 kt) relates to an especially large plume of SO_2 from Bagana, confirmed by viewing the latitude-longitude plot of the retrieved OMI data. It is almost twice as large as any other peak in the time-series. This could demonstrate the explosive behaviour sometimes reported at Bagana.[3,5] Potentially this larger SO_2 degassing event could be part of a longer cycle of larger events, not able to be captured in this time-series of 3 years. Notably, for comparison in McCormick Kilbride et al. (2019; Fig. 6) a large peak is present in the SO_2 dataset when binned monthly for in June 2005.[2] When examining this month of data daily, 10 peaks are above 18 kt, with the highest at 48 kt.[49] Though, for other examples, the entire middle of 2005, and end 2007 to beginning of 2008, show elevated SO_2 values when binned monthly. Therefore, this short-lived elevated event in March 2018 is dissimilar to the consistently high peaks in June 2005, and 2007-2008.

4.5 Conclusion

The thermal and SO_2 time-series are linked on a monthly scale, with thermal peaks preceding or matching SO_2 peaks. Both datasets show a drop in activity from January 2019, further supporting that the processes driving both data-sets are connected, and that Bagana has had a period of quiescence for the duration of 2019.

A periodicity of 4.5 months may link the two datasets when compiling all the graphs of daily, weekly and monthly totals, and the FFT cycles of significance, though this is a cautious link given uncertainty around the difference in sampling rates of the two methods.

The periodicity of 16 days evident in the SO_2 time-series is newly recognised at Bagana. Cycles of this length were seen in tiltmeter data at Soufriere Hills Volcano.[29,35] It was suggested that these cycles represent a charge-recharge phenomena during Vulcanian

activity. This could indicate that there is recharge of a shallow storage region which pressurises the system and degasses on a cycle of 16 days.

Chapter Five – Supporting Evidence to Enhance Interpretation of Cyclicity- Can InSAR and Amplitude Data from Sentinel-1, and Visible Data from Sentinel-2 Provide Supporting Evidence for Lava Flows and Enhance the Interpretation of SO_2 and Thermal Time-Series Data?

5.1 Introduction

The aim of this chapter is to investigate whether the presence of lava flows can be observed with InSAR and amplitude data from Sentinel-1. The observations will be compared with images from Sentinel-2. The gathered time-series of lava flow data will be compared with the SO_2 and thermal time-series data to investigate whether the InSAR and Sentinel-1 and Sentinel-2 data can be used to support interpretations of the cycles and processes causing the SO_2 and thermal cyclicity. This will demonstrate the benefits of using these multiple data streams together. This supports work that has previously been undertaken by Wadge et al. (2012) that uses amplitude images from TerraSAR-X to track pulsatory lava flows at Bagana in 2010-2012, and will aim to replicate the technique using Sentinel-1 data at Bagana for the first time.[1]

5.2 Objectives

- To acquire the Sentinel-1 Single Look Complex (SLC) and Ground Range Detected (GRD) products, from April 2017 (earliest available date for the dataset) to June 2019.

- To acquire the Sentinel-2 Level 1 products from the earliest available date to June 2019.

- To process the Sentinel-1 SLC and GRD images using the most appropriate methods to create InSAR and change detection amplitude images.

- Assemble a time-series to investigate signs of lava activity.

- Identify dates of potential lava flow activity and confirm intervals with Sentinel-2.

- Compare the Sentinel-2 derived dates with peaks in activity from the SO_2 and the thermal time-series.

- Provide an interpretation of the results that may describe the observed processes.

5.3 Data Acquisition

5.3.1 Sentinel-1A and -1B

Sentinel-1A was launched in 2014 by ESA, with Sentinel-1B following in 2016. Each satellite has a revisit time of 12 days, and 6 days as a 1A/1B pair. The sensors are C-band radar, and the resolution at nadir is 5 m by 20 m. Data is available from 2014 for Sentinel-1A and 2016 for Sentinel-1B.[70]

Sentinel-1 provides Synthetic Aperture Radar (SAR) data, which can be used to create Interferometric SAR (InSAR) and amplitude images. For amplitude images, GRD products are used, which have a higher level of processing, and a loss of the phase information. For InSAR images, SLC products are used, which have less processing, and still contain the necessary phase information to be able to perform InSAR.

The SLC and GRD products were downloaded from the Copernicus Hub, which provides access to all the archived data from the Sentinel missions.[71] This was done from the earliest available date (April 2017) to June 2019, to coincide with the data from the SO_2 and thermal time-series analyses (Chapters 2 and 3).

5.3.2 Sentinel-2A and -2B

Sentinel-2A and -2B were launched in 2015 and 2017, respectively. They have a 5 day revisit time, and 10-20 m spatial resolution at nadir. The sensor detects in Red, Green, Blue and Near Infrared (NIR). Data is available from 2015 (Sentinel-2A) and 2017 (Sentinel-2B) to the present.

The online image viewer of Sentinel-2 Playground allows the images to be viewed with a channel combination that highlights lava flows.[72] The user can select particular days and locations, and view the channels in their desired combination and then export the resulting image in jpeg file format. This allows for quick and easy access and manipulation of the data.

5.4 InSAR Data Processing.

5.4.1 Interferometry

Interferometric Synthetic Aperture Radar (InSAR) is a process by which, with two phase images of the same area, taken a period of time apart, we can determine if there has been any change in the 3D position of the surface. The change in path length can also be interpreted in terms of ground deformation.

For InSAR, the two main sources of noise are a variation in the water vapour content and spatial distribution between the two image acquisitions. Other sources are growth or removal of vegetation and the total loss of coherence, for instance when a new lava flow front covers part of an InSAR pairing.

5.4.2 InSAR Processing Method

The InSAR data from Sentinel-1A and -1B have been downloaded and processed for the period April 2017 to July 2019 to match SO_2 and thermal data. The Sentinel-1A data gives the most information when processed because of the look angle and direction of flight over Bagana in particular. It additionally gives good phase coherence, so this is where the processing efforts have been focussed. The images have been processed using the SNAP software toolbox from ESA, to give intervals of 12 days, 1 month, 3 months and 1 year. The most useful was the 1 month window, so this will be used to support the findings in Chapters 2 and 3.

A calibration and orbit file are applied to the images to ensure geolocation of the pixels. Topographic effects due to the terrain and radar geometry are removed by applying a Digital Elevation Model (DEM). The pattern that is left should show the ground deformation, and any atmospherically-generated noise.[73] Improvements to the process have been made by applying a more precise orbit file, and applying a more up-to-date (2011) DEM from an external source.[74]

5.5 Change Detection Amplitude Image Data Processing

5.5.1 Change Detection using Amplitude Data

Change detection works by overlaying two images taken a period of time apart, and colouring one image in the Red channel, and the second image in both the Green and Blue channels. Where there is coherence between the two images, the resulting RGB pixel will look white, where there are changes, the pixel will either be red or cyan. Cyan indicates rougher ground in the later image, so may show the presence and morphology of a lava flow.

5.5.2 Change Detection Processing Method

To process the Amplitude images, the Sentinel Applications Toolbox was used, provided by ESA.[75] As the Copernicus Hub did not have the full timeline of GRD products for the relevant time period, there was a modified processing chain for turning SLC products of the same scene, and ultimately the same starting data, into GRD images of the same scene.

The processing chain (listed in Appendix C) involved a calibration step, where the image was converted to σ_0, and the scene was cropped to the area of interest. Then a terrain correction was applied, using the more up-to-date TanDEM-X 90 m DEM, than the SNAP default SRTM DEM. The scene was then converted to decibel values and then co-registered with a scene from a set time interval apart. An RGB image was then created, with the first image in the Red band, and the second image in the Green and Blue bands. This method creates a similar output as for the Terra-SAR-X amplitude change detection images in Wadge et al. (2012; Figs. 3 and 4).[1]

The images were processed for different time intervals. The shortest was for 12 days, the longest was a year - it was determined that the 1 month-long interval gave a good time period for catching the movement of some features. With the shorter time periods, there was a risk of not having a long enough time interval for slower movements to generate a large enough signal to register. With the longer time intervals of a year, there was a risk of incoherence, making it hard to draw correlations between corresponding pixels and thus, not registering any signal.

5.6 Sentinel-2 Data Processing

On the Sentinel Playground, images were collected from July 2016 to June 2019. They are a Level 1C image, and the channel combination used is listed as “False Colour”, which uses bands 12 (SWIR 2.190 µm in Red Band), 11 (SWIR 1.610 µm in Green Band) and 4 (Red 0.665 µm in Blue Band). After investigating different combination available, this produced the clearest view and indication of any lava activity.

All images available for the time period that showed lava activity were downloaded, and they were then ready to use alongside the other data sources to confirm the presence of lava flows visually.

5.7 Results

5.7.1 Evidence for Lava Flows in InSAR, Amplitude and Sentinel-2 Data

Nine instances across the Sentinel-2 dataset of visible images have been identified that potentially show new lava flows, and one example of this is given in Fig. 5.1, alongside the corresponding Sentinel-1 Amplitude and InSAR images. The other instances are presented in Fig. 5.3 and Appendix D.

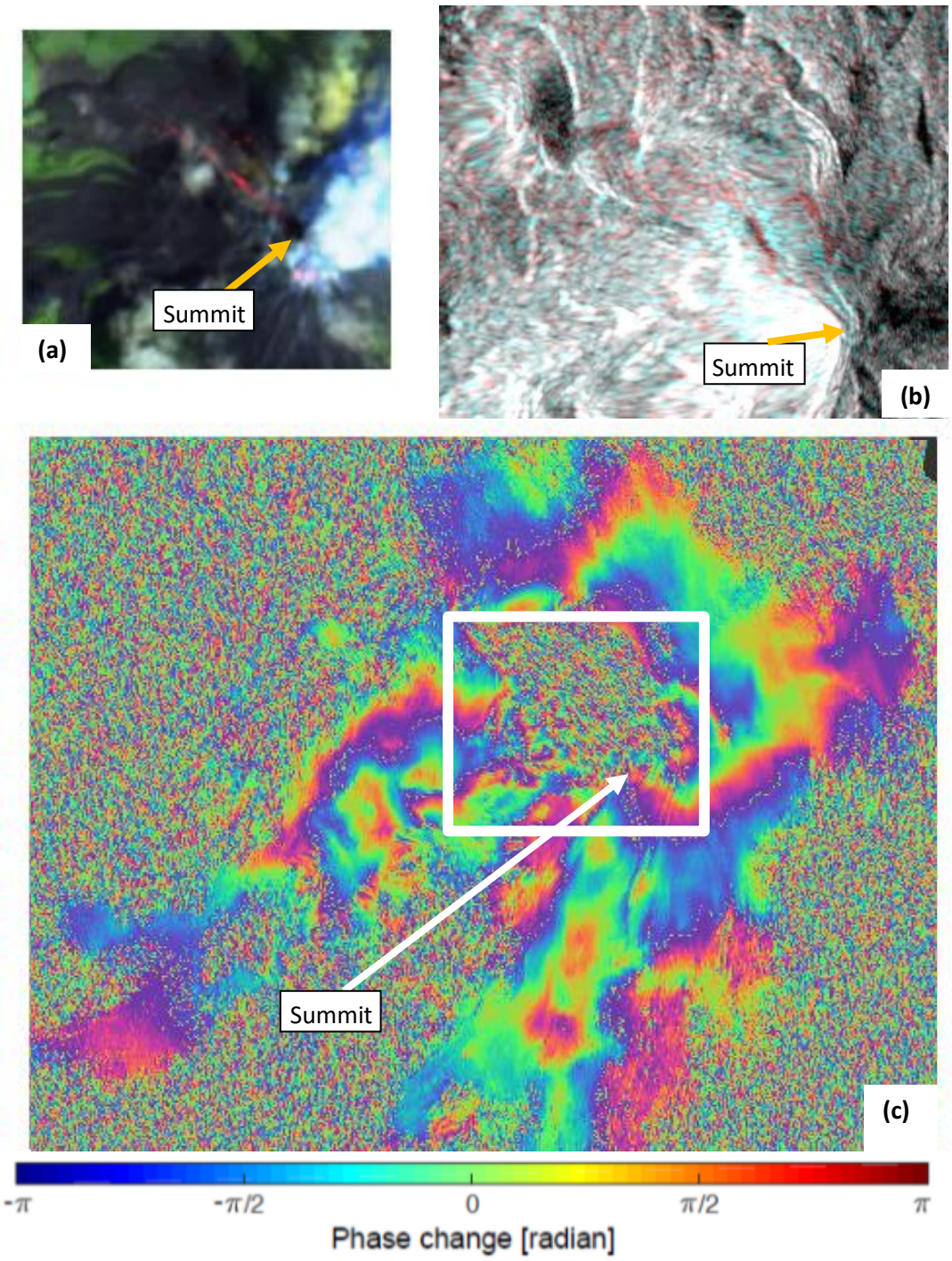

Figure. 5.1 A lava flow c. 14th December 2018, shown in (a) Sentinel-2 false colour (R-SWIR ,G-SWIR, B-Red) prominent in orange, (b) Sentinel-1A Amplitude change detection (1 month interval) as two bands of red (lava channel margins highlighted in red) and a weaker blue band (within the lava channel), and (c) Sentinel-1A wrapped InSAR (1 month interval) as a deformation pattern, with the white box denoting the area of images (a) and (b).

The bright cyan area seen on Fig. 5.1(b) corresponds with the positioning of the lava flow seen in the Sentinel-2 data (Fig. 5.1(a)), with the cyan showing rougher ground (more radar backscatter) than before, so it is likely a new blocky lava flow. The deformation signal in the InSAR image (Fig. 5.1(c)) shows a level of incoherence near the area where the lava flow is seen in the other two images. There is also a signal around the top of the southwestern flank, showing a semi-circular fringing, which is interpreted as a sign of deformation. The wrapped image shows looped rainbow fringing, where a full 2π of phase is given by a purple colour through to red, then orange, green and finishing in blue. With each change in ground height equivalent to one wave length, the fringing colour pattern begins again at purple and loops over the colours finishing at blue. The order that the colours come in denotes whether the ground has moved downwards (as listed above with purple to blue), or experienced uplift (blue to purple).

Descriptions of the nine instances of visible lava or dome-building activity in Sentinel-2 data, and their InSAR and Amplitude counterparts are show in Table 5.1. It is worth noting that the activity at Bagana shown by the dataset in Appendix D has been predominantly on the northern and north-western flanks.

The patterns seen in the Amplitude data are very reminiscent of the TerraSAR-X images in Wadge et al. (2012).[1] These images contain clear channels and pulses moving down them, with channel levees defined on each side of the lava flows. This similar structure is seen in the amplitude images in this study, with the clearest being Fig. 5.1(b) where edges of the lava flow are outlined in a clear red band on the upper flanks of Bagana.

Table 5.1 The dates of Sentinel-2 instances of identified lava flows or lava dome growth, and corresponding Sentinel-1 InSAR and Amplitude image interval dates. Each instance has notable features identified, with (S2) meaning Sentinel-2, (InSAR) for InSAR and (Amp) for Amplitude. See Appendix D for the images.

Sentinel-2	**Sentinel-1 InSAR**	**Sentinel-1 Amplitude**	**Features**	**Interpretation**
21/08/2016	Data not available	Data not available	(S2) Large flow on northern flanks and strong degassing	
07/02/2017	Data not available	Data not available	(S2) Small flow at summit and to north and strong degassing	
02/07/2017	03/06/2017-09/07/2017	03/06/2017-09/07/2017	(S2) Small flow at summit and minor degassing, (InSAR) repeated fringing seen to right of summit, (Amp) strong red pixels at summit	(InSAR) repeated fringing suggests deformation, (Amp) strong red pixels at summit suggest lava flow
03/01/2018	12/12/2017-05/01/2018	12/12/2017-05/01/2018	(S2) Small flow at summit and minor flows to north and strong degassing, (Amp) red pixels at summit with ends and edges of flows in blue	(Amp) red pixels at summit with ends and edges of flows in blue suggests lava flow
07/02/2018	17/01/2018-22/02/2018	17/01/2018-22/02/2018	(S2) Small flow to north of summit and strong degassing, (Amp) strong blue pixels from summit with red pixels at edge of flows	(Amp) red pixels at edge of flows suggest these may be the lava channel walls

07/07/2018	Not available	04/07/2018-09/08/2018	(S2) Small flow at summit and flows to north and west with strong degassing, (Amp) strong blue pixels from summit flow down northern flank terminating in a band of red pixels and small patches of blue pixels to west of summit	(Amp) strong blue pixels from summit suggest a lava flow, terminating to west of summit, showing the beginning of a change in direction of flow.
21/08/2018	16/07/2018-21/08/2018	16/07/2018-21/08/2018	(S2) Small flow from summit to the north, and degassing, (InSAR) butterfly fringing around summit with opposite directions of movement, (Amp) strong flow of blue pixels from summit down the northern flank	(InSAR) butterfly fringing around summit with opposite directions of movement could show dyke intrusion, (Amp) strong flow of blue pixels is a very active lava flow
25/10/2018	26/09/2018-01/11/2018	26/09/2018-01/11/2018	(S2) Glow seen and taken to be a flow to the north/north-west, (InSAR) a series of 2 fringes of same direction seen all around summit on three sides, (Amp) blue pixels flowing from summit to the north with red pixel edging	(InSAR) 2 fringes of same direction seen all around summit shows ground deformation deflation, (Amp) blue pixels show a lava flow and with red pixel edging shows channels

14/12/2018	13/11/2018-19/12/2018	13/11/2018-19/12/2018	(S2) Long flow from summit to north west with strong degassing, (Amp) strong flow of blue pixels from summit to the north/north-west with strong red edges to the flow	(S2) Flow north-west shows changed flow direction, (Amp) blue pixels show lava flow with strong red edges showing channel edges.

5.7.2 Comparing the Lava Flow Records with the SO_2 and Thermal Data

When compared with the SO_2 and thermal time-series on a weekly basis (Fig. 5.2), many of the peaks in the SO_2 and thermal data match with the Sentinel-1 and Sentinel-2 identified periods of lava activity. The first 4 instances of Sentinel-1 and Sentinel-2 identified lava activity are at fairly regular spacing of 5-6 months; this is not to say that the lava flows started on these dates, but that lava was present at Bagana. This correlates with the 4-5 month cyclicity found in the thermal and SO_2 data. The Sentinel-1 and Sentinel-2 instances coincide with peaks in the thermal data, and tend to precede SO_2 peaks. This is not to say that other flows have not occurred that would match the unmatched peaks in the thermal data, but they may be obscured on the Sentinel-2 images by clouds or strong degassing, so cannot be confirmed.

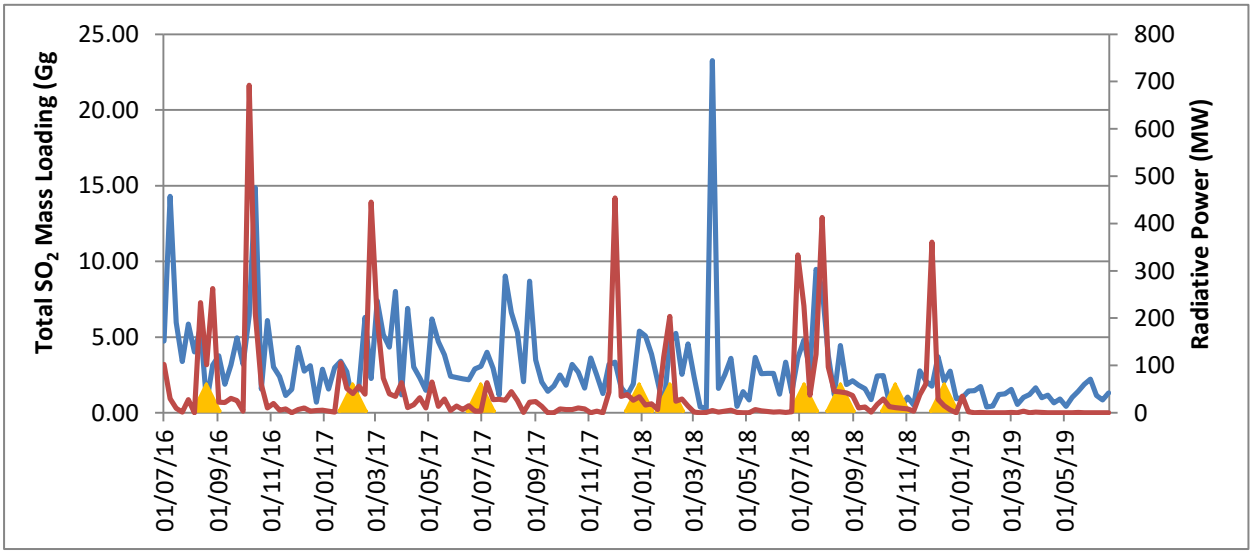

Figure. 5.2 The weekly SO_2 (blue) and thermal MIROVA (red) totals against instances of a lava flow present from the Sentinel-1 and -2 images, shown by an orange triangle on the date of the Sentinel-2 acquisition in the corresponding weekly bin.

After the fourth instance, the frequency of the Sentinel-1 and Sentinel-2 detected observations increases, with multiple examples in the latter-half of 2018. There are then no further instances for 2019, which corresponds the identified drop in SO_2 and thermal activity.

5.8 Discussion

The results would suggest that lava flows are the main cause of the peaks in thermal signature and corresponding SO_2 peaks from subsequent degassing of these flows. The InSAR data shows assumed ground deformation accompanying some of the flows, and the Amplitude data shows these flows stopping and starting in a way that the visible Sentinel-2 data alone cannot. It can also be seen that the activity at Bagana has been predominantly on the northern and north-western flanks.

The isolated SO_2 peak in March 2018 could show a change in behaviour, its arrival is also signalled by a change in the frequency of occurrences of lava flows shown by Sentinel-1 and Sentinel-2 data. For the period of a few months in mid-2018 there is the peak of SO_2 activity and nothing else. This is then followed by an increase in frequency of thermal peaks and Sentinel-1 and Sentinel-2 lava flow instances, with some increased SO_2 activity

and peaks. The second change in behaviour is exhibited from 2019, with a period of quiescence for the remainder of the time-series.

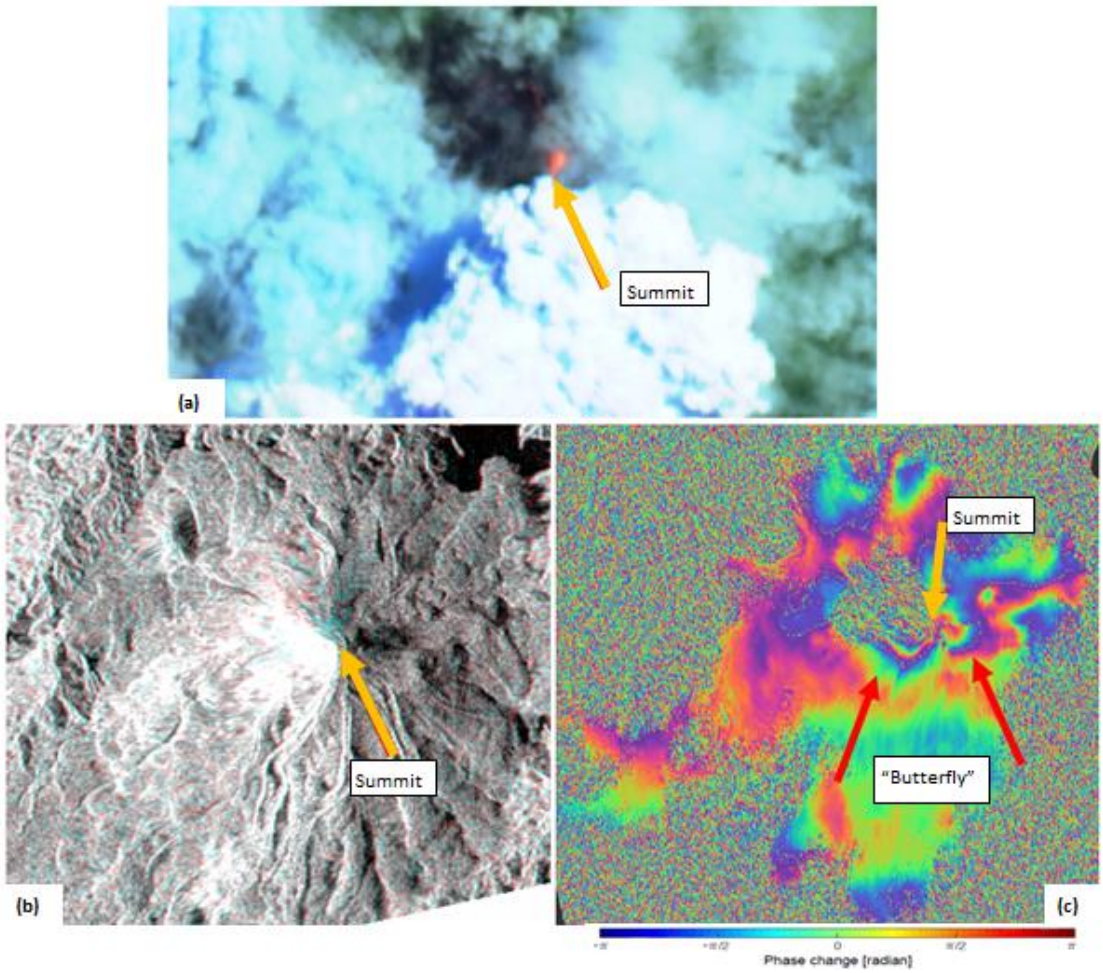

Figure 5.3 A lava flow c. 21st August 2018, shown in (a) Sentinel-2 false colour (R-SWIR ,G- SWIR ,B-Red) prominent in orange, (b) Sentinel-1A Amplitude change detection (1 month interval - 16th July 2018 - 21st August 2018) as a lobe of cyan, and (c) Sentinel-1A wrapped InSAR (1 month interval - 16th July 2018 - 21st August 2018) showing a "butterfly" deformation pattern.

The InSAR data show a "butterfly" pattern in the interval 16th July 2018 - 21st August 2018 (Fig. 5.3(c)), followed by a double fringe for the interval of 26th September 2018 - 1st November 2018, suggesting significant ground movement during this time, with two coinciding peaks from the thermal data around these dates. The butterfly pattern (Fig. 5.3(c)) strongly suggests a potential intrusion.[76] The double fringe suggests a more uniform change in ground movement across the volcano, related to the storage and release of the subsequent lava flow.

The ground movement may also be related to the change in activity, after the thermal activity recorded in the MIROVA data, around December 2018. One possible explanation is that a new lava dome is forming, and this has led to a reduction in degassing and lava flow activity for 2019. There has been a change to lava flows appearing more in the north-west than the north, where they flowed at the beginning of the time-series. Changes of direction in lava flows have been seen at SHV, where they indicated lava dome formation and were accompanied by a period of low flux.

5.9 Conclusions

The combination of these sources suggest that Bagana demonstrates three behaviours in its eruption style: firstly, a 4-6 month cycle in peaks of SO_2 and lava flow activity (shown by Amplitude and Sentinel-2 data) with elevated SO_2 background rates; secondly, periods of increased activity signalled by large SO_2 release (potential Vulcanian activity) then a reduction in SO_2 background rates accompanied by increased thermal activity and ground deformation (shown by the InSAR data); and thirdly, periods of quiescence with no thermal and low SO_2 activity. This is in contrast with previously reported two styles of activity.[1,5]

InSAR and Amplitude change detection images can be successfully deployed as an additional tool for lava flow identification. The data confirms that the SO_2 peaks are mainly tied to thermal peaks, which correspond to lava flows at Bagana. These datasets can be used to complement one another and to provide insights into eruption behaviours at Bagana, and thus potentially other volcanoes in similar settings.

Chapter Six – Conclusions

For the first time at Bagana volcano, a combination of SO_2, thermal, InSAR and Amplitude remote sensing data has been used to investigate the presence of cyclicity. This is in order to improve the understanding of the physical processes governing eruptive behaviour, and to relate the pulsatory behaviour observed at Bagana with global andesitic volcanoes in similar tectonic settings.

The most significant cycles observed during the 3-year time interval of July 2016 to June 2019 were 16 days for the SO_2 time-series, and 133 days for the thermal data. Overall, there was some matching of peaks between SO_2 and thermal data on a monthly timescale, with peaks seen at 4.5-5 month intervals, but also some discrepancies. Additionally, a notable period of quiescence has been observed since the beginning of 2019 in both datasets.

The inclusion of InSAR and Amplitude data has provided a catalogue of ground-truthing data, that has not been used alongside OMI and MIROVA data in this setting before. This combination and number of data sources is unique to this study.

The patterns of behaviour at Bagana of two eruption styles reported in previous work can be refined, with evidence to support three behaviours in Bagana's eruption style: firstly, a 4-6 month cycle in peaks of SO_2 and lava flow activity with elevated SO_2 background rates; secondly, periods of increased activity signalled by large SO_2 release followed by a reduction in SO_2 background rates accompanied by increased thermal activity and ground deformation; and thirdly, periods of quiescence with no thermal and low SO_2 activity.

In a global context, the most analogous cycles identified at other andesitic volcanoes are an 8-14 day cycle at SHV and a 1.7-7 month cycle of dome building at Popocatépetl. Both of these volcanoes support an interpretation that the shorter SO_2 cycle at Bagana is governed by a shallow-storage process, potentially conduit-based, and the thermal cycle relates to a larger scale and deeper process. This is the first time the behaviour of Bagana has been placed in this global context.

In comparison with other studies examining similar datasets and cyclicity at Bagana, this study has provided more evidence for different cycles present in SO_2 and thermal data. In addition, it supports the findings of Wadge et al. (2012) in the identification of cycles at

100 and 133 days, and a general 4.5-5 month peak in time-series data, that substantiate the evidence of an ~105 day cycle in lava flow data from TerraSAR-X.[1]

Further work at Bagana may seek to explore longer cycles at Bagana, to look for a potential SO_2 peak cycle on an anticipated multi-year time-period, as shown by the large peak in March 2018, and others recorded in McCormick Kilbride et al. (2019).[2] The analysis of a longer time period could be extended further back beyond 1st July 2016, and past 25th June 2019. However, an FFT could not be used with the gap in the dataset from June 2016, and from anomalous events in the dataset, where neighbouring volcanoes overprint the values obtained. Instead a Lomb periodogram would have to be the main method of assessing cycles, given its ability and design to deal with datasets that have an infrequent and variable sampling rate. This means there are fewer methods by which the cycles can be analysed to ascertain significance.

Additionally, further use could be made of alternative data sources in future work. The TROPOspheric Monitoring Instrument (TROPOMI) provides a finer resolution SO_2 dataset than OMI. However, due to its launch in October 2017, and not being operational until a while later, the data did not fully cover the period of interest of this study, so was not used in the time-series comparison. Shorter SO_2 cycles could also be examined, though without ground-based instruments it will be difficult to get sampling on a short enough timescale to detect them.

References

1. Wadge, G., S. Saunders and I. Itikarai, 2012: Pulsatory andesite lava flow at Bagana Volcano. Geochem., Geophys., Geosys., 13, Q11011, doi: 10.1029/2012GC004336
2. McCormick Kilbride, B. T., K. Mulina, G. Wadge, P. Webley, R. W. Johnson, I. Itikarai and M. Edmonds, 2019: Multiyear satellite observations of sulfur dioxide gas emissions and lava extrusion at Bagana volcano, Papua New Guinea. Frontiers in Earth Science, 7, doi: 10.3389/feart.2019.00009
3. Wadge, G., B. T. McCormick Kilbride, M. Edmonds and R. W. Johnson, 2018: Persistent growth of a young andesite lava cone: Bagana volcano, Papua New Guinea. Journal of Volcanology and Geothermal Research, 356. pp. 304-315, doi: 10.1016/j.jvolgeores.2018.03.012
4. Map of Bagana and surrounding ocean, Google Maps, TerraMetrics and Google, 2020. Date accessed 1/7/2020. https://goo.gl/maps/5jqnqfKtQPCqmYf18
5. McCormick, B. T., M. Edmonds, T. A. Mather, S. A. Carn, 2012: First synoptic analysis of volcanic degassing in Papua New Guinea. Geochem., Geophys., Geosys., 13, Q03008, doi: 10.1029/2011GC003945
6. Bultitude, R. J, 1976: Eruptive history of Bagana volcano, Papua New Guinea, between 1882 and 1975. R.W. Johnson (Ed.), Volcanism in Australasia, Elsevier, Amsterdam, pp. 317-336.
7. Bultitude, R. J. and R. J. S. Cooke, 1981: Note on activity from Bagana volcano from 1975 to 1980**.** R.W. Johnson (Ed.), Cooke-Ravian Volume of Volcanological Papers. Geological Survey of Papua New Guinea, Memoir 10, pp. 243-248.
8. Bultitude, R. J., R. W. Johnson, B. W. Chappell, 1978: Andesites of Bagana volcano, Papua New Guinea: chemical stratigraphy and a reference andesite composition**.** BMR J. Austr. Geol. Geophys., 3, pp. 281-295.
9. Basious, S., Panoramio (service no longer available – run by Google). Image taken in January 2013. Date accessed 1/7/2020. https://volcanohotspot.wordpress.com/2016/08/03/bagana-bougainville-island-p-n-g/
10. Newhall, C.G. and S. Self, 1982: The volcanic explosivity index (VEI): an estimate of the explosive magnitude for historical eruptions. J. Geophys. Res., 87(C2), pp. 1231–1238, doi: 10.1029/JC087iC02p01231
11. Chen, M.-C., C. Frohlich, F. W. Taylor, G. Burr and A. Quarles van Ufford, 2011: Arc segmentation and seismicity in the Solomon Islands arc, SW Pacific. Tectonophys, pp. 50747-50769, doi: 10.1016/j.tecto.2011.05.008
12. Syracuse, E. M. and G. A. Abers, 2006: Global compilation of variations in slab depth beneath arc volcanoes and implications. Geochem. Geophys. Geosys., 7(5), Q05017, doi: 10.1029/2005GC001045
13. Blake, D. H. and Y. Miezitis, 1968: Geology of Bougainville and Buka islands, New Guinea, Department of National Development, Bureau of Mineral Resources, Geology and Geophysics, Commonwealth of Australia. pp. 56.

14. Holm, R. J., G. Rosenbaum and S. W. Richards, 2016: Post 8 Ma reconstruction of Papua New Guinea and Solomon Islands: Microplate tectonics in a convergent plate boundary setting. Earth-Science Reviews, v. 156, pp. 66-81.
15. Lay, T., L. Ye, C. J. Ammon and H. Kanamori, 2017: Intraslab rupture triggering megathrust rupture coseismically in the 17 December 2016 Solomon Islands Mw 7.9 earthquake. Geophys. Res. Lett., 44, pp. 1286–1292, doi: 10.1002/2017GL072539
16. Rogerson, R. J., D. B. Hilyard, E. J. Finlayson, R. W. Johnson and C. O. McKee, 1989: The geology and mineral resources of Bougainville and Buka Islands, Papua New Guinea. Geological Survey of Papua New Guinea, Memoir 16, pp. 217.
17. Bultitude, R.J., 1981: Literature search for pre-1945 sightings of volcanoes and their activity on Bougainville Island. R.W. Johnson (Ed.), Cooke-Ravian Volume of Volcanological Papers. Geological Survey of Papua New Guinea, Memoir, vol. 10, pp. 227-242.
18. Guppy, H.B., 1887: The Solomon Islands: Their Geology, General Features and Suitability for Colonisation**,** vol. 21–22, Swan, Sonnenschein, Lowery and Company, London.
19. Mendoza-Rosas, A. T., A. Gómez -Vazquez and S. de la Cruz-Reyna, 2017: Statistical analysis of the sustained lava dome emplacement and destruction processes at Popocatépetl volcano, Central Mexico. Bulletin of Volcanology, 79 (6), 43, doi: 10.1007/s00445-017-1127-7
20. Gómez-Vazquez, A., S. De la Cruz-Reyna and A. T. Mendoza-Rosas, 2016: The ongoing dome emplacement and destruction cyclic process at Popocatépetl volcano, Central Mexico. Bulletin of Volcanology, 78 (58), doi: 10.1007/s00445-016-1054-z
21. Campion, R., H. Delgado-Granados, D. Legrand, N. Taquet, T. Boulesteix, S. Pedraza-Espitia and T. Lecocq, 2018: Breathing and coughing: The extraordinarily high degassing of Popocatépetl investigated with an SO_2 camera. Frontiers of Earth Sciences, 6, 163, doi: 10.3389/feart.2018.00163
22. Popocatépetl, Global Volcanism Project, 2019. Date accessed 01/02/2019. https://volcano.si.edu/volcano.cfm?vn=341090
23. Sanderson, R. W., J. B. Johnson and J. M. Lees, 2010: Ultra-long period seismic signals and cyclic deflation coincident with eruptions at Santiaguito, Guatemala. Journal of Volcanology and Geothermal Research, 198 (1-2), 35-44, doi: 10.1016/j.jvolgeores.2010.08.007
24. Johnson, J. B., J. J. Lyons, B. J. Andrews and J. M. Lees, 2014: Explosive dome eruptions modulated by periodic gas-driven inflation. Geophysical Research Letters, 41, 19, doi: 10.1002/2014GL061310
25. Johnson, J. B. and J. M. Lees, 2010: Sound produced by the rapidly inflating Santiaguito lava dome, Guatemala. Geophysical Research Letters, 37, 22, doi: 10.1029/2010GL045217
26. Harris, A. J. L., W. I. Rose and L. P. Flynn, 2003: Temporal trends in lava dome extrusion at Santiaguito 1922-2000. Bulletin of Volcanology, 65 (2-3), pp. 77-89, doi: 10.1007/s00445-002-0243-0

27. Genco, R., and M. Ripepe, 2010: Inflation-deflation cycles revealed by tilt and seismic records at Stromboli volcano. Geophysical Research Letters, 37, 12, doi: 10.1029/2010GL042925
28. Nishimura, T., M. Iguchi and M. Hendrasto, 2012: Activity of vulcanian eruptions at Sakurajima, Suwanosejima and Semeru volcanoes observed by seismic and geodetic measurements. AGU, Fall Meeting 2012, abstract ID: V31G-01.
29. Wadge, G., B. Voight, R. S. J. Sparks, P. D. Cole, S. C. Loughlin and R. E. A. Robertson, 2014: An overview of the eruption of SHV from 2000-2010. Geological Society London Memoirs, 39, pp. 1-40, doi: 10.1144/M39.1
30. Nicholson, E. J., T. A. Mather, D. M. Pyle, H. M. Odbert and T. Christopher, 2013: Cyclical patterns in volcanic degassing revealed by SO_2 flux time series analysis, Soufrière Hills Volcano, Montserrat. Earth and Planetary Science Letters, 375, pp. 209-221, doi: 10.1016/j.epsl.2013.05.032
31. Odbert, H. M., R. C. Stewart and G. Wadge, 2014: Cyclic phenomena at Soufrière Hills Volcano, Montserrat. Geological Society London Memoirs, 39, pp. 41-60, doi: 10.1144/M39
32. Flower, V. J. B. and S. A. Carn, 2015: Characterising volcanic cycles at Soufrière Hills Volcano: time-series analysis of multi-parameter satellite data. Journal of Volcanology and Geothermal Research, 304, pp. 82-93, doi: 10.1016/j.jvolgeores.2015.07.035
33. Voight, B. and co-authors, 1999: Magma Flow Instability and Cyclic Activity at Soufriere Hills Volcano, Montserrat, British West Indies. Science, 283 (5405), pp. 1138-1142, doi: 10.1126/science.283.5405.1138
34. Sparks, R. S. J. and S. R. Young, 2002: The eruption of Soufrière Hills Volcano, Montserrat (1995–1999): overview of scientific results. T. H. Druitt and B. P. Kokelaar (Eds), The Eruption of Soufrière Hills Volcano, Montserrat from 1995 to 1999, doi: 10.1144/GSL.MEM.2002.021.01.03
35. Costa, A., G. Wadge, R. Stewart and H. Odbert, 2013: Coupled sub-daily and multiweek cycles during the lava dome eruption of Soufrière Hills Volcano, Montserrat. Journal of Geophysical Research: Solid Earth, 118 (5), doi: 10.1002/jgrb.50095
36. Lamb, O. D., N. R. Varley, T. A. Mather, D. M. Pyle, P. J. Smith and E. J. Liu, 2014: Multiple timescales of cyclical behaviour observed at two dome-forming eruptions. Journal of Volcanology and Geothermal Research, 284, pp. 106-121, doi: 10.1016/j.jvolgeores.2014.07.013
37. Hautmann, S., J. Gottsmann, R. S. J. Sparks, A. Costa, O. Melnik and B. Voight, 2008: Modelling ground deformation caused by oscillating overpressure in a dyke conduit at Soufrière Hills Volcano, Montserrat. Tectonophysics, 471, pp. 87-95, doi: 10.1016/j.tecto.2008.10.021
38. OMSO2 README File v1.3.0, NASA, released 26/2/2008, updated 16/6/2016. https://aura.gesdisc.eosdis.nasa.gov/data/Aura_OMI_Level2/OMSO2.003/doc/README.OM SO2.pdf

39. Earthdata, NASA, 2018. Date accessed 1/12/2018. https://search.earthdata.nasa.gov/search/granules
40. Li, C., J. Joiner, N. A. Krotkov and P. K. Bhartia, 2013: A fast and sensitive new satellite SO_2 retrieval algorithm based on principal component analysis: Application to the ozone monitoring instrument. Geophys. Res. Lett., 40, 63146318, doi: 10.1002/2013GL058134
41. OMPIXCOR README FILE, NASA, released 6/12/2010. https://aura.gesdisc.eosdis.nasa.gov/data/Aura_OMI_Level2/OMPIXCOR.003/doc/README. OMPIXCOR.pdf
42. Sea Surface Temperature, NASA Earth Observations, NASA. Date accessed 1/7/2020. https://neo.sci.gsfc.nasa.gov/view.php?datasetId=MYD28M
43. Ozone Monitoring Instrument (OMI) Data User's Guide, NASA, released 5/1/2012. https://docserver.gesdisc.eosdis.nasa.gov/repository/Mission/OMI/3.3_ScienceDataProduct Documentation/3.3.2_ProductRequirements_Designs/README.OMI_DUG.pdf
44. Veefkind, P. and M. Sneep, released 20/3/2009: OMCLDO2 README file. http://projects.knmi.nl/omi/research/product/product_generator.php?info=read&product= Cloud&flavour=OMCLDO2&long=Cloud%20Pressure%20and%20Fraction%20using%20O%3C sub%3E2%3C/sub%3E-O%3Csub%3E2%3C/sub%3E%20absorption
45. Wang, Y. and C. Zhao, 2016: Can MODIS cloud fraction fully represent the diurnal and seasonal variations at DOE ARM SGP and Manus sites? J. Geophys. Res. Atmos., 122, pp. 329-343, doi: 10.1002/2016JD025954
46. Li, C., N. A. Krotkov, S. Carn, Y. Zhang, R. J. D. Spurr and J. Joiner, 2017: New-generation NASA Aura Ozone Monitoring Instrument (OMI) volcanic SO_2 dataset: algorithm description, initial results, and continuation with the Suomi-NPP Ozone Mapping and Profiler Suite (OMPS). Atmospheric Measurement Techniques, 10, pp. 445-458, doi: 10.5194/amt-10-445-2017
47. Fioletov, V. E., C. A. McLinden, N. Krotkov, J. Joiner, N. Theys, S. Carn and M. D. Moran, 2016: A global catalogue of large SO_2 sources and emissions derived from the Ozone Monitoring Instrument. Atmospheric Chemistry and Physics, 16, 11497-11519, doi: 10.5194/acp-16-11497-2016
48. OMI SO_2 AMF calculations, NASA, 2018. Date Accessed 30/4/2018. https://so2.gsfc.nasa.gov/Documentation/OMSO2AMFcorrections.pdf
49. McCormick Kilbride, B., personal communication with author, via email, March 2020.
50. Carn, S. A., V. E. Fioletov, C. A. McLinden, C. Li and N. A. Krotkov, 2017: A decade of global volcanic SO_2 emissions measured from space. Sci. Rep., 7, 44095, doi: 10.1038/srep44095
51. Carn, S., personal communication with author, via email, March 2018.
52. Crockett, R., 2019: A Primer on Fourier Analysis for the Geosciences. Cambridge University Press, pp. 191, doi: 10.1017/9781316543818

53. Carr, B. B., A. B. Clarke, M. de Michieli Vitturi, 2018: Earthquake induced variations in extrusion rate: A numerical modelling approach to the 2006 eruption of Merapi Volcano. Earth and Planetary Science Letters, 482, pp. 377-387, doi: 10.1016/j.epsl.2017.11.019
54. Luhr, J. F. and I. S. E. Carmichael, 1980: The Colima Volcanic Complex, Mexico. Contributions to Mineralogy and Petrology, 71 (4), 343372, doi: 10.1007/BF00374707
55. Reubi, O., J. Blundy and N. Varley, 2013: Volatiles contents, degassing and crystallisation of intermediate magmas at Volcán de Colima, Mexico, inferred from melt inclusions. Contributions to Mineralogy and Petrology, 165, 6, doi: 10.1007/s00410-013-0849-6
56. Luhr, J. F., 2002: Petrology and geochemistry of the 1991 and 1998-1999 lava flows from Volcán de Colima, Mexico: implications for the end of the current eruptive cycle. Journal of Volcanology and Geothermal Research, 117 (1-2), pp. 169-194, doi: 10.1016/S0377-0273(02)002317
57. Reyes-Dávila, G. A. and co-authors, 2016: Volcán de Colima dome collapse of July, 2015 and associated pyroclastic density currents. Journal of Volcanology and Geothermal Research, 320, pp. 100-106, doi: 10.1016/j.jvolgeores.2016.04.015
58. Saucedo,R. and co-authors, 2010: Eyewitness, stratigraphy, chemistry, and eruptive dynamics of the 1913 Plinian eruption of Volcán de Colima, México. Journal of Volcanology and Geothermal Research, 191(3-4), pp. 149-166, doi: 10.1016/j.jvolgeores.2010.01.011
59. Sahetapy-Engel, S. T and A. J. L. Harris, 2009: Thermal structure and heat loss at the summit crater of an active lava dome. Bulletin of Volcanology, 71 (1), pp. 15-28, doi: 10.1007/s00445-008-0204-3
60. Holland, A. S. P., I. M. Watson, J. C. Philips, L. Caricchi and M. P. Dalton, 2011: Degassing processes during lava dome growth: Insights from Santiaguito lava dome, Guatemala. Journal of Volcanology and Geothermal Research, 202 (1-2), pp. 153-166, doi: 10.1016/j.jvolgeores.2011.02.004
61. Voight, B., E. K. Constantine, S. Siswowidjoyo and R. Torley, 2000: Historical eruptions of Merapi Volcano, Central Java, Indonesia, 1768-1998. Journal of Volcanology and Geothermal Research, 100 (1-4), pp. 69-138, doi: 10.1016/S0377-0273(00)00134-7
62. Gertisser, R. and J. Keller, 2003: Temporal variations in magma composition at Merapi Volcano: magmatic cycles during past 2000 years of explosive activity. Journal of Volcanology and Geothermal Research, 123 (1-2), pp. 1-23, doi: 10.1016/S0377-0273(03)00025-8
63. Ratdomopurbo, A. and co-authors, 2013: Overview of the 2006 eruption of Mt. Merapi. Journal of Volcanology and Geothermal Research, 261, pp. 87-97, doi: 10.1016/j.jvolgeores.2013.03.019
64. Thouret, J. C., F. Lavigne, K. Kelfoun and S. Bronto, 2000: Toward a revised hazard assessment at Merapi volcano. Journal of Volcanology and Geothermal Research, 100 (1-4), pp. 479-502, doi: 10.1016/S0377-0273(00)00152-9
65. MIROVA. Date accessed 1/2/2020. http://www.mirovaweb.it/?action=about

66. Wooster, M. J., B. Zhukov and D. Oertel, 2003: Fire radiative energy for quantitative study of biomass burning: derivation from the BIRD experimental satellite and comparison to MODIS fire products. Remote Sensing of Environment, 86(1), pp. 83-107.
67. Moderate Resolution Imaging Spectrometer, About, NASA. Date accessed 1/2/2020. https://modis.gsfc.nasa.gov/about/
68. Near Real Time Volcanic Hotspot Detection System. Date accessed 1/2/2020. http://www.mirovaweb.it/
69. Flower, V. J. B., S. A. Carn and R. Wright, 2016: The impact of satellite sensor viewing geometry on time-series analysis of volcanic emissions. Remote Sens. Environ. 183, pp 282–293, doi: 10.1016/j.rse.2016.05.022
70. Sentinel 1, ESA, 2020. Date accessed 1/3/2020. https://sentinel.esa.int/web/sentinel/missions/sentinel-1
71. Copernicus Open Access Hub, ESA, 2020. Date accessed 1/3/2020. https://scihub.copernicus.eu/dhus/#/home
72. Sentinel Playground, Sentinel Hub, ESA, 2020. Date accessed 1/3/2020. https://www.sentinel-hub.com/explore/sentinel-playground
73. Training Kit HAZA03, Land Subsidence with Sentinel-1 using SNAP, ESA, 2020. Date accessed 1/3/2020. https://rus-copernicus.eu/portal/wp-content/uploads/library/education/training/HAZA03_LandSubsidence_MexicoCity_Tutorial.pdf
74. The TanDEM-X 90m Digital Elevation Model, 2019. Date accessed 16/02/2019. https://geoservice.dlr.de/web/dataguide/tdm90/
75. STEP, Science Toolbox Exploitation Platform, Download, ESA, 2018. Date accessed 1/4/18. https://step.esa.int/main/download/
76. Salzer, J. T., M. Nikkhoo, T. R. Walter, H. Sudhaus, G. Reyes-Dávila, M. Breton and R. Arambula, 2014: Satellite radar data reveal short term pre-explosive displacements and a complex conduit system at Volcán de Colima, Mexico. Frontiers in Earth Science, 2, 12, doi: 10.3389/feart.2014.00012

Glossary of Terms

AMF – Air Mass Factor

a.s.l. – Above Sea Level

BRD – Band Residual Difference

CI – Confidence Interval

CMA – Centre of Mass Altitude

CSV – Comma Separated File

dB – decibel

DEM – Digital Elevation Model

DFT – Discrete Fourier Transform

DOAS – Differential Optical Absorption Spectrometer

DU – Dobson Unit

ESA – European Space Agency

FFT – Fast Fourier Transform

FoV75 – Field of View 75%

FT – Fourier Transform

GES DISC – Goddard Earth Sciences Data and Information Services Center

GRD – Ground Range Detected

InSAR – Interferometric Synthetic Aperture Radar

km – kilometres

kt – kilotonnes

m – metres

MIR – Middle Infra-Red

MIROVA – Middle InfraRed Observation of Volcanic Activity

mm – millimetres

MODIS – Moderate Resolution Imaging Spectroradiometer

MODVOLC - (not an acronym, but a name of an algorithm)

NASA – National Aeronautics and Space Administration

nm – nanometres

OMI – Ozone Monitoring Instrument

OMPS - Ozone Mapping and Profiler Suite

ORA – OMI Row Anomaly

O2 – Oxygen

PBL – Planetary Boundary Layer

PCA – Principal Component Analysis

RCF – Radiative Cloud Fraction

RGB – Red, Green, Blue

s – seconds

SAR – Synthetic Aperture Radar

SHV – Soufrière Hills Volcano

SLC – Single Look Complex

SNAP – Sentinel Applications Platform Toolbox

SO_2 – Sulphur Dioxide

SRTM – Shuttle Radar Topography Mission

SZA – Solar Zenith Angle

TOMS – Total Ozone Mapping Spectrometer

TRL – Lower Tropospheric Layer

TROPOMI - TROPOspheric Monitoring Instrument

UTC – Coordinated Universal Time

UV – Ultraviolet

UV-DOAS – Ultraviolet Differential Optical Absorption Spectroscopy

VEI – Volcanic Explosivity Index

3D – 3-Dimensional

Acknowledgements

Thank you to Andrew Prata and Catherine Hale for their invaluable advice on OMI SO_2 processing. Thank you to Brendan McCormick Kilbride for the provision of data for comparisons drawn in the analysis of the OMI SO_2 data. Thank you to the Monitoring Committee (Helen Dacre and Jon Blower) for their advice on the progress of this study. Thank you to BGS and the University of Reading for the funding to complete this study. Thank you to the two supervisors to this study, Geoff Wadge and Julia Crummy. And thank you to family and friends for reading the thesis and providing support (Ellen Couchman-Crook, Michael Couchman-Crook, Tom Halliday and Levi Curry).

Appendix A – OMI code

This is the Python code used to process the OMI SO_2 totals for Chapter 2.

```
# -*- coding: utf-8 -*-

import h5py
import numpy as np

# Read in OMI SO2 data
path = '<insert_path_to_file>'
fn = '<insert_file_name>'
dataset = h5py.File(path+fn,'r')
data_fields = dataset['HDFEOS']['SWATHS']['OMI Total Column Amount SO2']['Data Fields']
geo_fields = dataset['HDFEOS']['SWATHS']['OMI Total Column Amount SO2']['Geolocation Fields']
so2_pbl = data_fields['ColumnAmountSO2_PBL'][:, :] # changed from BRD
rad_cld_frac = data_fields['RadiativeCloudFraction'][:, :]
lats = geo_fields['Latitude'][:, :]
lons = geo_fields['Longitude'][:, :]
time = geo_fields['Time'][:]
dataset.close()

nadir_lats = lats[:, 29]

so2_data = so2_pbl

# Mask missing and fill values
fill_value = -1.2676506E30  # note this is the same as the missing value
so2_data_ma = np.ma.masked_equal(so2_data, fill_value)

# Mask row anomalies & discard exterior pixel for better data quality
so2_data_ma[:, 0:3] = np.ma.masked
so2_data_ma[:, 54:59] = np.ma.masked
# Anomaly 1: 53-54 (Since June 25th, 2007)
so2_data_ma[:, 53:54] = np.ma.masked
# Anomaly 2: 37-44 (Since May 11th, 2008)
so2_data_ma[:, 37:44] = np.ma.masked
# Anomaly 3: 27-44 (Since January 24th, 2009)
so2_data_ma[:, 27:44] = np.ma.masked
# Anomaly 4: 42-45 (Since July 5th, 2011)
so2_data_ma[:, 42:45] = np.ma.masked
# Anomaly 5: 41-45 (Since August 9, 2011)
so2_data_ma[:, 41:45] = np.ma.masked
# Suspected Anomaly 6: 26-27 (28 March, 2017)
#so2_data_ma[:, 26:27] = np.ma.masked

# Mask noise
so2_noise = 0.5  # [DU]
so2_data_ma = np.ma.masked_where(so2_data_ma <= so2_noise, so2_data_ma)

# Mask data with radiative cloud fraction greater than or equal to 0.3
so2_data_ma = np.ma.masked_where(rad_cld_frac >= 0.3, so2_data_ma)

ma_extent = [153.8, 156.3, -7.4, -4.7] # Box around Bagana

lons_ma, lats_ma = lons, lats

```

```
# Mask values outside latitude range (defined in ma_extent array).
lats_ma = np.ma.masked_outside(lats, ma_extent[2], ma_extent[3])
# Apply mask of lats to so2 and lons arrays
so2_data_ma = np.ma.masked_where(np.ma.getmask(lats_ma), so2_data_ma)
lons_ma = np.ma.masked_where(np.ma.getmask(lats_ma), lons)
# Mask values outside longitude range (defined in ma_extent array).
lons_ma = np.ma.masked_outside(lons_ma, ma_extent[0], ma_extent[1])
# Apply mask of lons to so2 and lats arrays
so2_data_ma = np.ma.masked_where(np.ma.getmask(lons_ma), so2_data_ma)
lats_ma = np.ma.masked_where(np.ma.getmask(lons_ma), lats_ma)

# Read in OMI pixel coordinates
fn_pix = '<insert_name_of_OMPIXCOR_file>'
dataset_pix = h5py.File(path+fn_pix,'r')
data_fields_pix = dataset_pix['HDFEOS']['SWATHS']['OMI Ground Pixel Corners UV-2']['Data Fields']
omi_pix = data_fields_pix['FoV75Area'][:]
dataset_pix.close()

total_mass_loading = 0.

for i in range(so2_data.shape[0]):
    for j in range(so2_data.shape[1]):
        row_area = omi_pix[j] * 1000000.  # convert km^2 to m^2
        # along sum non-masked pixels
        if so2_data_ma[i, j]:
            so2_mass = so2_data_ma[i, j] * (row_area) * 2.86e-2 * (0.36/0.547)  #  so2 mass [g] = area [m^2] * mass_per_unit_area [g m^-2] * cor.AMF
            # sum total mass
            total_mass_loading = total_mass_loading + so2_mass

total_mass_loading = total_mass_loading
print (total_mass_loading) # Print to get total in grams
```

Appendix B – Cloud Cover

Examples of the cloud cover scenes from Aqua-MODIS. The minimal cloud scenes are a rarity in the region, with most scenes being classified as mostly or totally cloudy. Bougainville Island is outlined in yellow and Bagana is near the middle

Minimal:
(0-15%)

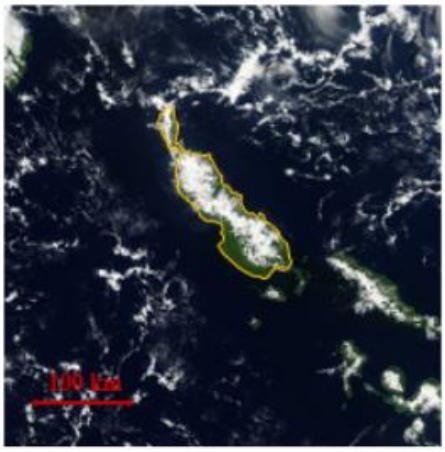

Mostly:
(40-80%)

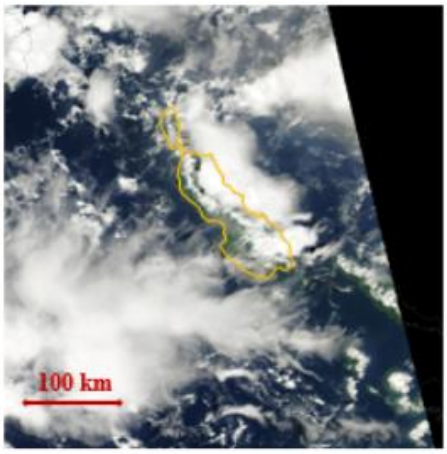

Partial:
(15-40%)

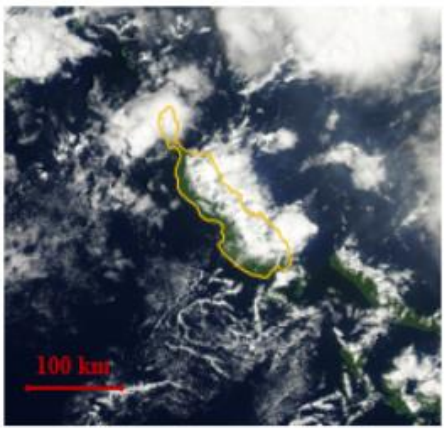

Total:
(80-100%)

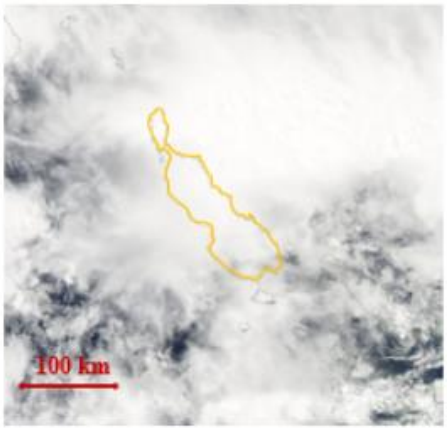

Appendix C – Change Detection Processing

The processing chain for the change detection images with Sentinel-1 data using the SNAP Toolbox.

Calibration Step: *Radar > Radiometric > Calibrate*

Cropping image Step: *Raster > Subset*

Terrain Correction Step: *Radar > Geometric > Terrain > Range-Doppler Correction*

Convert Values to Decibel Step: *Raster > Data Conversion > Convert to/from dB*

Co-registration Step: *Radar > Coregistration > Stack Tools > Create Stack*

RGB Image Creation Step: *Image 1 > R, Image 2 > G & B*

Appendix D – Sentinel-1 and Sentinel-2 Images

The red arrows on each picture indicate the features highlighted in Table 5.1.

D.A. Sentinel-2 - 2016-08-21, Sentinel-1 - unavailable

D.B. Sentinel-2 - 2017-02-07, Sentinel-1 - unavailable

D.C. Sentinel-2 - 2017-07-02, Sentinel-1 InSAR - 2017-06-03 to 2017-07-09, Sentinel-1 Amplitude - 2017-06-03 to 2017-07-09

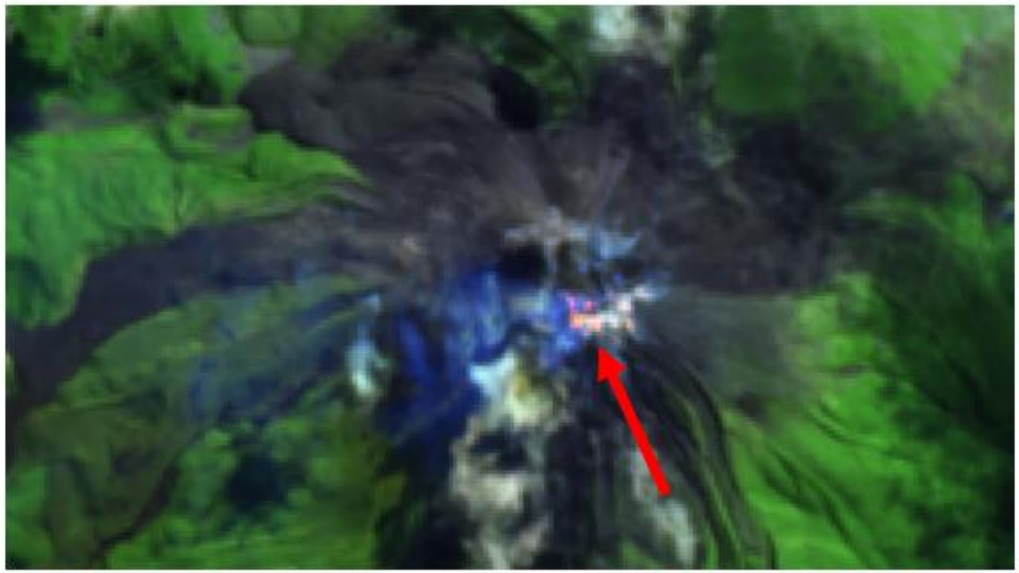

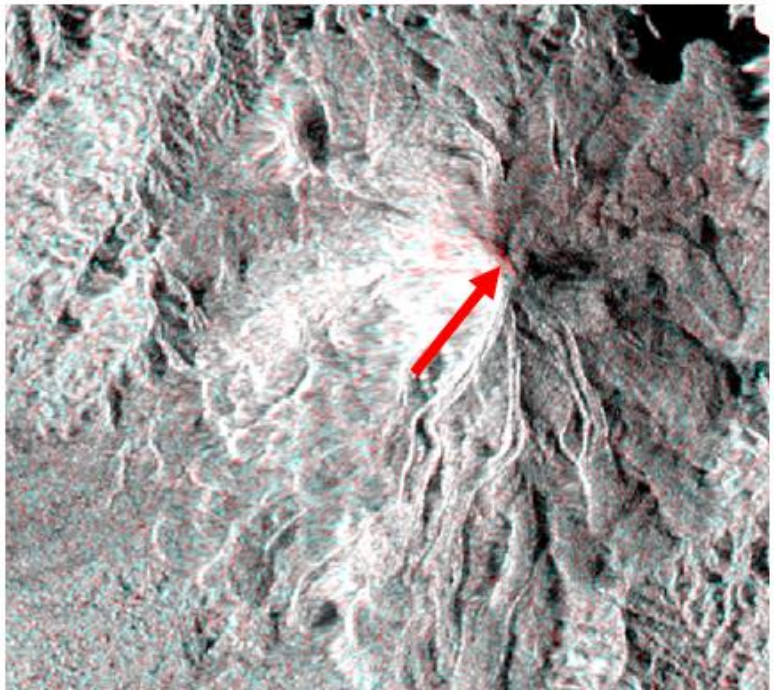

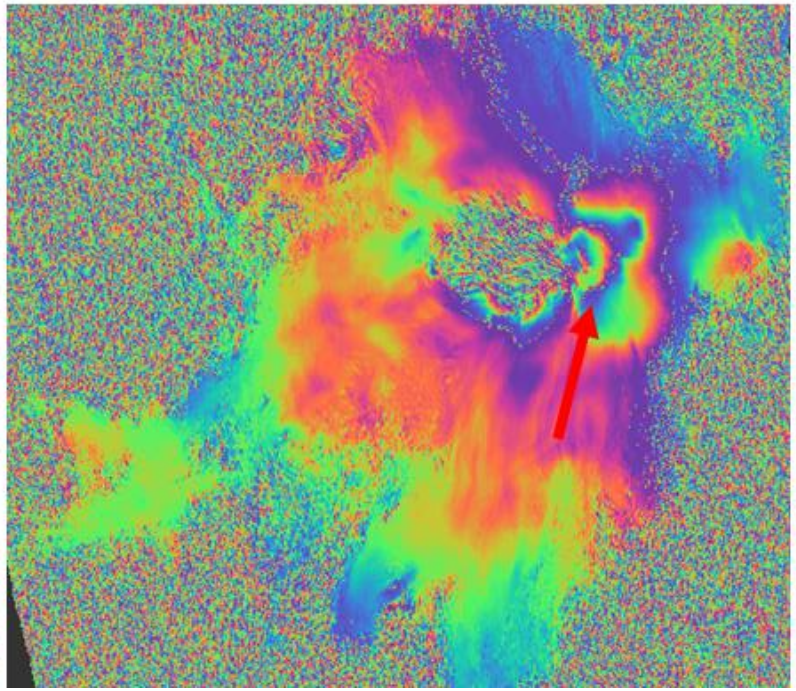

D.D. Sentinel-2 - 2018-01-03, Sentinel-1 InSAR - 2017-12-12 to 2018-01-05, Sentinel-1 Amplitude - 2017-12-12 to 2018-01-05

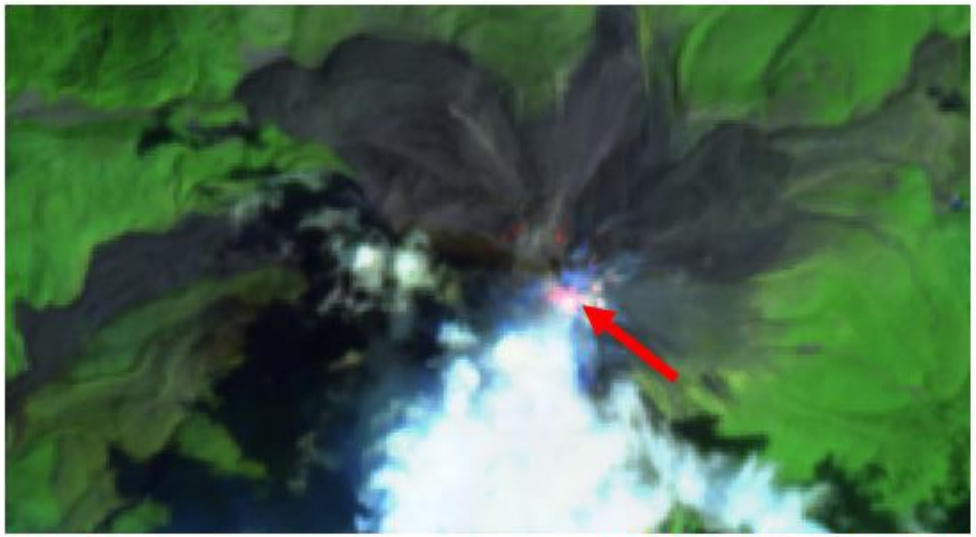

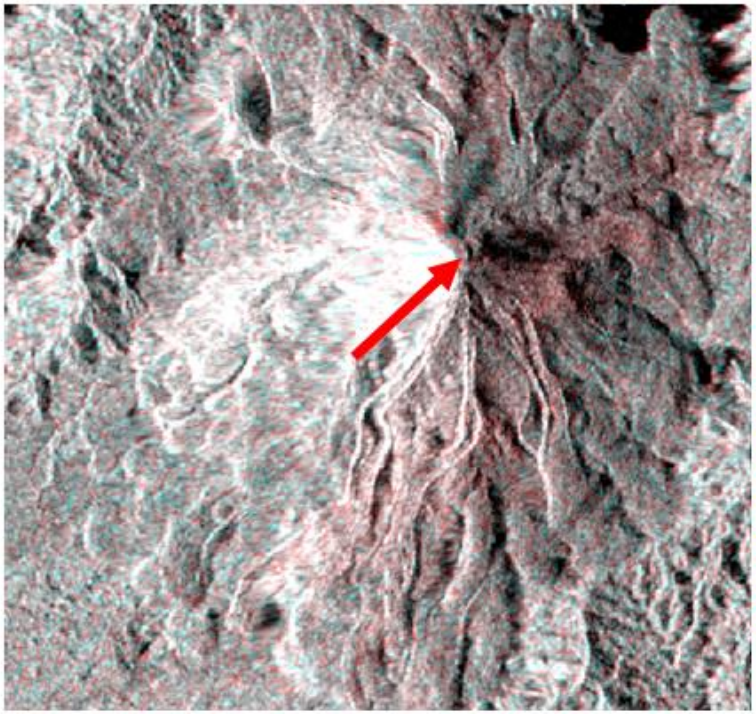

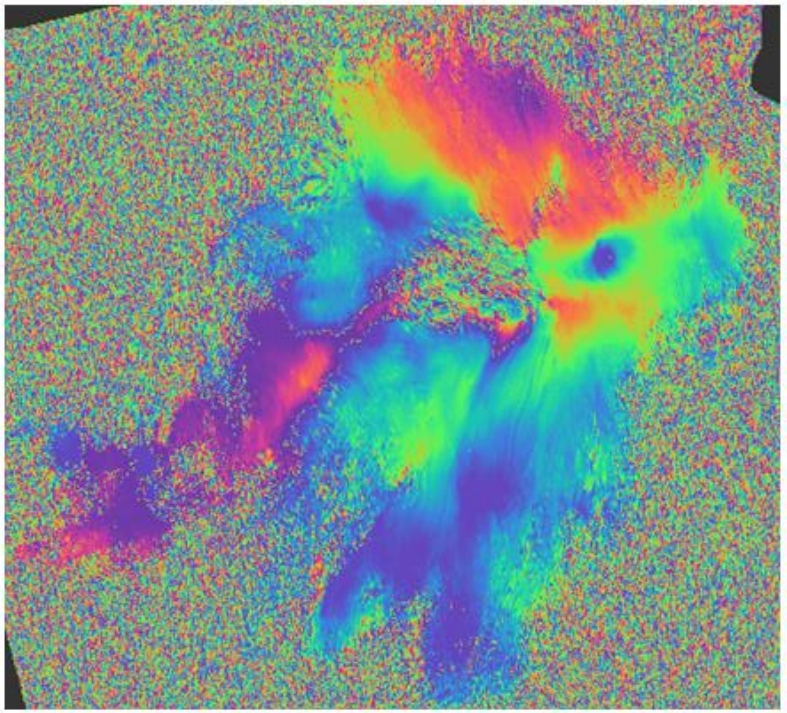

D.E. Sentinel-2 - 2018-02-07, Sentinel-1 InSAR – 2018-01-17 to 2018-02-22, Sentinel-1 Amplitude - 2018-01-17 to 2018-02-22

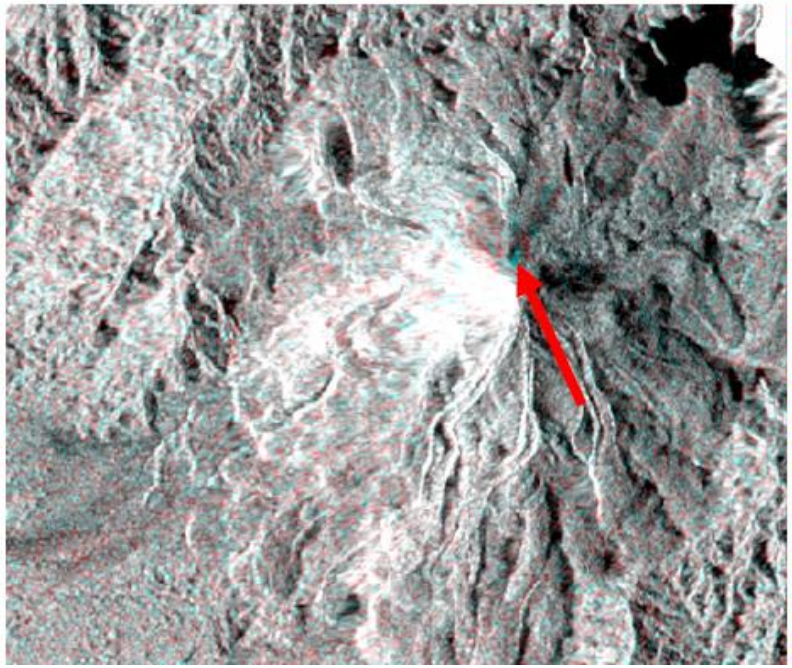

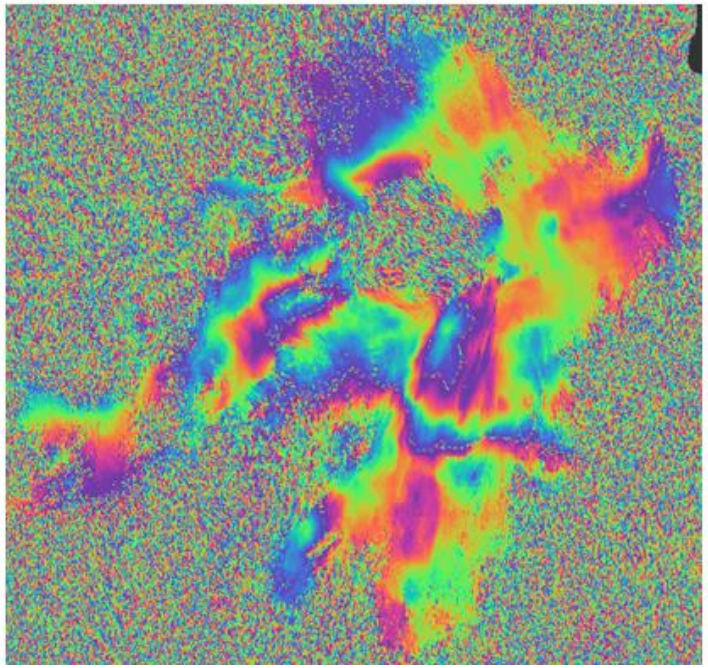

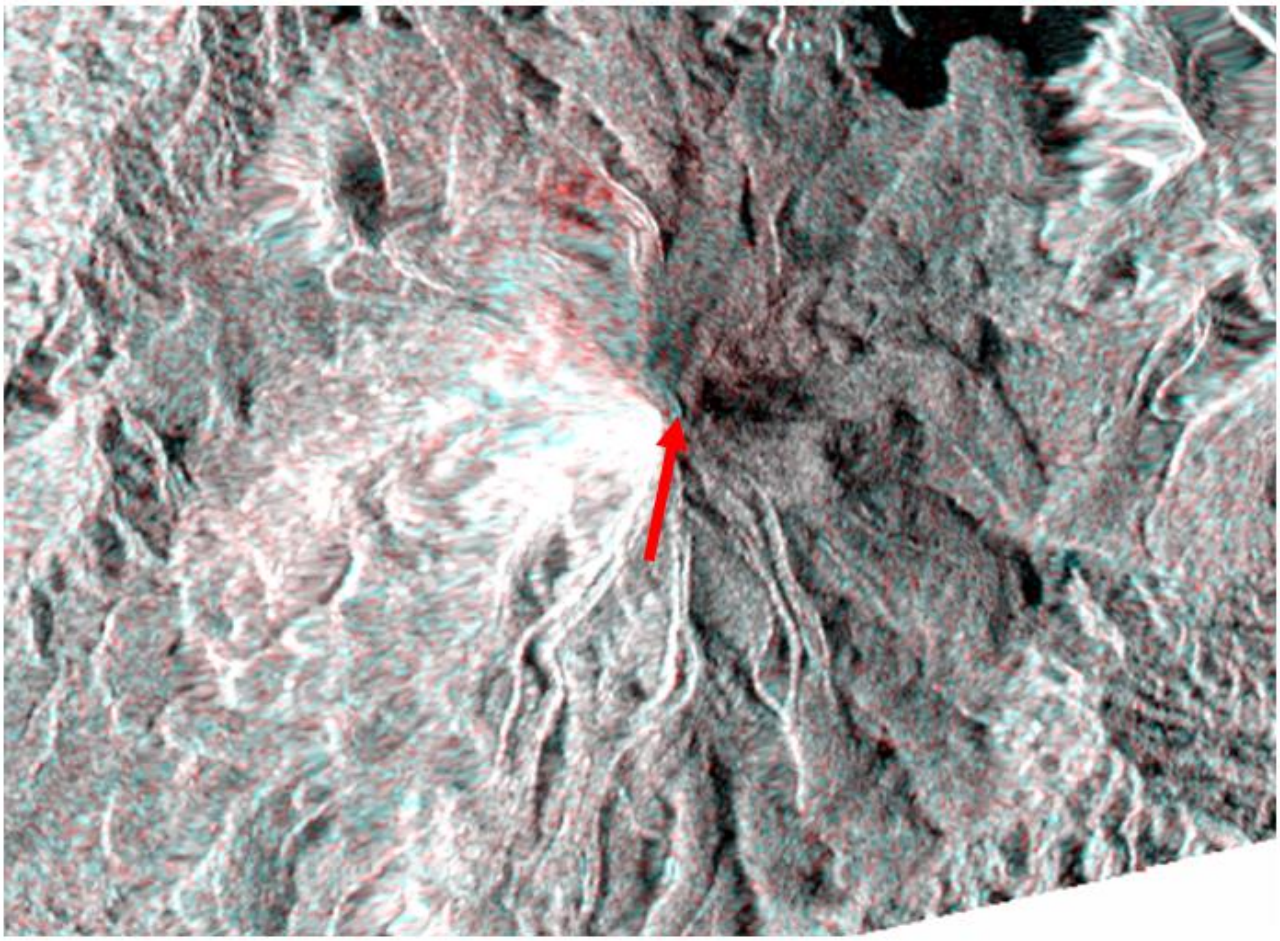

D.F. Sentinel-2 - 2018-07-0, Sentinel-1 Amplitude - 2018-07-04 to 2018-08-09

D.G. Sentinel-2 - 2018-08-21, Sentinel-1 InSAR - 2018-07-16 to 2018-08-21, Sentinel-1 Amplitude - 2018-07-16 to 2018-08-21

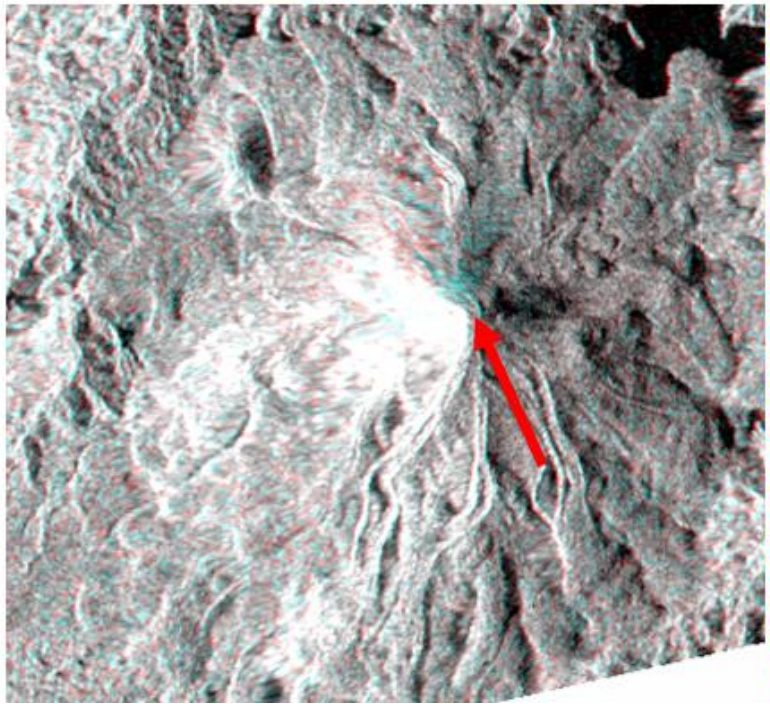

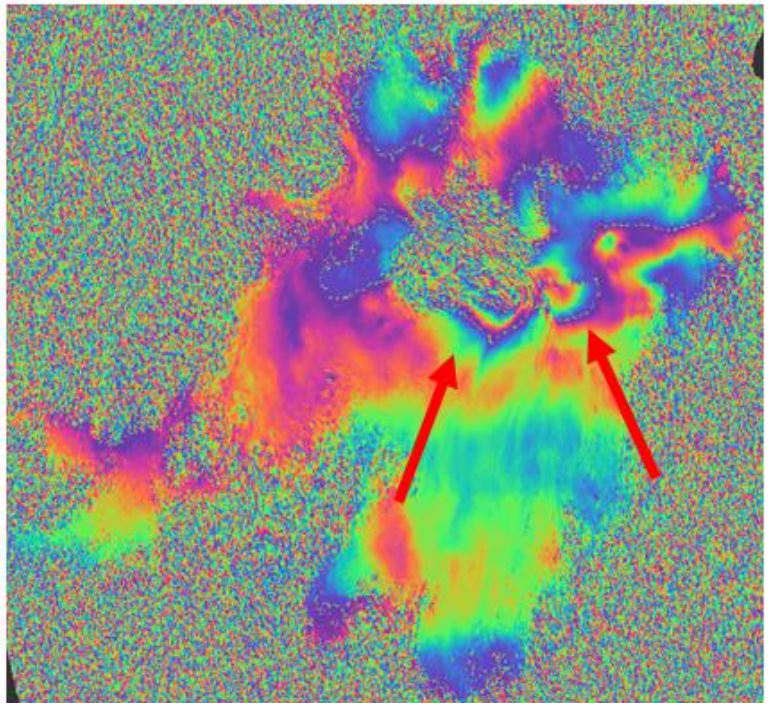

D.H. Sentinel-2 - 2018-10-25, Sentinel-1 InSAR - 2018-09-26 to 2018-11-01, Sentinel-1 Amplitude - 2018-09-26 to 2018-11-01

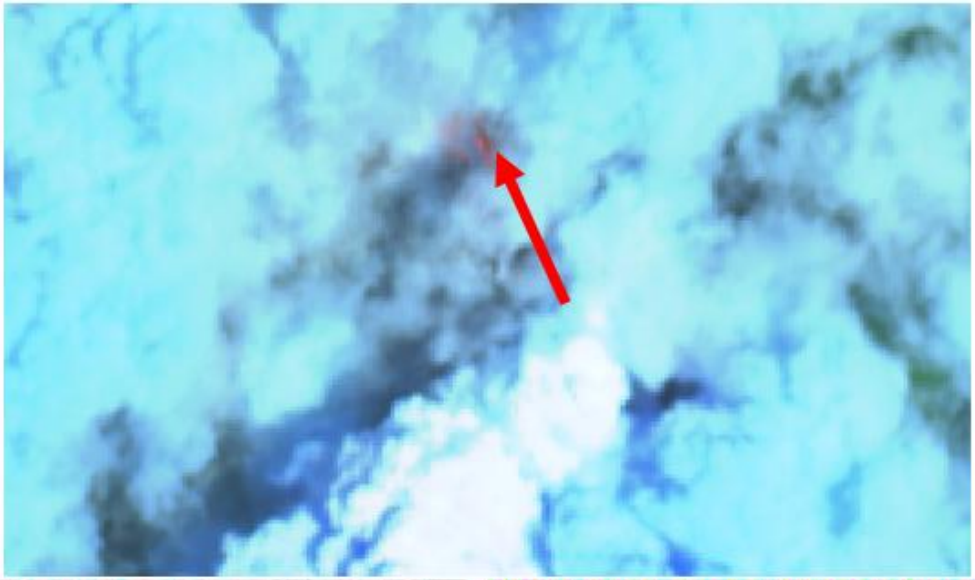

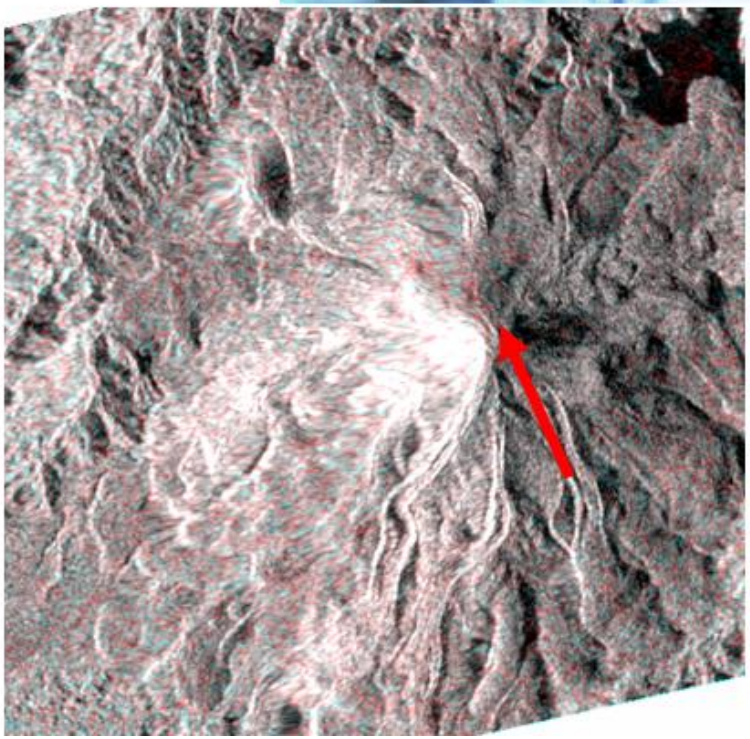

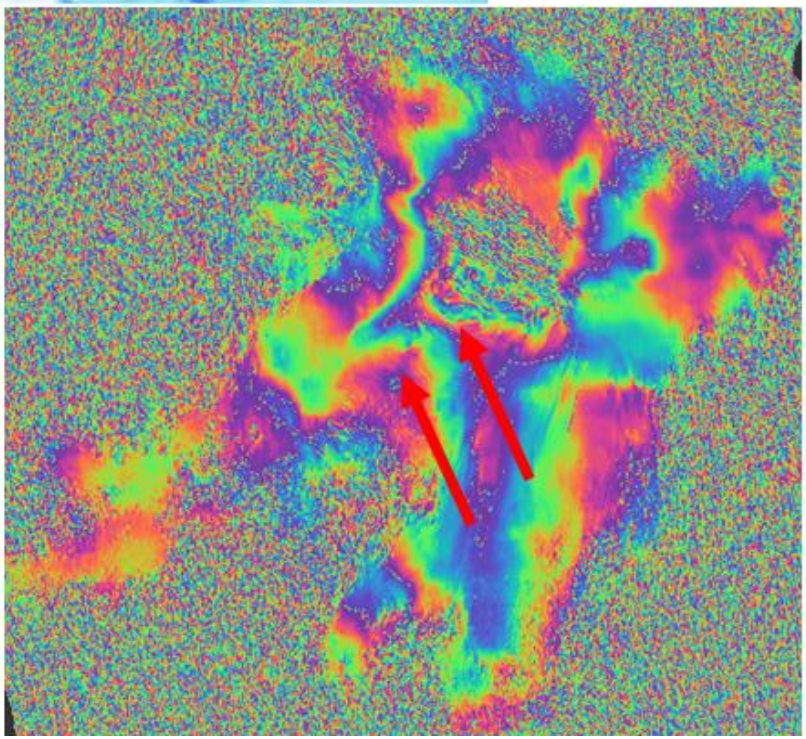

D.I. Sentinel-2 - 2018-12-14, Sentinel-1 InSAR - 2018-11-13 to 2018-12-19, Sentinel-1 Amplitude - 2018-11-13 to 2018-12-19